LONG-TERM STABILIZATION OF ARSENIC-BEARING SOLID RESIDUALS UNDER LANDFILL CONDITIONS

by

Madhumitha Raghav

_____

A Dissertation Submitted to the Faculty of the

DEPARTMENT OF CHEMICAL AND ENVIRONMENTAL ENGINEERING

In Partial Fulfillment of the Requirements

For the Degree of

DOCTOR OF PHILOSOPHY

WITH A MAJOR IN ENVIRONMENTAL ENGINEERING

In the Graduate College

THE UNIVERSITY OF ARIZONA

2013

THE UNIVERSITY OF ARIZONA

GRADUATE COLLEGE

As members of the Dissertation Committee, we certify that we have read the dissertation prepared by Madhumitha Raghav, titled Long-term Stabilization of Arsenic-bearing Solid Residuals under Landfill Conditions and recommend that it be accepted as fulfilling the dissertation requirement for the Degree of Doctor of Philosophy.

_____Date:

Wendell P. Ela

_____Date:

A.Eduardo Sáez

_____Date:

James Farrell

_____Date:

Jon Chorover

Final approval and acceptance of this dissertation is contingent upon the candidate's submission of the final copies of the dissertation to the Graduate College.

I hereby certify that I have read this dissertation prepared under my direction and recommend that it be accepted as fulfilling the dissertation requirement.

_____Date:

Dissertation Director: Wendell P. Ela

STATEMENT BY AUTHOR

This dissertation has been submitted in partial fulfillment of the requirements for an advanced degree at the University of Arizona and is deposited in the University Library to be made available to borrowers under rules of the Library.

Brief quotations from this dissertation are allowable without special permission, provided that an accurate acknowledgement of the source is made. Requests for permission for extended quotation from or reproduction of this manuscript in whole or in part may be granted by the head of the major department or the Dean of the Graduate College when in his or her judgment the proposed use of the material is in the interests of scholarship. In all other instances, however, permission must be obtained from the author.

SIGNED: Madhumitha Raghav

ACKNOWLEDGEMENTS

I want to thank my advisors Dr.Wendell Ela and Dr.Eduardo Sáez for all their support, mentorship and encouragement during my time here at the University of Arizona. They have always been receptive to my ideas and patiently guided me whenever I needed direction. I also wish to thank all my teachers from the University of Arizona and elsewhere who are responsible for instilling a sense of passion in me for environmental issues.

I will always be thankful to my family - my parents, Dr.Raghavan and Mrs.Prema Raghavan, and my sister, Nivedita Raghav. My father has been the main inspiration behind me pursuing a PhD. My mother has been a strong support system throughout my graduate studies and my life in the US. My sister has always believed in me and rooted for me. This dissertation would not have been possible without their constant love, affection, support and motivation.

I wish to thank my best friend, Sriram Srinivasan for his wonderful company during my graduate studies and for being someone I can always count on. I also wish to thank my roommate and friend Dr.Aakriti Tandon, for her encouragement and support during my journey towards a PhD.

I wish to thank all my friends in the Department of Chemical and Environmental Engineering, especially Sahar and Hector for their friendship. I also want to thank Dr. Jilei Shan and Dr.Fernando Alday for being amazing mentors during the first few years of my graduate studies.

XRD, SEM, TEM, EDS and elemental mapping analyses were performed by University Spectroscopy and Imaging Facility at the University of Arizona. I wish to thank Phillip Anderson and Steven Hernandez for performing these analyses.

ICP-MS analysis was performed by the Analytical Section of the Hazard Identification Core and Arizona Laboratory for Emerging Contaminants (ALEC) at the University of Arizona from our NIEHS-supported Superfund Research Program Grant. I wish to thank Mike Kopplin and Mary Kay Amistadi for performing these analyses. Synchrotron XRD data for schwertmannite solids were obtained at the Stanford Synchrotron Radiation LightSource. I wish to thank Dr. Jon Chorover and Dr. Robert Root respectively for sharing beam time and performing these analyses.

I am grateful for the financial support from the National Institute of Environmental Health Sciences (NIEHS) supported Superfund Basic Research Program (Grant (NIH ES-04940)) Research Program (Grant (NIH ES-04940)) and the Science Foundation of Arizona.

Last but not the least I am grateful to Lord Shrirama, for giving me the strength and perseverance to achieve my goals and guiding me through difficult times in life.

DEDICATION

To all the people in my life who have seen great potential in me. It is your strong belief in my capabilities that has made me strive to reach greater heights.

TABLE OF CONTENTS

LIST OF FIGURES 8

LIST OF TABLES 14

ABSTRACT 15

CHAPTER 1: INTRODUCTION 17
1. Occurrence of Arsenic 17
2. Arsenic Chemistry 18
3. Arsenic Treatment Technologies in Drinking Water 19
4. Conventional Treatment Technologies for ABSRs 20
5. Biogeochemistry of Landfills 21
6. Iron Biogeochemistry and Fate of Associated Arsenic 22
7. Motivation 25
8. Objectives 26
9. Dissertation overview 28

CHAPTER 2: UNDERSTANDING ABIOTIC FERRIHYDRITE REMINERALIZATION BY FERROUS IONS 39
ABSTRACT 39
1. Introduction 41
2. Materials and Methods 43
2.1. Preparation of Synthetic Ferrihydrite 43
2.2. Experimental System 45
2.3. Solids Characterization 47
2.4. ZVI-Magnetite Quantification 47
3. Results and Discussion 50
4. Concluding Remarks 61
Acknowledgements 63

CHAPTER 3: SCOPING CANDIDATE MINERALS FOR STABILIZATION OF ARSENIC-BEARING SOLID RESIDUALS 73
ABSTRACT 73
1. Introduction 75
2. Materials and Methods 78
2.1. Ferrihydrite Preparation 78
2.2. Characterization and Analytical Methods 79

TABLE OF CONTENTS - *Continued*

2.3. Scorodite Synthesis 81
2.4. Arsenate Hydroxyapatite Synthesis 83
2.5. Tooeleite Synthesis 83
2.6. Ferrous Arsenate Synthesis 84
2.7. Arsenated-Schwertmannite Synthesis 85
3. Results and Discussion 86
4. Conclusions 93
Acknowledgements 94

CHAPTER 4: MICROENCAPSULATION OF ARSENIC-BEARING SOLID RESIDUALS FOR LONG-TERM STABILIZATION UNDER LANDFILL CONDITIONS 108
ABSTRACT 108
1. Introduction 110
2. Materials and Methods 115
2.1. Preparation of Synthetic Arsenic-loaded Ferrihydrite 115
2.2. Characterization and Analytical Methods 116
2.3. PHREEQC Modeling 118
2.4. Experimental Setup 119
2.4.1.Vivianite Synthesis Trials - Instantaneous Addition vs. Continuous Dosing 119
2.4.2. Mixed System Synthesis Trials (Pre-formed Vivianite and ABSR) 120
2.4.3. Microencapsulation Trials 120
3. Results and Discussion 121
4. Conclusions 130
Acknowledgements 131

CHAPTER 5: CONCLUSIONS 142

APPENDIX A: CHARACTERIZATION TECHNIQUES FOR ANALYSIS OF SOLIDS FROM MICROENCAPSULATION PROCEDURE 148

APPENDIX B: MICROENCAPSULATION TRIALS USING ALUMINUM HYDROXIDE 163

REFERENCES 171

LIST OF FIGURES

Figure 1.1. Eh-pH diagram for arsenic at 25 °C and 101.3 kPa 31

Figure 1.2. Arsenic speciation and inter-transformations. 32

Figure 1.3.Conceptual diagram for transformations of arsenic-bearing ferrihydrite and resulting arsenic partitioning among secondary mineralization products under reducing conditions.....33

Figure 2.1. XRD spectra for product solid taken (a) initially, (b) after 5 hrs, (c) after 16 hrs, and (d) after 10 days. All experiments were performed using a magnetic stirrer with initial ferrihydrite:ZVI ratio of 1.0 and pH 6.8±0.2. M-Magnetite, Z-ZVI 65

Figure 2.1. XRD spectra for product solid taken (a) initially, (b) after 16 hrs, non-magnetic fraction, (c) after 16 hrs, magnetic fraction, (d) after 3 days, non-magnetic fraction, (e) after 3 days, magnetic fraction, (f) after 10 days, non-magnetic fraction, and (g) after 10 days, magnetic fraction. All experiments were performed using an overhead stirrer with initial ferrihydrite:ZVI ratio of 1.0 and pH 6.8±0.2. M-Magnetite, Z-ZVI, G-Goethite.....66

Figure 2.3. Magnetite generated as function of time using a magnetic stirrer (♦), overhead stirrer (■) and an overhead stirrer with a magnetic bead attached to the propeller shaft (▲). Conditions as in Figs. 1 and 2. The 16 hour data for the overhead stirrer and the overhead stirrer with the magnetic bead attached to the propeller shaft overlap with each other. Error bars are standard errors from three replicates and were generated for 25% of the sampled data-points chosen randomly 67

Figure 2.4. XRD spectra for initial ferrihydrite (a); solid products of ferrihydrite transformation when Fe^{2+} was added: at 3.13 mg of Fe^{2+}/hr for 4 days on the magnetic stir plate (b); at 3.13 mg of Fe^{2+}/hr for 4 days on the overhead stirrer (c); at 30.61 mg of Fe^{2+}/hr for 5 hr on the magnetic stir plate (d); and at 30.61 mg of Fe^{2+}/hr for 5 hr on the overhead stirrer (e).....68

Figure 2.5. XRD spectra for solid products of ferrihydrite transformation in the presence of ZVI on: overhead stirrer with a magnetic bead attached to the propeller (a); overhead stirrer without any magnetic bead attached (b); and magnetic stir plate (c). All experiments were performed with an initial Fe (III):ZVI ratio of 1.0 and an initial pH of 6.8±0.2 69

LIST OF FIGURES - *Continued*

Figure 2.6. Zero-valent iron remaining as a function of time using a magnetic stirrer (♦), an overhead stirrer (■), and an overhead stirrer with a magnetic bead attached to the propeller shaft(▲). Initial amount of ZVI added to each system = 0.3g. The 2-day data points for all three systems overlap with each other. Error bars are standard errors from three replicates and were generated for 25% of the sampled data-points chosen randomly. 70

Figure 2.7. XRD spectra for solid products of iron-arsenic solid transformation in the presence of ZVI on the magnetic stirrer. Solids with the following Fe/As ratios were used: (a) ferrihydrite with no arsenic, (b) Fe/As=100, (c) Fe/As=20, and (d) Fe/As=5.7. All experiments were performed with an initial Fe (III):ZVI ratio of 1.0 and an initial pH of 6.8±0.2. M- 100% peak for magnetite, Z-100% peak for zero-valent iron 71

Figure 2.8. Summary of transformation pathways of amorphous ferric hydroxide under different arsenic loadings and presence/absence of high Fe (II) concentrations. *High Fe^{2+} concentrations can either be localized (this study) or uniformly distributed (other studies). Hansel et al. (2003) observed that a threshold Fe (II) concentration level of 0.3 mM is required for magnetite nucleation. **Suggested/ presumed short-term mineralogy (not confirmed in this study). Presence of high arsenic concentrations inhibit transformation of ferrihydrite to goethite by interfering with both the dissolution of ferrihydrite and the re-precipitation of goethite. Long-term arsenic sequestration/release will depend on the relative rates of ferrihydrite dissolution and re-precipitation as goethite in the presence of high concentrations of arsenic. 72

Figure 3.1. XRD spectra for solids generated from scorodite synthesis trials at 160 °C for 24 hours, a Fe/As molar ratio of 1.0, and initial pH as indicated. 96

Figure 3.2. Arsenic concentration from Toxicity Characteristic Leaching Procedure for candidate minerals. FA oxic - Ferrisymplesite synthesized under oxic conditions, Sch - Arsenated-Schwertmannite, FA anoxic - Parasymplesite synthesized under anoxic conditions, Sco - Scorodite, Apa - Arsenate Hydroxyapatite (with no Fe and As/P < 0.2), Too - Tooeleite, Si-Too - Silica-amended Tooeleite. Note: Error bars were not be obtained for scorodite and arsenate-hydroxyapatite. 97

Figure 3.3. XRD spectra of solids generated from arsenate hydroxyapatite synthesis trials using different As/P ratios. All the solids were synthesized at 100 °C, an initial synthesis pH of 11 and reaction time of 24 hours.. 98

LIST OF FIGURES - *Continued*

Figure 3.4. XRD spectra for solids obtained from the iron arsenate hydroxyapatite synthesis trials using different Fe/As ratios. All the solids were synthesized at 100 °C, Ca/(As+P) ratio of 5/3 and P/As ratio =1. The initial pH was 12 and the reaction time was 24 hours.....99

Figure 3.5. Solid synthesized from a.) pure Fe(II) and As(V) solutions following the procedure in Johnston and Singer (2007). b.) Fe/As = 20.46 solid, zero-valent iron [Fe(III)/ZVI = 10], at room temperature, inside the glove box purged with N_2. c.) Fe/As = 20 solid, zero-valent iron [Fe(III)/ZVI = 10], at room temperature, outside the glove box. Note: PS – Parasymplesite, FS – ferrisymplesite. There were no unidentified peaks. Only the major peaks have been labeled in all three cases. 100

Figure 3.6. Arsenic leachate concentration from Simulated Landfill Leachate test on ferrous arsenate (FA) anoxic - Parasymplesite synthesized inside the glove box, FA oxic - Ferrisymplesite synthesized outside the glove box, and Sch - Arsenated-Schwertmannite. 101

Figure 3.7. a.) XRD reference stick pattern for schwertmannite and Synchrotron XRD spectra for solid synthesized after 18 days from b.) lab synthesized arsenic-loaded ferrihydrite (Fe/As molar ratio = 20.46) following a procedure modified from Carlson et al. (2002) for arsenated-schwertmannite and b.) ferrihydrite following a procedure modified from Bigham et al. (1990) for schwertmannite synthesis.....102

Figure 4.1. XRD spectra for final solid in vivianite synthesis trials using instantaneous addition of ferrous and phosphate solutions and total phosphorus to Fe(II) molar ratios of: a.) TOTP/Fe(II) = 333.33, b.) TOTP/Fe(II) = 190.47, c.) TOTP/Fe(II) = 82.67, d.) TOTP/Fe(II) =15, e.) TOTP/Fe(II) = 5, f.) TOTP/Fe(II) = 4, g.) TOTP/Fe(II) = 3... 132

Figure 4.2. XRD spectra of a.) arsenic loaded ferrihydrite (Fe/As = 4) and final solids from synthesis trials under continuous dosing conditions for vivianite (b-d) and the mixed system (arsenic-loaded ferrihydrite solid mixed with pre-formed vivianite) (e, f). The feed rates used in each case for the Fe(II) and phosphorus solutions are: b.) 180 mL/hr, c.) 90 mL/hr d.) 36 mL/hr e.) 90 mL/hr and f.) 36 mL/hr. 133

Figure 4.3. SEM images of solid synthesized from pure vivianite synthesis trial with continuous dosing of ferrous and phosphate solutions at a.) 180mL/hr (duration = 1 hour), b.) 90 mL/hr (duration = 2 hour) and c.) 36 mL/hr (duration = 5 hour) 134

LIST OF FIGURES - *Continued*

Figure 4.4. SEM image and Energy Dispersive X-Ray (EDX) elemental analysis results for final solids obtained from microencapsulation trials using simultaneous continuous dosing of Fe(II) and phosphorus solutions at feed rates of 90 mL/hr each.....135

Figure 4.5. Aqueous phosphorus concentrations at equilibrium for different solids included in this study. Note: PHREEQC predicted values are reported for all solids marked with an *. Experimentally observed values for aqueous phosphorus concentrations are reported in all other cases. Final pH was 7.2 ± 0.1. Viv – vivianite solid, Mixed - arsenic loaded ferrihydrite mixed with pre-formed vivianite, Encap - solid obtained from the microencapsulation trial... 136

Figure 4.6. Aqueous arsenic concentrations at equilibrium for different solids included in this study. Note: PHREEQC predicted values are reported for all solids marked with an *. Experimentally observed values for aqueous arsenic concentrations are reported in all other cases. A total suspension volume of 760 mL was assumed for all PHREEQC calculations. All cases contained 1±0.05 g of arsenic loaded ferrihydrite (equivalent to approx 200 mg of arsenic). Final pH was 7.2 ± 0.1. FeAs* - arsenic loaded ferrihydrite in deionized water, FeAs+P* - arsenic loaded ferrihydrite in 1718 mg/L phosphorus solution (this is the total phosphorus concentration in equilibrium with vivianite solid as determined by PHREEQC), Mixed - arsenic loaded ferrihydrite mixed with pre-formed vivianite, Encap – solid obtained at equilibrium from the microencapsulation trial described in this study.... 137

Figure 4.7. Aqueous arsenic concentrations after 50 hours of exposure to acetic acid leaching for solids included in this study. Note: PHREEQC predicted values are reported for all solids marked with a *. Experimentally observed values for aqueous arsenic concentrations are reported in all other cases. Final pH was 4.9 ± 0.2. FeAs - arsenic loaded ferrihydrite, Mixed - arsenic loaded ferrihydrite mixed with pre-formed vivianite, Encap – solid obtained from the microencapsulation trial.....138

Figure A1. Vivianite solid synthesized using instantaneous addition of 50 mL of 0.07 M sodium phosphate (Na_2HPO_4) solution and 50 mL of 0.02325 M ferrous chloride tetrahydrate ($FeCl_2.4H_2O$) solution to 23 mL of deionized water (TOTPO4/Fe(II) = 3), without any arsenic-loaded ferrihydrite solid added. Note: Final pH observed = 7.15. For SEM elemental mapping, accelerating voltage used: 15 kV and magnification used: 5030.....153

Figure A2. Arsenic-loaded ferrihydrite (Fe/As molar ratio = 4) solid. Note: SEM accelerating voltage: 20 kV, magnification: 900.....154

LIST OF FIGURES - *Continued*

Figure A3. Solid from microencapsulation trial using instantaneous addition of ferrous and phosphate solutions to a suspension containing the arsenic-loaded ferrihydrite solid (Fe/As = 4). 17 ml of 0.3 M sodium phosphate and 17 ml of 0.1 M ferrous chloride were added to 0.2 g of arsenic-loaded ferrihydrite suspended in 100 ml. Two such doses of Fe (II) and phosphate solutions followed at 20 minute intervals of each other. Final pH observed = 7.2. Note: SEM accelerating voltage: 20 kV, magnification: 1800 155

Figure A4. FTIR spectra of different solids synthesized as part of vivianite microencapsulation efforts ▬▬ Fe/As = 4 solid with phosphate sorbed on the surface ▪▪▪▪▪▪ Mixed Fe/As = 4 solid and pre-formed vivianite ▬▬ Vivianite solid using continuous dosing ▬ ▬ Solid from encapsulation experiment using continuous dosing ═══ Fe/As = 4 solid 156

Figure A5. FTIR spectra of arsenic loaded ferrihydrite (Fe/As = 4) and vivianite mixed in the different ratios ═══ 100% Fe/As = 4 solid ▬▬ 75% Fe/As = 4 solid, 25% vivianite

- - - 50% Fe/As = 4 solid, 50% vivianite ▬▬ 25% Fe/As = 4 solid, 75% vivianite

▪▪▪▪▪▪ 100% vivianite.. 157

Figure A6. TEM image of arsenic-loaded ferrihydrite (Fe/As = 4).....158

Figure A7. TEM image of arsenic loaded ferrihydrite (Fe/As = 4) with 0.3M phosphate added. 159

Figure A8. TEM image of vivianite solid synthesized using continuous dosing of Fe(II) and phosphate solutions fed simultaneously at 90 mL/hr each.....160

LIST OF FIGURES - *Continued*

Figure A9. TEM image of mixed solid (arsenic-loaded ferrihydrite Fe/As = 4 and pre-formed vivianite) synthesized under continuous dosing at a feed rate of 90 mL/hr for Fe(II) and phosphate solutions.....161

Figure A10. TEM image of solid obtained from microencapsulation trial under continuous dosing at a feed rate of 90 mL/hr for Fe(II) and phosphate solutions. 162

Figure B1: Aqueous total arsenic concentrations before leaching in the 'Al Hyd'- aluminum hydroxide system, 'Mixed'- mixed system (Fe/As = 4 solid and pre-formed aluminum hydroxide solid) and 'Encap' - microencapsulation system. Note: The final pH in all systems was 6.8 ±.1. The arsenic detected in the pure aluminum hydroxide system was probably because the concentrations were close to detection limit for arsenic.....167

Figure B2: Aqueous total arsenic concentrations after leaching in the 'Al Hyd' - aluminum hydroxide system, 'Mixed' - mixed system (Fe/As = 4 solid and pre-formed aluminum hydroxide solid) and 'Encap' - microencapsulation system. Note: The final pH in all systems was 4.85 ± 0.15. Arsenic detected in the pure aluminum hydroxide system indicates low levels of contamination. If this contamination was present in the mixed and microencapsulation systems as well that would only mean that the actual arsenic concentrations in the system are lower. Hence, this observation does not change the interpretation of our results.....168

Figure B3: Aqueous total aluminum concentrations before leaching in the 'Al Hyd' - aluminum hydroxide system, 'Mixed' - mixed system (Fe/As = 4 solid and pre-formed aluminum hydroxide solid) and 'Encap' - microencapsulation system. Note: The final pH in all systems was 6.8 ±.1. 169

Figure B4: Aqueous total aluminum concentrations after leaching in the 'Al Hyd' - aluminum hydroxide system, 'Mixed' - mixed system (Fe/As = 4 solid and pre-formed aluminum hydroxide solid) and 'Encap' - microencapsulation system. Note: The final pH in all systems was 4.85 ± 0.15. 170

LIST OF TABLES

Table 1.1. Arsenic treatment technologies in drinking water.....35

Table 1.2. Composition of landfill leachate (Source: Kjeldsen et al. 2002) 37

Table 1.3. Arsenic Retention Capacities of Selected Iron Minerals (Source: Alday 2010) 38

Table 3.1. Summary of synthesis parameters for synthesis of scorodite under different temperatures.....103

Table 3.2. Results of SEM-EDX analysis of tooeleite and solid synthesized from silica-coating of tooeleite.....104

Table 3.3. Characterization of ferrous arsenate (parasymplesite) synthesized from arsenic-loaded ferrihydrite.....105

Table 3.4. Summary of evaluation results of candidate minerals for Arsenic Crystallization Technology 106

Table 4.1. Compilation of arsenic leaching and final transformation products in biological columns operated under simulated landfill conditions 139

Table 4.2. PHREEQC calculated supersaturation indices for vivianite in synthesis trials using instantaneous addition of ferrous and phosphate solutions (Note: TOTP and Fe(II) concentrations are initial concentrations after dilution of the stock solutions) 140

ABSTRACT

The maximum contaminant level (MCL) for arsenic in drinking water was reduced to 10 parts per billion in 2006 by the USEPA. As a result, approximately 10,000 tons of arsenic-bearing residuals (ABSRs) are estimated to be generated every year from water treatment processes. It has also been established that the standard Toxicity Characteristic Leaching Procedure (TCLP), underestimates arsenic leaching from ABSRs, particularly under mature, mixed solid waste landfill conditions. This makes it critical to investigate stabilization technologies that would ensure long-term stability of arsenic residuals after disposal.

Arsenic is ubiquitously associated with iron oxides in natural environments as well as water treatment residuals. Hence, knowledge of iron oxide transformations under landfill conditions is critical to understanding the fate and mobility of the associated arsenic. In this work, the effect of high local Fe(II) concentrations on ferrihydrite transformation pathways was studied. Magnetite was the sole transformation product in the presence of high local Fe(II) concentrations. In the absence of high Fe(II) concentrations, goethite was the major transformation product along with minor quantities of magnetite. These results have implications for arsenic mobility from ABSRs since goethite and magnetite have different arsenic sorption capacities and mechanisms.

Two technologies were investigated for the stabilization of ABSRs – Arsenic Crystallization Technology (ACT) and Microencapsulation. The strategy for ACT was to convert ABSRs into minerals with a high arsenic capacity and long-term stability under

landfill conditions. Scorodite, arsenate hydroxyapatites, ferrous arsenate, arsenated schwertmannite, tooeleite and silica-amended tooeleite, were synthesized and evaluated for their potential to serve as arsenic sinks using TCLP and a simulated landfill leachate test. Ferrous arsenate type solids and arsenated schwertmannite showed most promise in terms of low arsenic leachability and favorable synthesis conditions.

Microencapsulation involved coating arsenic-loaded ferrihydrite with a mineral having high stability under landfill conditions. Based on results from a previous study, vivianite was investigated as a potential encapsulant for ABSRs. A modified version of the TCLP was used to evaluate the effectiveness of microencapsulation. Although vivianite did not prove to be a promising encapsulant, our efforts offer useful insights for the development of a successful microencapsulation technology for arsenic stabilization.

Keywords: Iron-oxides; Arsenic residuals; Landfills; Magnetite; Goethite; Ferrous iron; Arsenic Crystallization Technology (ACT); Ferrous Arsenate; Schwertmannite; Tooeleite; Microencapsulation; Vivianite.

CHAPTER 1: INTRODUCTION

1. Occurrence of Arsenic

Arsenic is a ubiquitous element that occurs in natural soils, sediments and rocks in the form of various arsenic-containing minerals (Mandal and Suzuki 2002). The dissolution of these minerals via slow geologic processes results in the introduction of arsenic into groundwater sources (Smedley and Kinniburgh 2002). Some industrial processes such as mining and wood preservation activities also introduce arsenic into the environment via the generated waste streams (Smedley and Kinniburgh 2002; Wilson and Hawkins 1978).

Arsenic concentrations in groundwater vary between 0.5-5000 µg/L (Welch et al. 2000). The concentrations are generally below 10 µg/L, but in some countries, including India, Bangladesh, Mexico and Vietnam, concentrations as high as 500 µg/L have been reported (USEPA 2001). In the United States, arsenic concentrations exceeding 10 µg/L have been frequently observed especially in the southwest (Welch et al. 2000). It is well-recognized that long-term exposure to arsenic even at relatively low concentrations can lead to deleterious health effects, especially carcinogenic effects (WHO 2001). Hence, the USEPA lowered the Maximum Contaminant Level (MCL) for arsenic from 50 µg/L to 10 µg/L in 2006 (USEPA 2001). This has resulted in a significant increase in the amount of arsenic waste generated in water treatment plants. It has been estimated that approximately 10,000 tons of arsenic-bearing waste residuals are generated every year (Impellitteri and Scheckel 2006).

2. Arsenic Chemistry

Arsenic is a metalloid that is both redox and pH sensitive. In nature, arsenic can be present in one of the following stable redox states: −3 (e.g. arsine gas, AsH_3), −1 (e.g. alkyl arsenic), 0 (zero-valent elemental arsenic), +3 (the arsenites) and +5 (the arsenates). In aqueous solution, arsenic occurs as the arsenite and/or arsenate species. These two oxyanions can bind to one or more hydrogen ions to form various inorganic hydrolysis species: arsenate species include H_3AsO_4, $H_2AsO_4^-$, $HAsO_4^{2-}$ and AsO_4^{3-} while arsenite species are H_3AsO_3, $H_2AsO_3^-$, $HAsO_3^{2-}$ and AsO_3^{3-}. The dissociation constants for As (III) and As (V) are $pK_{a1} = 9.22$, $pK_{a2} = 12.10$, $pK_{a3} = 13.4$ and $pK_{a1} = 2.22$, $pK_{a2} = 6.96$, $pK_{a3} = 11.5$ respectively. The speciation of arsenic in aqueous solution is dependent on pH and redox conditions as shown in the Eh-pH diagram in Figure 1.

Apart from inorganic arsenic species mentioned above, organic species are also relevant under high concentrations of organic matter. Huang et al. (2009) found that methylated arsenic species contributed to about 15-50% of the total arsenic released from biologically pretreated municipal solid waste. The authors observed that the organic arsenic species were more mobile than the inorganic species which is consistent with the results from other studies (Lafferty and Loeppert 2005; Huang and Matzner 2006).

Similarly, dissolved arsenic sulfide species can also form under reducing conditions in the presence of relatively high reduced sulfur concentrations. Couture and Cappellen (2011) suggest that the formation of highly soluble arsenate (oxy)thioanions might be

responsible for the increased mobility of arsenic under reducing conditions. Bostick et al. (2005) proposed a similar enhancement in solubility of arsenic due to the formation of thioarsenite complexes in neutral to alkaline arsenic sulfide solutions. Recent studies have also demonstrated the transformation of monomethylarsonic acid (MMA^V) and dimethylarsinic acid (DMA^V) to highly toxic thiol-organoarsenic species in municipal landfill leachate (Li et al. 2010; Li et al. 2011). Figure 2 shows the different inorganic and organic arsenic species that have been observed in municipal solid waste landfills and their inter-transformation pathways.

3. Arsenic Treatment Technologies in Drinking Water

The most commonly used technologies for arsenic removal from drinking water include – precipitation/ coprecipitation, adsorption, ion exchange and membrane filtration (USEPA 2002). Oxidation of As(III) to As(V) is usually done either prior to or as part of all these processes in order to increase the efficiency of arsenic removal. Penta-valent arsenic exists predominantly as anionic species in the pH range relevant to water treatment processes. Hence, As(V) exhibits higher affinity for charged surfaces and is removed more efficiently than As(III), which exists pre-dominantly as the uncharged H_3AsO_3 species in the pH range 2-9. More details on conventional arsenic treatment technologies are provided in Table 1.

4. Conventional Treatment Technologies for ABSRs

Toxicity Characteristic Leaching Procedure (TCLP) is the current EPA recommended test to evaluate the potential for arsenic mobilization from a solid waste (USEPA 1992). Solids that pass the test need not be disposed in hazardous waste landfills, which are more expensive and complex than regular municipal solid waste landfills. All the above arsenic removal technologies generate a residual solid, which may be disposed in municipal solid waste landfills, since they routinely pass the TCLP (Impellitteri and Scheckel 2006, Mohan and Pittman 2007). However, it has been established that both the TCLP and California Waste Extraction Test (CA-WET) protocols underestimate arsenic leaching under mature landfill conditions (Ghosh et al 2004). Hence, the large volumes of arsenic-bearing solid residuals (ABSRs) generated by the treatment technologies have to be safely disposed so as to avoid subsequent groundwater, soil, or wastewater contamination. Vitrification, solidification/stabilization using Portland cement, concrete or fly ash, and polymer encapsulation are the conventional technologies used for toxic waste stabilization. Vitrification is the EPA recommended Best Demonstrated Available Technology (BDAT) for stabilization of arsenic-bearing solids. But the high temperatures involved (2630-3330^{o}F) make this technology cost-prohibitive (USEPA 2002). Several studies have investigated the use of solidification/stabilization and polymer encapsulation for the pre-treatment of arsenic waste before disposal (Dutre and Vandecasteele 1998; Dawadi et al. 2004; Singh and Pant 2006; Chintalapati et al. 2009; Carter et al. 1995; Shaw et al. 2008). But, the effectiveness of these technologies in ensuring long-term stability of the arsenic residuals under mature, mixed-solid waste landfill conditions is

not clear. More details on these technologies are provided in the Introduction section of Chapter 4.

5. Biogeochemistry of Landfills

Mature, mixed solid waste landfills are characterized by slightly alkaline pH, low redox potential, biological activity, long retention time, and rich organic content. It has been established that both the TCLP and CA-WET protocols underestimate arsenic leaching under mature landfill conditions due to their poor simulation of mature landfill conditions mentioned above. These conditions have the propensity to cause increased mobilization of arsenic associated with conventional sorbents (Ghosh et al. 2004). Landfills are known to undergo the following four phases of decomposition – (i.) an initial aerobic phase, (ii.) an anaerobic acid phase, (iii.) an initial methanogenic phase, and (iv.) a stable methanogenic phase (Christensen and Kjeldsen 1995). It has been hypothesized that once all the available refuse has been decomposed, the landfill would become aerobic, since the rate of diffusion of oxygen would exceed rate of microbial oxygen depletion (Christensen and Kjeldsen 1995). But model calculations have also shown that the enhanced release of heavy metals and other contaminants due to return of aerobic conditions in the landfills will not occur for thousands of years (Bozkurt et al. 2005). Hence, even though landfills undergo aging from aerobic to anoxic and back again to aerobic conditions, majority of research has focused on the fate of arsenic and other trace contaminants under anaerobic landfill conditions.

Lee at al. (2008) used discriminant analysis and geochemical modelling to delineate three redox zones of aquifers in the Lanyang plain and the speciation of arsenic in each zone. It was observed that the distribution of the oxidizing zone was well correlated with the region of infiltration of oxygenated rainfall and decreased with distance and depth from this region. A similar redox zonation could be expected in active mixed solid waste landfills, with the conditions becoming more anaerobic with depth. It has been suggested that different parts of a landfill are usually at different stages of decomposition which is also responsible for the wide range in leachate composition as shown in Table 2 (Kjeldsen 2002). The values of these parameters are found to vary not only across different landfills but also at different regions within the same landfill.

6. Iron Biogeochemistry and Fate of Associated Arsenic

Arsenic is ubiquitously associated with iron-oxides in natural systems and the residuals generated from arsenic removal processes in water-treatments systems (Smedley and Kinniburgh 2002; Benner et al. 2002; Vircikova et al. 1995). Studies using X-ray Absorption Spectroscopy (XAS) and Fourier Transformation Infrared (FTIR) Spectroscopy have reported that arsenic sequestration in an iron oxide is due to but not limited to the following mechanisms: co-precipitation, adsorption by the formation of surface precipitates and/or formation of inner- and outer-sphere complexes (Manning et al. 1998; Goldberg and Johnston 2001; Wang et al. 2008; Wang et al. 2011; Mitchell et al. 2011). The fate of arsenic in the ABSRs under landfill conditions would hence depend

on the nature of its association with iron oxides and its mobilization and/or re-sequestration under landfill conditions. It is also well-established that the iron-oxide system is very redox-sensitive; one iron oxide transforming into another depending on various conditions such as pH, temperature, presence of ferrous ions and anions like chloride and sulfate (Liu et al. 2005; Liu et al. 2008; Pedersen et al. 2005; Yee et al. 2006; Hansel et al. 2005) . Iron-oxide transformations (both biotic and abiotic) have been studied and reported to have significant implications for the leachability and mobility of arsenic under anaerobic conditions (Yee et al. 2006; Hansel et al. 2005; Kocar et al. 2006; Pedersen et al. 2006).

Microbially mediated dissimilatory Fe(III) reduction and abiotic Fe(III) reduction have both been identified as important pathways for arsenic mobilization (Masscheleyn et al. 1991; Cummings et al. 1999; Bose and Sharma 2002; Islam et al. 2004). It is also known that iron reducing bacteria are ubiquitous in landfill leachate (Ludvigsen et al. 1999). Several studies have investigated the mobilization of arsenic into groundwater due to microbial oxidation of organic matter derived either from natural (e.g.; peat and clay layers) or anthropogenic sources (e.g.; organic carbon input from irrigation pumping) coupled with microbially mediated dissimilatory Fe(III) reduction (Dowling et al. 2002; McArthur et al. 2004; Burgess and Pinto 2005). Such processes would also be significant in landfills which are generally rich in organic content.

Under strongly reducing conditions arsenic is sequestered via sorption and co-precipitation with iron sulfide phases like mackanawite, greigite, pyrite and precipitation of arsenic sulfide phases like realgar and orpiment (Farquhar et al. 2002; Wilkin and Ford 2006; Wolthers et al. 2005; O'Day et al. 2004; Kirk et al. 2004), whereas under strongly oxidizing conditions arsenic mobility is controlled mainly by sorption/co-precipitation with Fe, Al or Mn-oxide phases (Fuller and Davis 1989; W. Cullen, K. Reimer 1989; Bowell 1994; Sadiq 1997). Hence, arsenic mobilization has been observed to be highest under shifting redox conditions (Bose and Sharma 2002). Such conditions are expected in a mixed solid waste landfill, with different parts of the landfill being in different conditions (especially redox conditions) as noted earlier.

Several studies have found that Fe(II)-catalyzed transformation of Fe(III) oxides under reducing conditions to secondary iron minerals like magnetite, green rust, siderite and ferrous iron carbonate can partially sequester arsenic (Kocar et al. 2006; Pedersen et al. 2006; Tufano and Fendorf 2008). It is possible that these secondary mineral phases could be transient under the prolonged reducing conditions expected in landfills. Hence, it is important to have an understanding of the mechanisms and kinetics of iron oxide transformations and, stability of the secondary minerals in complex landfill systems. Figure 3 shows the different transformations that arsenic-loaded ferrihydrite can undergo under reducing conditions (Kocar et al. 2010).

7. Motivation

Recent batch and column studies have considered the mobilization of arsenic from ABSRs under reducing conditions in landfills (Ghosh et al. 2004; Mohapatra et al. 2005; Cortinas et al. 2008; Stuckman et al. 2011). Long-term laboratory-scale anaerobic column studies have identified solid associated transport, reductive sorbent dissolution, and microbially mediated arsenic reduction and changes in iron biomineralization as the dominant mechanisms for arsenic mobilization from ABSRs under landfill conditions (Cortinas et al. 2008; Ghosh et al 2006a; Alday 2010). In these studies, iron-based ABSRs transformed into secondary minerals siderite, goethite, vivianite and green rust accompanied with more than 80% release of arsenic compared to only about 10% release of iron. The transformations that the iron minerals undergo determine the ultimate stability of the associated arsenic under landfill conditions owing to differences in arsenic retention capacities of the original ferrihydrite solid (ABSR) and of its transformation products (Table 3).

It is clear that the secondary minerals that precipitate have appreciably lower arsenic sequestration capacities than ferrihydrite. Therefore, it is safe to expect that landfill stimulated biotransformation of iron-based ABSRs will cause release of the associated arsenic. Arsenic leaching from ABSRs under landfill conditions can pose a serious threat to the quality of ground and surface waters. Even in the case of the modern lined landfills, arsenic leaching could pose a risk due to problems with handling the contaminated leachate. Landfill leachate is periodically pumped out and sent to a storage

facility and then eventually to a treatment facility. Enhanced arsenic leaching under mature landfill conditions would result in high arsenic concentrations in the leachate and consequentially high arsenic loadings in the solid waste generated after leachate treatment. The solids generated from the treatment of landfill leachate are generally used for biosolid application. Hence, high arsenic loadings in these solids could potentially pose a serious health hazard.

Given the complexity of landfill systems, it is essential to have a good understanding of processes that could affect the release/sequestration of arsenic under landfill conditions. It also seems critical to direct efforts towards developing stabilization technologies to ensure long-term stability of arsenic-bearing solids under mixed solid waste landfill conditions.

8. Objectives

The main objective of this study was to develop arsenic stabilization technologies that ensure long-term stability of arsenic residuals after disposal. Since knowledge of iron-oxide transformations and subsequently the fate of the associated arsenic under landfill conditions are imperative to the development of such technologies, efforts were directed towards studying the same. Ferrous ion is known to be a significant parameter influencing ferrihydrite transformation and release of associated contaminants such as arsenic. Landfills are heterogeneous systems rich in diverse microbial communities. Localized hot-spots with elevated ferrous ion concentrations can be expected under such

environments. Hence, the effect of high local Fe(II) concentrations on ferrihydrite transformation was investigated. Lab synthesized arsenic-loaded ferrihydrite was used in all our experiments as a surrogate for the arsenic-bearing solid residuals generated after water treatment.

In this dissertation, two technologies for long-term arsenic stabilization under landfill conditions are discussed - (i.) Arsenic Crystallization Technology (ACT) and (ii.) microencapsulation of ABSRs by stable mineral phases. The objective of ACT is to convert arsenic-bearing solid residuals into crystalline mineral phases with high arsenic capacity and low solubility under landfill conditions. Research efforts included – selection of candidate minerals for ACT, synthesis starting from synthetic arsenic-loaded ferrihydrite and evaluation of their effectiveness as long-term arsenic sinks using various leaching tests.

The objective of microencapsulation was to encapsulate arsenic-bearing ferrihydrite particles with a mineral with high stability under landfill conditions. The encapsulating solid is not intended to be an arsenic sink but rather a protective layer around the arsenic-bearing solid core.

9. Dissertation overview

This dissertation is divided into 5 chapters as described below:

Chapter 1 provides a general introduction, motivation for this work and objectives. Arsenic chemistry, arsenic treatment/removal technologies from drinking water, arsenic waste stabilization techniques before disposal in landfills and biogeochemistry in landfills are some of the topics discussed.

The objective of the **Chapter 2** was to different transformation pathways/products of lab synthesized ferrihydrite under the presence and absence of locally high Fe(II) concentrations. The ultimate goal is to gain insights into the implications of such transformations for the sequestration/release of arsenic associated with iron based water treatment residuals under landfill conditions.

Chapter 3 provides detailed description of an Arsenic Crystallization Technology (ACT) developed for the long-term stabilization of arsenic-bearing solid residuals (ABSRs) under mixed-solid waste, municipal landfill conditions. This chapter describes the criteria used for the selection of candidate minerals, synthesis of the minerals and evaluation of arsenic leachability using standard and modified leaching tests. This chapter also includes literature review for each of the candidate minerals considered – ferrous arsenate, arsenated-schwertmannite, tooeleite and silica-amended tooeleite. The feasibility and effectiveness of these candidate minerals was compared with scorodite and arsenate hydroxyapatite, two minerals evaluated as candidates in a previous ACT study performed in our laboratory. Scorodite ($FeAsO_4.2H_2O$) is an Fe(III)-As(V) mineral which was a

promising ACT candidate because of its high arsenic capacity (25-30% wt/wt) and low arsenic solubility (Robins 1987; Harris and Krause 1993). Hydroxyapatites are known to be relatively stable over a broad pH range and arsenate can substitute for phosphate in their structure (Mahapatra et al. 1989; Lee et al. 2009). High arsenic loading (approximately 25% wt/wt) and low arsenic solubility (Johnston and Singer 2007) made ferrous arsenate ($Fe_3(AsO_4)_2.8H_2O$) a promising candidate for ACT. Arsenated-schwertmannite was included in this study due to the reported structural incorporation of arsenate in the schwertmannite [$(Fe_8O_8(OH)_x(SO_4)_y$ .nH2O, where $8 - x = y$ and $1.0 \leq y \leq 1.75$] structure (Regenspurg and Peiffer 2005; Burton et al. 2009). Tooeleite $Fe_6(AsO_3)_4SO_4(OH)_4.4H_2O$, is an iron arsenite oxyhydroxy-sulfate mineral, investigated due to its high arsenic capacity (~20-25% wt/wt) (Morin et al. 2007, Nishimura and Robins 2008). Amendment of tooeleite with silica was also attempted to make the solid further resistant to leaching.

Chapter 4 provides a description of a microencapsulation technique investigated for the long-term stabilization of arsenic-bearing solid residuals (ABSRs) under mixed-solid waste, municipal landfill conditions. Microencapsulation was studied as a technique to coat ABSR with a recalcitrant mineral phase. The goal is to have the arsenic associated with the ABSR phase in the core and a stable mineral phase (with no arsenic) in the coating. Previous biological column studies under simulated landfill conditions performed in our laboratory (not as part of this dissertation) suggested that vivianite, a ferrous phosphate mineral was stable under simulated landfill conditions over atleast a period of 600 days (Alday 2010). Hence, vivianite was chosen as an encapsulant to coat

arsenic-loaded ferrihydrite and study arsenic leachability using a modified acetic acid leaching test.

Chapter 5 includes general conclusions for the entire research performed as part of this dissertation and some recommendations for future work.

Appendix A includes a discussion of additional characterization efforts pursued to confirm the formation of a vivianite coating around the arsenic-loaded ferrihydrite core. These include Scanning Elemental Microscopy (SEM) elemental mapping, Transmission Electron Microscopy (TEM) imaging and Powder Fourier Transform Infrared (FTIR) Spectroscopy analysis.

Appendix B provides details of microencapsulation trials of arsenic-loaded ferrihydrite using amorphous aluminum hydroxide solid.

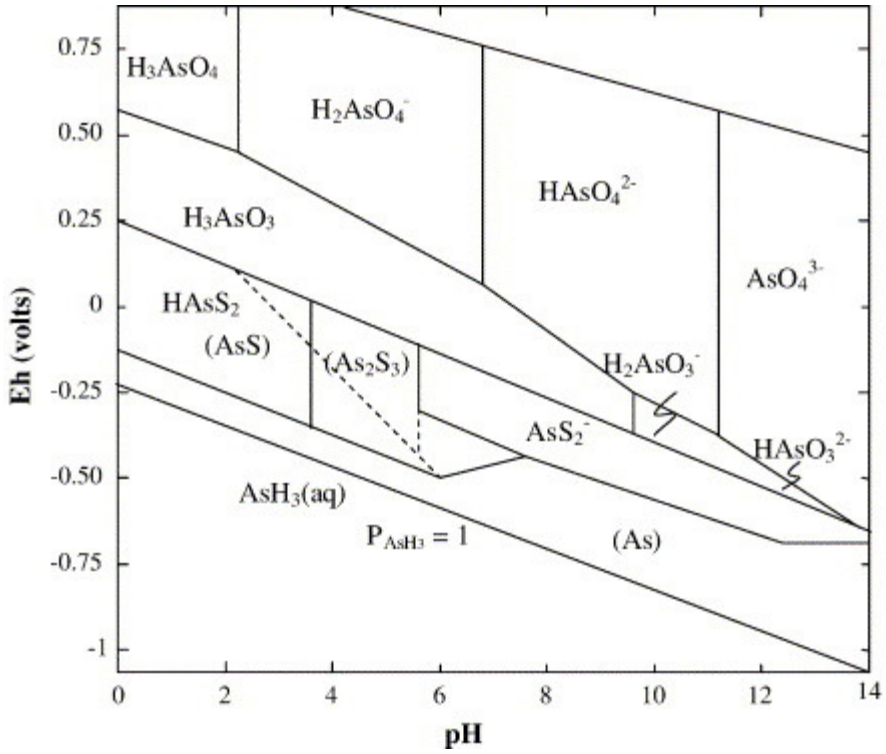

Figure 1.1. Eh-pH diagram for arsenic at 25 °C and 101.3 kPa (Source: Wang and Mulligan 2006)

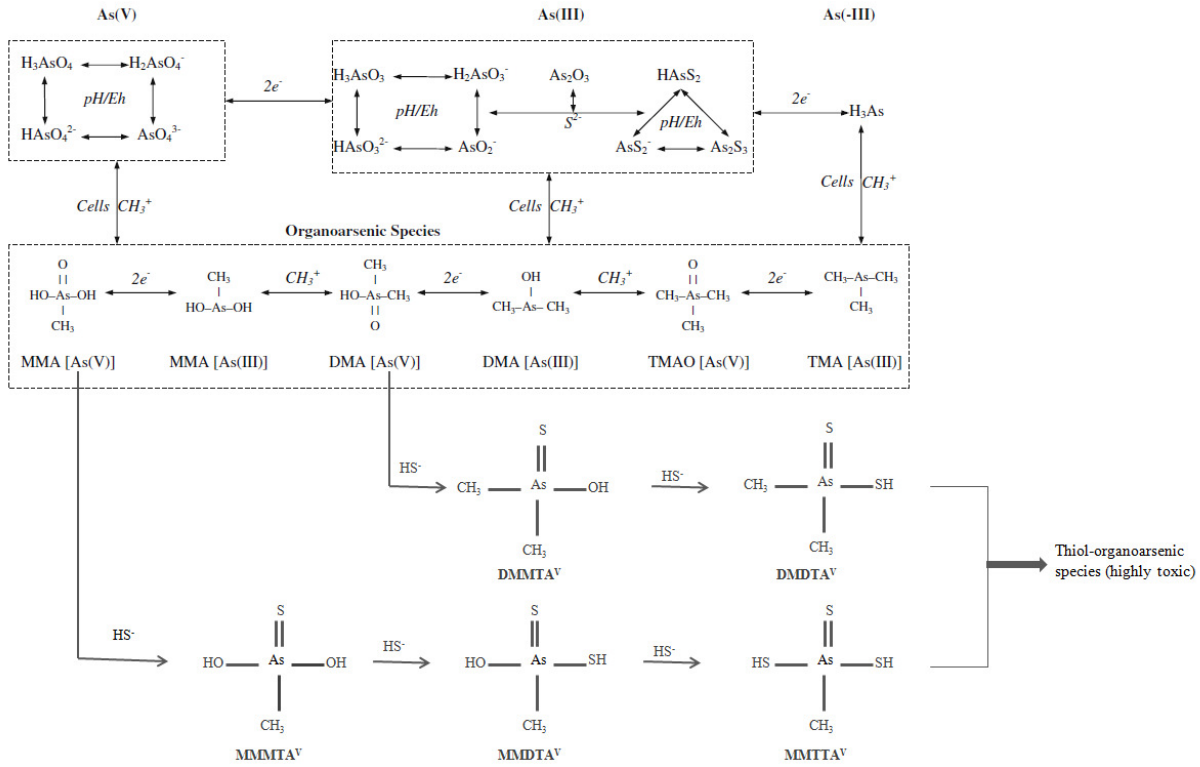

Figure 1.2. Arsenic speciation and inter-transformations (Modified from: Li et al. 2011; Wang and Mulligan 2006)

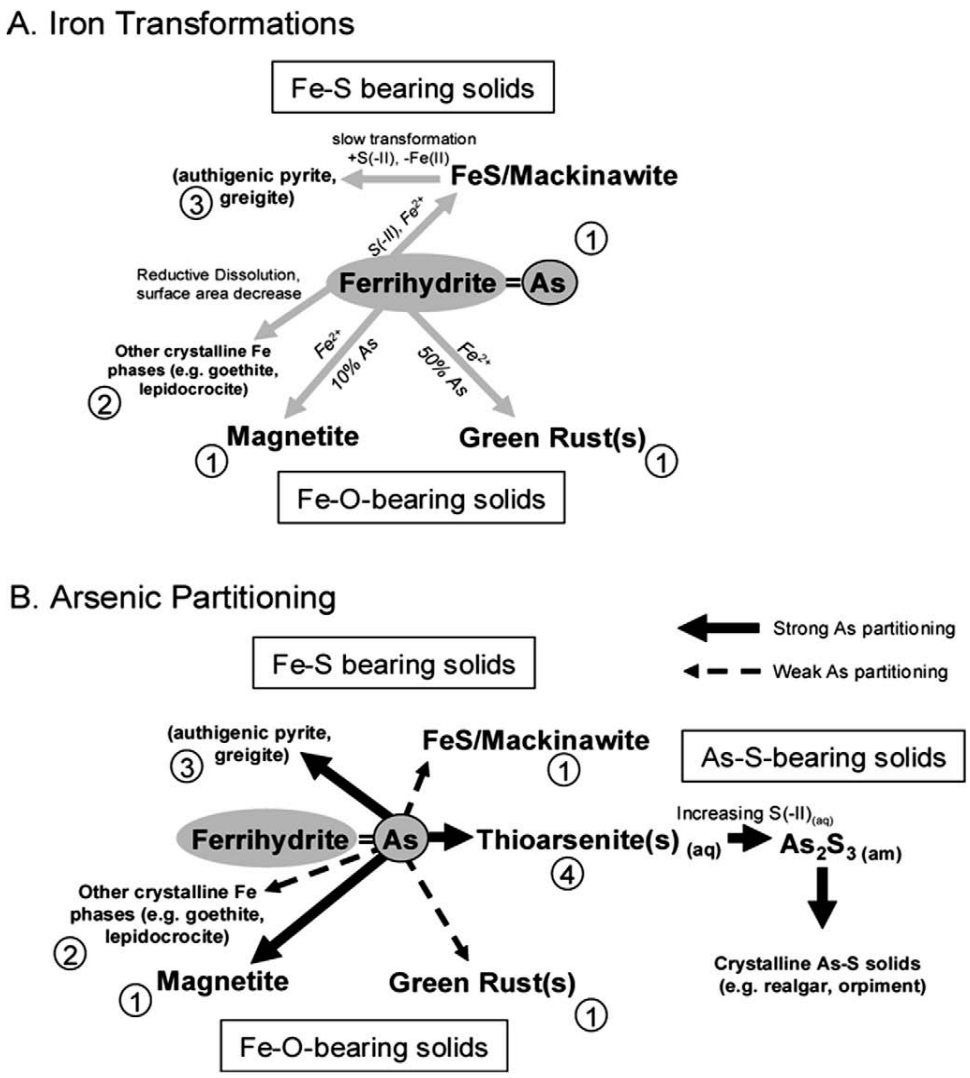

Figure 1.3. Conceptual diagram for transformations of arsenic-bearing ferrihydrite and resulting arsenic partitioning among secondary mineralization products under reducing conditions (Source: Kocar et al. 2010)

(1) Arsenic partitions strongly with and residual ferrihydrite, but appreciably less with FeS or green rust(s). Transformations from ferrihydrite to magnetite and green rust(s) are mediated by Fe^{2+}, which is produced during S(-II)(aq) reaction with Fe(III)(s) (Kocar et al. 2010). (2) Arsenic is released from ferrihydrite during reductive dissolution and

transformation to other crystalline phases, such as lepidocrocite (Pedersen et al. 2007). (3) Arsenic partitions strongly with authigenic greigite and pyrite (Wilkin and Ford 2006; Lowers et al. 2007), which form under long-term diagenesis. Arsenic may also associate with mackinawite when co-precipitated in solution at high As concentrations (Farquhar 2002), but is weakly associated with amorphous FeS at low concentrations (Bostick and Fendorf 2003). (4) In the presence of excess S(-II)(aq), As(III) may form soluble As–S (thioarsenite) complexes (Bostick et al. 2005; Wilkin 2003). With increasing S(-II)(aq), As precipitates to form amorphous As_2S_3, or other crystalline As–S phases.

Table 1.1. Arsenic treatment technologies in drinking water

Treatment technology	Description	Advantages	Disadvantages
Precipitation/ Coprecipitation	This technique involves the addition of chemical coagulants or precipitant and pH adjustment to precipitate a solid matrix, which traps the dissolved, colloidal or suspended contaminants. The solids are then removed by sedimentation or filtration. Arsenic is most commonly coprecipitated with ferric and aluminum hydroxides.	• Can be used to treat a wide range of contaminants and water characteristic such as heavy metals and hardness. • Treatment effectiveness is not significantly affected by the presence of other contaminants.	• Needs skilled labor and hence cost-effective only for large-scale treatment systems.
Adsorption	Arsenic contaminated water is passed through a fixed bed packed with media with high adsorption capacity for arsenic. Examples of adsorption media commonly used include activated carbon, activated alumina and granular ferric hydroxide.	• Less complex and needs less skilled labor than precipitation/ coprecipitation. Ideal for use in smaller treatment systems.	• Presence of other contaminants or anions (e.g.; phosphate, carbonate, organic matter) can significantly affect removal efficiency. • The adsorption media has to be regenerated periodically.
Membrane filtration	Arsenic is removed by passing the water through a semi-permeable membrane which traps the arsenic. Depending on the pore size of the membrane, dissolved arsenic or particulates containing arsenic can be	• Can remove a wide range of contaminants. • Do not require chemical addition for separation.	• Presence of organics causes membrane fouling. • Expensive and generates more residual than other technologies.

	removed. Includes microfiltration, ultrafiltration, nanofiltration and reverse osmosis.		
Ion exchange	Ion exchange involves exchanging ions held electrostatically on a solid surface for ions of similar charge in solution (the contaminant). Strong base anion exchange resins are used for the treatment of arsenic contaminated waters because they are effective over a broad pH range.	• Well defined medium and capacities. • Fairly pH independent.	• High cost associated with media and operation. • Other ions such as sulfate and nitrate have higher adsorption affinity for most strong base anion resins and compete with arsenic for iron exchange sites. This reduces efficiency of removal and increases the frequency of media regeneration. • Chloride exchange resins add chloride to the water making it corrosive and also decrease pH of the water.

Table 1.2. Composition of landfill leachate (Source: Kjeldsen et al. 2002)

Parameter	**Range**
pH	4.5-9
Specific conductivity (μScm^{-1})	2500-35000
TOC (mg/L)	30-29000
Total Phosphorous (mg/L)	0.1-23
Chloride (mg/L)	150-4500
Sulphate (mg/L)	8-7750
Bicarbonate (mg/L)	610-7320
Iron (mg/L)	3-5500
Manganese (mg/L)	0.03-1400
Silica (mg/L)	4-70
Arsenic (mg/L)	0.01-1

Table 1.3. Arsenic Retention Capacities of Selected Iron Minerals (Source: Alday 2010)

Mineral	Specific Surface Area ($m^2 g^{-1}$)	Arsenate adsorption capacity ($\mu molg^{-1}$)	Arsenate adsorption capacity (mol As /mol Fe)	Arsenite adsorption capacity ($\mu molg^{-1}$)	Arsenite adsorption capacity (mol As /mol Fe)
Ferrihydrite	600[a]	2246[b]	0.24	2901[b]	0.31
Goethite	54[b]	173[b]	0.016	173[b]	0.016
Magnetite	90[b]	-	-	332[b]	0.025
Siderite	1.58[c]	5.15[d]	0.0006	6.11[d]	0.00071
Vivianite	0.21[e]	-	-	-	-

[a] Roden and Zachara, 1996

[b] Dixit and Hering, 2003

[c] McCormick et al., 2002

[d] Guo et al., 2007

[e] Thinnappan et al. 2008

CHAPTER 2: UNDERSTANDING ABIOTIC FERRIHYDRITE REMINERALIZATION BY FERROUS IONS

M.Raghav[1], A.E.Sáez[2], and W.P.Ela[2,*]

[1] Graduate Research Assistant, Dept. of Chemical and Environmental Engineering, The Univ. of Arizona, Tucson, AZ 85721.

[2] Professor, Dept. of Chemical and Environmental Engineering, The Univ. of Arizona, Tucson, AZ 85721.

[*] Corresponding author. Tel.: (520) 626-9323; fax: (520) 621-6048; email address: wela@email.arizona.edu

ABSTRACT

In this work, we study the abiotic remineralization of ferrihydrite under reducing conditions, obtained by adding zero-valent iron (ZVI) to a suspension of ferrihydrite particles. Under similar conditions, the ferrihydrite-ZVI system proceeded along two different transformation pathways differentiated by whether a magnetic stirrer or an overhead stirrer was used for mixing. XRD characterization of the solid products showed that magnetite was the sole product of ferrihydrite transformation when a magnetic stirrer was used, whereas both goethite and magnetite were formed when an overhead stirrer was used. The two systems also behaved differently in terms of transformation kinetics and amount of magnetite formed. The quantification of magnetite generated was performed using a procedure developed in this study. The role of four mechanisms was investigated to explain the differences observed between the two systems, namely - (i)

presence/absence of high local Fe(II) concentrations, (ii) mechanical abrasion, (iii) presence/absence of a magnetic field, and (iv) presence/absence of a crystalline ZVI surface. Ferrous ions are expected to be concentrated near the magnetic bead on the magnetic stirrer as opposed to a more dispersed distribution on the overhead stirrer. This mechanistic study concluded that the presence of high local Fe(II) concentrations in the ferrihydrite-ZVI system leads to magnetite formation and the absence of the same leads to mixed goethite/magnetite or magnetite-free systems. These findings have significant implications for the mobilization of arsenic from solids as the conditions move from oxidizing to reducing, such as often occurs in engineered landfills and natural carbon-rich sediments.

KEYWORDS: Arsenic; Iron-compounds; Phase transformation; Water treatment; Landfills

1. Introduction

Under oxidizing conditions iron (III) (hydr)oxide minerals play a key role in the solid sequestration of contaminants such as arsenic in the natural environment as well as in treatment systems for removing arsenic from water (Benner et al. 2002; Smedley and Kinniburgh 2002; Vircikova et al. 1995). It is also well established that the iron (III)(hydr)oxide system is redox sensitive; one iron oxide transforming into another depending on various conditions such as pH, temperature, presence of ferrous ions and anions like chloride and sulfate (Liu et al. 2005a; Liu et al. 2005c; Liu et al. 2008a; Pedersen et al. 2005; Yee et al. 2006; Hansel et al. 2005; Mukiibi et al. 2008). In natural and engineered environments, reductive dissolution of the ferric minerals is commonly cited as a primary mechanism causing arsenic mobilization (Kocar et al. 2006; Pedersen et al. 2006; Hansel et al. 2005; Ghosh et al. 2006a). However, the degree of iron mobilization often does not correlate well with the degree of arsenic release (Islam et al. 2004; Horneman et al. 2004; Burnol et al. 2007; van Geen et al. 2006; Kocar et al. 2006; Ghosh et al. 2006a). This decoupling of iron and arsenic release into the aqueous phase has been linked to the formation of secondary iron minerals with reduced arsenic adsorption capacity (Pedersen et al. 2006; Kocar et al. 2006; Tufano and Fendorf 2008; O'Day et al. 2004). For instance, typical specific surface area of ferrihydrite (600 m^2 g^{-1}) is higher than that of its transformation products, goethite and magnetite (54 m^2 g^{-1} and

90 m^2 g^{-1}, respectively) (Dixit and Hering 2003). Maximum sorbed concentrations of arsenite at pH 8 on goethite and magnetite are much lower (173 ± 13 µmol g^{-1} and 332 ± 30 µmol g^{-1}, respectively) than on ferrihydrite (3514 ± 157 µmol g^{-1}) (Dixit and Hering 2003). On the other hand, Mamindy-Pajany et al. (2011) reported adsorption capacities of 1.4 µmol m^{-2} and 5.4 µmol m^{-2} for As (V) on commercial goethite (11.61 ± 0.19 m^2/g) and magnetite (1.60 ± 0.01 m^2/g), respectively. It is therefore important to understand the mineralogical transformations that iron (III) (hydr)oxides undergo to ascertain the degree to which these transformations will subsequently impact the sequestration of the arsenic.

Magnetite (Fe_3O_4) is commonly observed to form from iron (III) (hydr)oxide minerals, such as commercial arsenic water treatment sorbents in the presence of iron-reducing bacteria, when conditions transition from aerobic to anoxic (Benner et al. 2002; Liu et al. 2008b). As a mixed-valent iron oxide, magnetite is an intermediate phase between the aerobically stable Fe(III) (hydr)oxides and the anaerobically stable Fe(II) sulfides and oxides/hydroxides. Goethite is a crystalline Fe(III) oxy-hydroxide that is known to form as a transformation product of ferrihydrite (Cornell and Schwertmann 2003). Several studies have shown that the presence of ferrous ions catalyzes this transformation (Benner et al. 2002; Pedersen et al. 2005; Hansel et al. 2003; Hansel et al. 2005).

Physical heterogeneity within soils is known to give rise to localized biogeochemical gradients due to the presence of both advection (in large pores) and diffusion (in smaller micropores) dominated domains (Bai and Roegiers 1997; Tokunaga et al. 2003; Tufano et al. 2009; Pallud et al. 2010). The localized build-up of Fe(II) due to Fe(III) reduction is

hence common in heterogeneous systems such as landfills. Aqueous Fe(II) concentration is an important parameter influencing the transformation of ferrihydrite to secondary Fe minerals and hence sequestration and release of contaminants like arsenic (Benner et al. 2002; Pedersen et al. 2005; Hansel et al. 2003; Hansel et al. 2005).

The objective of this paper was (i) to understand the different transformation pathways/products of ferrihydrite under the presence or absence of locally high Fe(II) concentrations, and (ii) to gain insights into the implications of such transformations for the sequestration/release of arsenic associated with iron based water treatment residuals under landfill conditions. It should be mentioned that the goal here was not to develop a remedial process for the stabilization of arsenic in the water treatment residuals, but to interrogate the factors causing an iron-rich oxic system to generate different secondary minerals when it transitions into a reducing system and, consequently, have greater or lesser arsenic retention capacity.

2. Materials and Methods

2.1. Preparation of Synthetic Ferrihydrite

Synthetic ferrihydrite was prepared based on a modified procedure for ferrihydrite synthesis reported by Mukiibi et al. (2008). 1 L of 1 M anhydrous ferric chloride solution was titrated with 10 M NaOH to a pH of 7.0 within 1 hour. The pH was brought up to 7 to mimic the arsenic removal process using coagulation and adsorption on ferric hydroxide in water treatment facilities. It has been reported that best arsenic removal is

achieved at pH values less than 7.2-7.5 (Jekel and Amy 2006). The suspension was allowed to settle and equilibrate for 48 hours, until the pH stabilized at 7.0. The pH fluctuated by ± 0.3 during this period and was adjusted back to 7 as necessary using 0.1 M HCl or 0.1 M NaOH. The pH of the suspension was monitored for 48 hours to ensure that the pH had stabilized at 7.0. The precipitate was then vacuum filtered using 0.22 μm membrane filters to achieve a water content of approximately 75% wt and rinsed multiple times with deionized water to remove residual salts. The whole procedure was carried out at room temperature. The solid was transferred to HDPE storage jars, sealed tightly using parafilm, and stored at 4°C for later use.

Synthetic arsenic-bearing solid residuals (ABSRs) were also produced to study the effect of arsenic's presence on ferrihydrite transformations. The synthesis procedure used was similar to the procedure described above except that sodium arsenate solution was added to the Fe(III) solution before the pH was brought up to 7. Three different solids with Fe/As molar ratio of 5.7, 20 and 100 were synthesized.

The total iron and arsenic content of the synthesized solids was determined by microwave digestion of known amounts of the solids. Solid samples of 0.5 g (wet weight) were weighed and digested in 14.5 mL of concentrated nitric acid for 20 minutes using a CEM MDS 2100 Microwave Digestion System. Five replicates were run in each case. Digested samples were diluted and analyzed for iron content using the phenanthroline test (Clesceri et al. 1998) and for arsenic content using an Inductively Coupled Plasma Mass Spectrometer (ICPMS, Agilent 7500a).

Deoxygenated water used in this study was prepared by heating deionized water in a 2-L conical flask to 90±4 °C for 1 hour while bubbling nitrogen in the headspace. The flask was then sealed tightly, stored inside a Terra Universal Critical Environment Solutions glove box purged with nitrogen at room temperature (20-25 °C) and the water used as needed.

2.2. Experimental System

Batch experiments were conducted using the synthesized ferrihydrite and ZVI as the reducing agent. Analytical grade zero-valent iron (200 mesh, 99+% purity on metals basis) was used as purchased (Alfa Aesar). All the experiments were performed inside the glove box. The synthesized ferrihydrite solid was used to prepare a suspension containing 0.3 g of Fe (III) in 100 mL of deoxygenated water. The initial pH was 6.8±0.2 in all the experiments. The system was continuously stirred using an overhead stirrer, a magnetic stirrer or an overhead stirrer with a magnetic stir bar attached (at 300 rpm in all cases) as dictated by the specific trial objective (described later). Individual batches were sacrificed at time intervals of 16 hrs, 3 days or 10 days. In one set of trials, a measured amount of ZVI was added to the solution in order to achieve an initial 1:1 ratio of Fe^{3+}: Fe^{0} in the system. In a second set of trials, Fe^{2+} was added directly in lieu of ZVI. In these cases, 0.3 g of the ferrihydrite solid as Fe^{3+} was added to 20 mL of deoxygenized water and homogenized on a magnetic stir plate for half an hour before addition of the Fe^{2+}. The initial pH of this solution was 6.8±0.2, similar to the experiments conducted with ZVI.

Trials using direct injection of Fe^{2+} (added as ferrous sulfate) used one of two rates for addition – a fast rate of 30.6 mg of Fe^{2+}/hr for 5 hours to mimic the fastest rate of Fe^{2+} generation observed in the experiments with ZVI, and a slower rate of 3.1 mg of Fe^{2+}/hr for 4 days to mimic the average slow rate of Fe^{2+} generation observed in the experiments with ZVI (see Results and Discussion). Ferrous sulfate solutions of concentrations 0.0342 M and 0.0670 M were used for the fast and slow rate experiments, respectively, in order to bring the final volume of the batch to 100 mL. In the case of the experiments with the fast rate of Fe^{2+} addition, the pH was maintained at 6.8 ± 0.2 by adding 0.3 M NaOH, as needed. This was done to mimic pH trends in the system employing the magnetic stirrer with ZVI added as the source of Fe^{2+}, where the pH was nearly constant at 6.8 (results not shown). In case of the experiments with slow rate of Fe^{2+} addition, no pH adjustment was made and the pH was observed to decrease to 4.2 and rise up to ≈ 5.8 at the end of 4 days. This was done to mimic pH trends in the system employing the overhead stirrer with ZVI added as the source of Fe^{2+} (results not shown).

Experiments were also conducted with arsenic added in order to study the effect of arsenic on ferrihydrite transformations in the presence of high local Fe(II) concentrations. Transformations of the three iron-arsenic solids (Fe/As molar ratio =5.7, 20 and 100) were studied by performing experiments analogous to the ones performed with the ferrihydrite solid, at an initial pH of 6.8±0.2 and initial Fe^{3+}: ZVI ratio of 1:1.

2.3. Solids Characterization

Solid samples for X-ray diffraction (XRD) were collected by filtering approximately 100 mL of solution through a 0.22 μm filter and rinsing the solid on the filter multiple times with deoxygenated water. The solids were then dried inside the glove box purged with nitrogen. All the steps were carried out inside the glove box and the dried solids were collected in tightly sealed vials and stored inside the glove box until taken out for solid characterization.

The crystalline phases in the bulk samples were identified using XRD patterns collected on a Bruker D8 ADVANCE diffractometer using Cu$K\alpha$ radiation. The samples were scanned from 5° to 90° for over 285 minutes and diffraction patterns were recorded. Patterns were matched against those in the International Centre for Diffraction Data (ICDD) database.

2.4. ZVI-Magnetite Quantification

A method was developed as part of this study for the quantitative analysis of magnetite generated and ZVI remaining in the system at the end of each experiment. This method is somewhat analogous to that used for the determination of chemical oxygen demand (COD).

Step 1: Dissolution of magnetite and zero-valent iron by concentrated sulfuric acid

A weighed mass of the magnetic fraction (residual ZVI and magnetite) collected at the end of an experiment was added to 100 mL of deoxygenated water in an Erlenmeyer

flask. The flask's top was connected to a vertical glass column containing water; 200 mL of 9 M sulfuric acid were added to the solution and allowed to react for 45 minutes. During preliminary method development trials, this was determined to be sufficient time to dissolve all the solids for the maximum total weight of solids expected if all the ferrihydrite transformed to magnetite. By measuring the displacement of the water level in the glass column, the volume of hydrogen generated in the reaction was determined.

Step 2: Oxidation of reduced iron in solution by potassium dichromate

After 45 minutes, an excess (2 times of stoichiometric demand, assuming all the remaining solid was ZVI) of potassium dichromate was added to oxidize all the reduced iron in the system. After 20 minutes, a 2 mL aqueous sample was taken. The aqueous sample was diluted immediately and analyzed for total iron.

Step 3: Addition of ferrous sulfate to reduce the residual potassium dichromate

Following step 2, excess ferrous sulfate was added to the solution. A 2 mL aqueous sample was taken after 1 hr, diluted and analyzed for Fe (II) concentrations using the phenanthroline method.

The amount of ferrous sulfate oxidized by potassium dichromate allowed for the determination of the amount of potassium dichromate consumed in step 1 to oxidize all the reduced iron in magnetite and ZVI.

The moles of electrons that must be withdrawn to fully oxidize all reduced iron in the system ($TOTe^-$) and the total number of moles of iron (TOTFe) from both magnetite and ZVI are given by

$$N_m + 3N_z = TOTe^- \quad \text{Eq. (1)}$$

$$3N_m + N_z = TOTFe \quad \text{Eq. (2)}$$

where N_m and N_z are the number of moles of magnetite and ZVI, respectively.

$TOTe^-$ is calculated as the number of electrons transferred from dichromate to oxidize all the remaining reduced iron to Fe^{3+} and generate hydrogen by the reaction of the zero-valent iron with sulfuric acid (procedure detailed below),

$$2Fe^0 + Cr_2O_7^{2-} + 14H^+ \rightarrow 2Fe^{3+} + 2Cr^{3+} + 7H_2O \quad \text{Eq. (3)}$$

$$6Fe^{2+} + Cr_2O_7^{2-} + 14H^+ \rightarrow 6Fe^{3+} + 2Cr^{3+} + 7H_2O \quad \text{Eq. (4)}$$

$$2Fe^0 + 6H^+ \rightarrow 2Fe^{3+} + 3H_2 \quad \text{Eq. (5)}$$

Ferrihydrite is not detected by XRD owing to its amorphous nature, so in all trials the possibility existed that some untransformed ferrihydrite could remain at the end of the experiment. Both magnetite and ZVI were separated from any non-magnetic solid species by collection on a Teflon-coated magnetic bead. The process was repeated using a fresh magnetic bead to confirm that the magnetic fraction remaining in the suspension after this point was insignificant. A similar technique for separation and recovery of magnetic

minerals has been employed by Horneman et al. (2004). The magnetic bead with the magnetite and ZVI was recovered and directly used in the ZVI-magnetite quantification procedure.

For validation purposes, known amounts of magnetite and ZVI were mixed and analyzed using the procedure described above. Magnetite was synthesized based on the standard procedure in Schwertmann and Cornell (1991) via partial oxidation of ferrous chloride solution. The magnetite thus synthesized and pure ZVI were mixed at different ratios (Magnetite/Total weight = 0 to 1) with at least 3 replicates of each ratio.

A student's t-test was performed on the data set and the results were found to be statistically significant at the 95% confidence interval (not shown here).

3. Results and Discussion

Baseline experiments to characterize ferrihydrite transformation products were conducted using a magnetic stirrer or an overhead stirrer with ZVI addition, keeping all other conditions constant. Solid samples collected after 10 days from the magnetic stirrer were black in color for the magnetic stirrer system (indicative of magnetite), and from the overhead stirrer system they were yellowish green (indicative of goethite and/or green rust). The XRD spectra of solids from the magnetic stirrer system (Fig. 1) showed that magnetite and residual ZVI were the only crystalline phases. Magnetic fraction separation showed that the non-magnetic fraction remaining in the solid was insignificant. In the overhead stirrer system, the product consisted of a mixture of goethite, magnetite and residual ZVI (Fig. 2).

Four possible mechanisms were considered to explain the different transformation products observed in the magnetic and overhead stirrer trials – (i) Fe^{2+} concentration levels near the solid surface, (ii) abrasion and grinding, (iii) presence or absence of a magnetic field, and (iv) presence or absence of a ZVI surface. Initially, ZVI oxidation is the only source of Fe^{2+} in both the systems. However, Fe^{2+} generation is locally concentrated on the stir bar to which ZVI particles adhere in the magnetic stirrer case, as opposed to the overhead stirrer case where the Fe^{2+} generation is distributed throughout the reactor volume since ZVI particles are completely dispersed. In what follows, we analyze possible effects of each mechanism.

The role of Fe^{2+} as a catalyst in accelerating the transformation of ferrihydrite to various iron-oxide minerals including goethite and magnetite has been discussed extensively in the literature (Benner et al. 2002; Pedersen et al. 2005; Hansel et al. 2003; Hansel et al. 2005). Pedersen et al. concluded that iron (III) (hydr)oxides undergo phase transition to more stable phases due to the catalytic action of Fe (II) adsorbed on the surface. They explained that the adsorbed Fe (II) exchanged for Fe (III) in terminal octahedral positions. The Fe (II)-O bond being more labile than the Fe (III)-O bond caused the crystal structure to disintegrate resulting in the dissolution of ferrihydrite followed by re-precipitation of more stable phases like goethite by Ostwald ripening.

On the other hand, Fe (II) sorption also drives solid-state conversion of ferrihydrite to magnetite (Cornell 1988; Tronc et al. 1992). In column experiments using ferrihydrite-coated sands, a direct correlation has been observed between Fe (II) concentrations and

the solid phases present, both temporally and spatially (Hansel et al. 2003; Benner et al. 2002). Hansel et al. (2003) demonstrated that both the Fe^{2+} generation rate and flow-induced Fe^{2+} concentration profiles play an important role in determining the transformation products of ferrihydrite. Goethite precipitated at the influent end of the column where Fe^{2+} concentrations were low, whereas magnetite formed under the presence of the high Fe^{2+} concentrations present near the effluent end of the column.

In another study by Tufano et al. (2009), it was established that gradients in Fe^{2+} concentrations in diffusion-controlled systems might result in spatial patterns that lead to varied secondary mineral formation. In their experiments, magnetite and green rust formed at the inlet of a pore where the Fe^{2+} concentrations were high. At increasing distances from the pore entrance where lower Fe^{2+} concentrations exist, goethite was the predominant phase.

In our system when the magnetic stir plate is used, high local Fe^{2+} concentrations exist near the magnetic bead due to the accumulation of ZVI particles in that region. This is in contrast to the more dispersed generation of Fe^{2+} in the case of the overhead stirrer. Hence, the ferrihydrite in the magnetically stirred system is exposed to high concentrations of Fe^{2+} and transformation to magnetite is favored over dissolution-reprecipitation of ferrihydrite to goethite.

These results are consistent with those found by Yang et al. (2010) in a recent study of the kinetics of Fe (II)-catalyzed transformation of 6-line ferrihydrite under anaerobic flow conditions. They reported that at a concentration of 0.36 mM Fe^{2+}, goethite was the major

phase formed as a result of ferrihydrite transformation, with minor amounts of magnetite being detected. At higher concentrations of 1.8 mM and 18 mM Fe^{2+}, magnetite was the only secondary phase that formed. This was described as being due to the presence of higher electron current density when high Fe^{2+} concentrations were present, which allows for rapid internal structural rearrangement of the ferrihydrite particles to form magnetite nuclei. In the case of low Fe^{2+} concentrations, the electron current density is low, which results in a slower rearrangement of ferrihydrite particles allowing for dissolution of ferrihydrite and re-precipitation as goethite.

Our results show that once goethite started forming on the overhead stirrer, magnetite generation was inhibited. This is evident from comparison of the amount of magnetite generated at 16 hr, 2 days and 4 days (Fig. 3). Magnetite inhibition was explained by Tufano et al. (2009) as being due to the removal of tetrahedral Fe (III) centers in ferrihydrite that are presumed to be necessary for the Fe (II)-induced nucleation of magnetite. Magnetite has an inverse spinel structure with Fe (II) atoms in the octahedral positions and Fe (III) atoms both at the tetrahedral and octahedral positions (Cornell and Schwertmann 2003). Hence, tetrahedral Fe (III) centers in ferrihydrite could help lower the free energy required for magnetite nucleation in the presence of Fe (II). But the presence of tetrahedral Fe(III) in ferrihydrite is still an unresolved issue, with more evidence mounting against it (Rancourt and Meunier, 2008, Manceau 2009, Manceau 2011, Manceau 2012). Hence, the reason for the observed inhibition of magnetite generation in our study once goethite formation started is still unclear.

The relative amounts of ZVI and magnetite in experiments on both the magnetic and overhead stirrer in our study were determined using the ZVI-magnetite quantification technique described in the Materials and Methods section. In the magnetically stirred system, the possibility of any untransformed ferrihydrite remaining in the system was ruled out by using a magnetic bead to separate the magnetic and non-magnetic fractions. After separation, there was no residual non-magnetic fraction remaining. In the case of the overhead stirrer, the non-magnetic fraction was significant. The objective behind quantifying the amounts of magnetite and ZVI was to elucidate the relative importance of the different operative mechanisms. In other words, it was to quantitatively demonstrate the differences between the amount of magnetite formed and the amount of ZVI consumed in the two systems employing the overhead and magnetic stirrer.

In order to test the hypothesis that high local Fe^{2+} concentrations were responsible for the differences in the transformation products in the two systems, experiments were performed in the overhead stirrer system as well as the magnetic stirrer system by adding a ferrous sulfate solution directly, instead of using ZVI as a source of Fe^{2+}. In these trials, the objective was to approximate the Fe^{2+} generation rates observed in the magnetic and overhead stirrer systems when ZVI was used as the Fe^{2+} source, but to do so without ZVI present (and hence determine if the presence of ZVI solid, per se, was a significant factor). The rates of Fe^{2+} generation in the two systems were calculated from the rates of ZVI consumption. These were in turn estimated by using the ZVI-magnetite quantification procedure (described above) to determine the amount of ZVI consumed over different time periods. It was determined that 0.15 g of Fe^{2+} were generated in the

magnetic stirrer system in 5 hours, and from the XRD spectra and ZVI-magnetite quantification, it was confirmed that all the ferrihydrite solid was transformed into magnetite within this period. Similarly, it was determined that 0.3 g of Fe^{2+} were generated in the overhead stirrer system in 4 days, while the ferrihydrite started transforming into both magnetite and goethite.

A syringe pump was used to supply Fe^{2+} at two different rates – a faster rate (30.6 mg of Fe^{2+}/hr for 5 hr) to mimic Fe^{2+} generation from ZVI on the magnetic stirrer, and a slower rate (3.1 mg of Fe^{2+}/hr for 4 days) to mimic that on the overhead stirrer. Experiments at both rates were performed in the magnetic stirrer system as well as in the overhead stirrer system.

XRD analysis of the products (Fig. 4) showed that the faster inflow rate of Fe^{2+} yielded magnetite in both systems, whereas the experiments with the slower inflow rate of Fe^{2+} resulted in no transformation of ferrihydrite to goethite or magnetite (no crystalline solid products were detected by XRD) in either system. In one replicate experiment with the magnetic stirrer and the slow Fe^{2+} supply rate, weak peaks for goethite were detected, indicating that small amounts of goethite were being formed. It is not clear why no ferrihydrite transformation to goethite was observed within 4 days as had been observed on the overhead stirrer when ZVI was used as the source of Fe^{2+}.

One explanation could be that the estimates for Fe^{2+} inflow rate were based on the amount of ZVI consumed in 4 days on the overhead stirrer assuming a linear rate for Fe^{2+} generation over this period. This is a likely simplification of the actual Fe^{2+} generation

rate on the overhead stirrer throughout the reaction time, as the rate was more likely faster during the initial stages of the experiment and slowed down once magnetite and goethite generation began, due to passivation of the ZVI surface. A detailed kinetic study of the rate of Fe^{2+} generation from ZVI was not the focus of this study and hence was not undertaken to test the degree to which the rate was non-linear. Nevertheless, these experiments do prove that at a faster inflow rate of Fe^{2+} and consequently higher Fe^{2+} concentrations, magnetite is the only product formed, irrespective of whether the overhead stirrer or the magnetic stir plate was used, thus also negating the presence/absence of a magnetic field being a significant determinant.

In the case of the magnetically stirred system, mechanical abrasion/ grinding of the ZVI particles between the magnetic bead surface and the vessel bottom could help keep the ZVI surface clean, hence maintaining its surface reactivity, and leading to a relatively high rate of Fe^{2+} generation. An experiment was set up in the overhead stirrer system with a magnetic bead attached to the propeller shaft of the stirrer to examine the importance of this mechanism in explaining the observed phenomena. This was expected to create localized high Fe (II) concentrations while excluding any abrasion effects. Individual batch trials were set up and once again sacrificed after 16 hrs, 3 days and 10 days. The XRD spectra of the 10-day long experiment is shown in Fig. 5.

It is clear that the products after 10 days in the overhead stirrer system with a magnetic bead attached to the propeller are goethite and magnetite, which replicates results without the magnetic bead attached to the propeller. This was contrary to our expectation, which

assumed high local Fe^{2+} concentrations would be present at the magnetic surface and that magnetite would be the only product. It was confirmed that all the ZVI particles stay on the bead and do not shear off during mixing by the overhead stirrer, via visual observation in a system where zero-valent iron was added in the absence of ferrihydrite. An explanation for this unexpected result could be that when ZVI is used as a source of Fe^{2+} the creation of high local Fe^{2+} concentrations depended on the presence of abrasion to maintain the surface reactivity of the zero-valent iron surface.

Mechanical abrasion may thus play an indirect role in pre-disposing the ferrihydrite-ZVI system to form magnetite by allowing the creation of high local Fe^{2+} concentrations. To confirm this, we compared the amount of ZVI remaining after different time-periods on the magnetic stir plate, overhead stirrer and the overhead stirrer with the magnetic bead attached to the propeller (Fig. 6). We observed rapid consumption of ZVI on the magnetic stirrer initially and then the amount of ZVI stayed constant in the system.

In contrast, the ZVI consumption rate is much slower in the case of the overhead stirrer both with and without the magnetic bead attached to the propeller. We also observed that ZVI consumption continues for 4 days of the experiment, whereas in the case of the magnetic stirrer, the ZVI consumption stopped after 5 hrs. The initial rapid consumption of the ZVI on the magnetic stir plate is consistent with mechanical abrasion maintaining the surface reactivity of ZVI in this system.

An experiment was conducted to test the possibility that the presence of a magnetic field predisposes the ferrihydrite towards transforming to magnetite. A magnetic stir plate was

placed underneath the beaker containing the same amounts of ferrihydrite and zero-valent iron as described earlier. The magnetic stir plate was kept turned on but at zero rpm so that there was no motion/abrasion of the zero-valent particles while still ensuring the presence of a magnetic field. An overhead stirrer (at 300 rpm) was used to mix the suspension. All other initial parameters were maintained the same as described previously. Upon separating out the magnetic fraction and performing the ZVI-magnetite quantification procedure, the amount of magnetite formed in this system (not shown) was found to be insignificant compared to that formed on the magnetic stir plate. Hence, the presence of a magnetic field was eliminated as an important mechanism in the context of the objectives of this study. It should be noted that it was not the authors' objective to gain quantitative insights into effects of the intensity of the magnetic field on ferrihydrite transformation pathways/products but rather to test whether the magnetic field generated by the magnetic stirrer may lead the ferrihydrite-ZVI system towards the observed transformation pathways/products.

Another factor considered was whether the presence of nucleation sites (in this case the ZVI particles) co-located with the high Fe^{2+} concentrations, was necessary for magnetite formation. The zero-valent iron particles would act not only as a source of ferrous ions but also as potential nucleation sites for the formation of magnetite particles. Since ZVI is the main source of Fe^{2+} in our experiments – it was difficult to unequivocally delineate surface effects from Fe^{2+} concentration effects. However, from the experiments with direct Fe^{2+} addition it is evident that when high Fe^{2+} concentrations are present, a

crystalline surface (i.e., ZVI particles) is not required in order to dispose the system to form magnetite.

Other researchers have observed the transformation of ferrihydrite to magnetite due to the presence of high local concentrations of an electron donor. Burton et al. (2011) observed the transformation of As (III)-bearing ferrihydrite-coated quartz sand to mackinawite, magnetite and goethite after 28 days of advective-flow column experiments. The columns were inoculated with *Desulfovibrio vulgaris,* a sulfate-reducer. It was observed that magnetite formation was dominant near the influent end of the columns where intense sulfidogenesis was happening. This was explained as being due to the presence of high sulfide concentrations locally near the inflow end of the column resulting in high electron current density needed for the solid-state transformation of ferrihydrite to magnetite. We think that in our study, the high local concentrations of Fe (II) that would be generated due to the localization of the electron donor (zero-valent iron in this case) on the magnetic bead in the magnetically stirred system resulted in the transformation of ferrihydrite to magnetite.

Experiments to study the effect of arsenic's presence on the transformation of amorphous ferric hydroxide at relatively high local Fe^{2+} concentrations were performed only in the magnetic stirrer system since the objective was to see if the presence of arsenic inhibited the ferrihydrite transformation to magnetite. The XRD spectra (Fig. 7) of final solid products from these experiments indicated that magnetite was formed in all three systems, but the peaks for magnetite were progressively weaker as the Fe/As ratio in the

original solid was decreased from Fe/As = 100 to Fe/As= 20 and Fe/As = 5.7. Only a trace amount of magnetite formed in the latter case (Fig. 7). The peaks for zero-valent iron showed the opposite trend. Despite the fact that XRD results are qualitative, the relative amplitudes of ZVI and magnetite determined from the XRD peaks are 22: 6: 1 and 1: 1: 3 written as respective fractions in experiments with Fe/As =5.7: Fe/As=20: Fe/As=100. This clearly indicates variations in the relative amounts of the two minerals.

This result is consistent with observations from other studies that found that the presence of arsenic limits the transformation of ferrihydrite to magnetite (Kocar et al. 2006; Herbel and Fendorf 2006). Kocar et al. (2006) used biotic columns loaded with As (V)-bearing ferrihydrite to study arsenic elution. Secondary mineral formation showed partial transformation of ferrihydrite to magnetite. The columns were inoculated with *Shewanella putrefaciens*, an organism capable of reducing both Fe (III) and As (V) and had arsenic loadings (Fe/As = 22 and 111) similar to the ones used in this study. The highest level of transformation to magnetite in all these columns was observed near the outlet of the columns (at around 15 cm from the inlet in a 20 cm long column). Dominant iron mineralogy from Extended X-ray Absorption Fine Spectra (EXAFS) measurements at this section of the columns in the Kocar et al. study indicated ~9 mol% magnetite after 25 days in the columns loaded with As (V)-bearing ferrihydrite, as opposed to 59 mol% magnetite after 16 days of reaction in the columns loaded with ferrihydrite but no arsenic. The level of transformation to magnetite, though much lower than that observed in similar columns without any arsenic, was still appreciable (Hansel et al. 2003). Ferrihydrite transformation to goethite was not observed in any of their columns loaded

with arsenic even though goethite was a major transformation product in similar columns with no arsenic. Pedersen et al. (2006) studied the effect of low arsenic concentrations on iron oxide transformations. They observed no inhibition of ferrihydrite transformation to goethite at low arsenic loadings (Fe/As $\geq$ 200). A flowchart summarizing the transformation products of ferrihydrite under different arsenic loadings and Fe (II) concentrations (observed in this and other studies) is shown in Fig 8.

4. Concluding Remarks

This study looked at the differences in ferrihydrite transformation pathways caused by differences in local Fe^{2+} concentration. When magnetic solids (i.e., ZVI, magnetite) are concentrated on a magnetic stir bar rather than dispersed throughout the fluid, magnetite was the sole product of the ferrihydrite/ZVI system. In contrast, both goethite and magnetite were detected when an overhead stirrer was employed for mixing. Various mechanisms were considered to explain the observed differences between the two systems - the presence or absence of localized high Fe^{2+} concentrations, mechanical abrasion/grinding effects on the ZVI particles, role of ZVI particles as nucleation sites for magnetite synthesis and the presence/absence of a magnetic field.

In the system studied, high Fe^{2+} concentrations could only be obtained if the Fe^{2+} source (ZVI) was locally concentrated (i.e., on a magnetic stir bar) and the ZVI surface was refreshed by abrasion. This study confirmed that the presence of high local Fe^{2+} concentrations caused ferrihydrite transformation to magnetite. Preliminary experiments

with ZVI and three different Fe/As ratios showed that the amount of magnetite formed decreased with increasing loading of arsenic. Lower arsenic loadings of Fe/As=100 and Fe/As=20, which are more representative of the loadings achieved in actual arsenic-bearing solid residuals generated after water-treatment, still showed significant transformation to magnetite.

These findings have implications for arsenic release in natural systems and landfills. Arsenic is ubiquitously associated with iron (hydr)oxides in natural systems and the residuals generated from arsenic removal processes in water treatments systems. Iron oxide transformations (both biotic and abiotic) have been studied and reported to have significant implications for the leachability and mobility of arsenic in natural aquatic systems and landfills (Kocar et al. 2006; Pedersen et al. 2006; Hansel et al. 2005; Ghosh et al. 2006a). The possible transformations that the iron minerals undergo may determine the ultimate stability of the associated arsenic owing to differences in their arsenic retention capacities. Spatial heterogeneity in the distribution of iron oxides, microbes and/or reducing agents in soils can result in locally high Fe^{2+} concentrations. The findings from this study show that local Fe^{2+} concentrations can pre-dispose ferrihydrite to transform into magnetite or goethite. These minerals have different sequestration capacities for arsenic due to differences in their surface areas.

Recent XAS, EXAFS and FT-IR studies have reported that arsenic sequestration in an iron oxide is due (but not limited) to the following mechanisms: co-precipitation, adsorption by the formation of surface precipitates and/or formation of inner- and outer-

sphere complexes (Manning et al. 1998; Hansel et al. 2003; Wang et al. 2008; Morin et al. 2009; Wang et al. 2011). The mode of arsenic sequestration/incorporation is different for different minerals. For instance, it has been observed that As (V) can be incorporated within the magnetite structure during co-precipitation experiments (Wang et al. 2011; Coker et al. 2006). Wang et al. (2011) demonstrated that during the Fe (II)-induced transformation of As (V)-sorbed lepidocrocite to magnetite, arsenate tetrahedra were incorporated within magnetite nanoparticles with increasing loading of arsenic. Such a trapping mechanism for arsenate has not yet been established with sufficient spectroscopic evidence in the case of goethite. The mode of association of the arsenic with an iron oxide is expected to have a significant influence on the fate and mobility of the associated arsenic. Thus, local Fe^{2+} concentrations can have significant implications for the sequestration or release of arsenic by determining the transformation products of ferrihydrite under reducing conditions.

Acknowledgements

This work was supported by the National Institute of Environmental Health Sciences (NIEHS) Grant No. P42 ES04940. The authors declare that they have no conflict of interest. This paper's contents are solely the responsibility of the authors and do not necessarily represent the official views of NIEHS. The authors wish to thank Phil Anderson of the University Spectroscopic Imaging Facility at the University of Arizona for performing the XRD analyses. The authors also wish to acknowledge the work of an undergraduate student, I-Tso Chen, who assisted with sample preparation for XRD and SEM analysis, and microwave digestions for aqueous iron analysis.

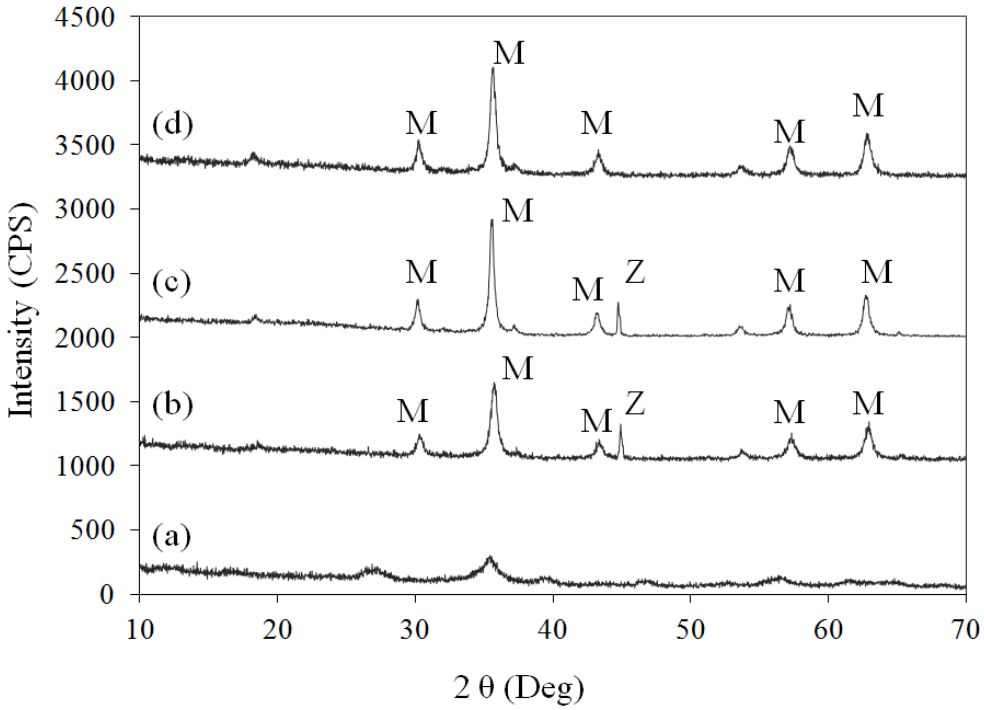

Figure 2.1. XRD spectra for product solid taken (a) initially, (b) after 5 hrs, (c) after 16 hrs, and (d) after 10 days. All experiments were performed using a magnetic stirrer with initial ferrihydrite:ZVI ratio of 1.0 and pH 6.8±0.2. M-Magnetite, Z-ZVI.

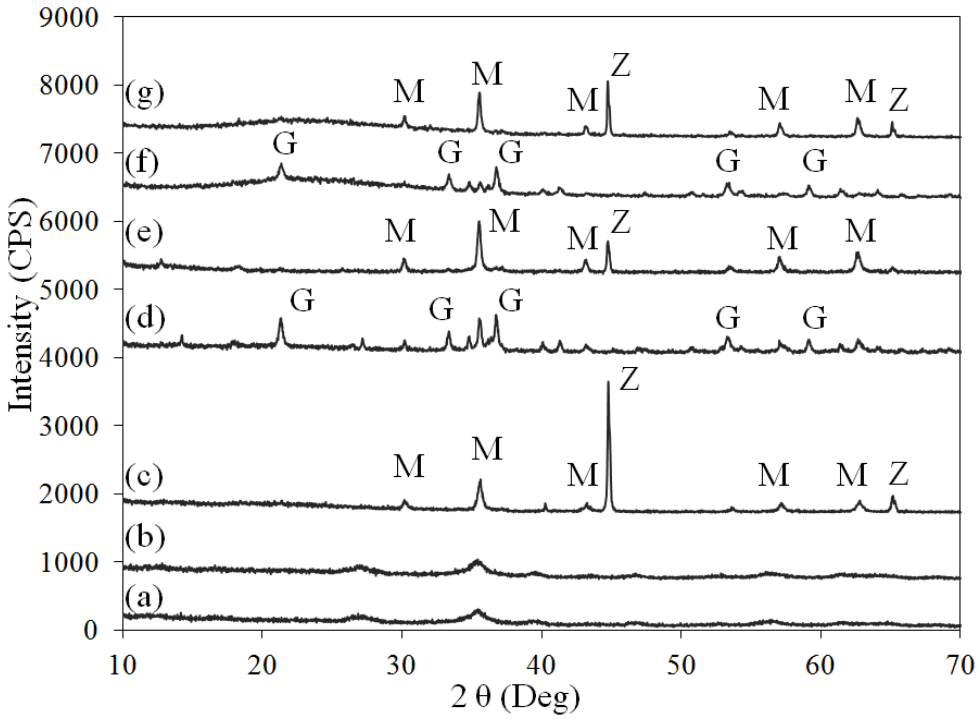

Figure 2.2. XRD spectra for product solid taken (a) initially, (b) after 16 hrs, non-magnetic fraction, (c) after 16 hrs, magnetic fraction, (d) after 3 days, non-magnetic fraction, (e) after 3 days, magnetic fraction, (f) after 10 days, non-magnetic fraction, and (g) after 10 days, magnetic fraction. All experiments were performed using an overhead stirrer with initial ferrihydrite:ZVI ratio of 1.0 and pH 6.8±0.2. M-Magnetite, Z-ZVI, G-Goethite.

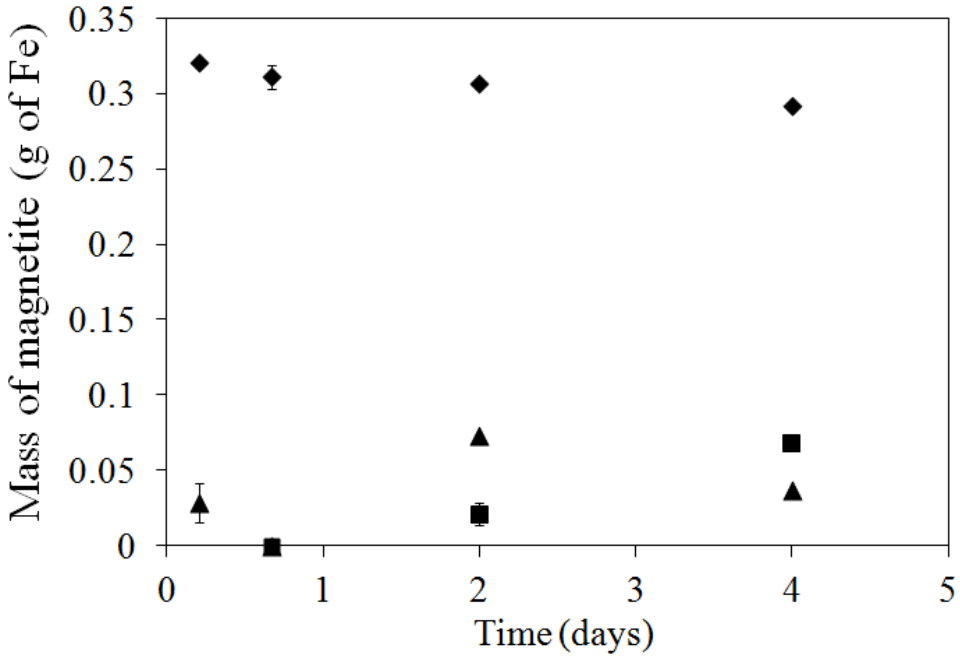

Figure 2.3. Magnetite generated as function of time using a magnetic stirrer (♦), overhead stirrer (■) and an overhead stirrer with a magnetic bead attached to the propeller shaft (▲). Conditions as in Figs. 1 and 2. The 16 hour data for the overhead stirrer and the overhead stirrer with the magnetic bead attached to the propeller shaft overlap with each other. Error bars are standard errors from three replicates and were generated for 25% of the sampled data-points chosen randomly.

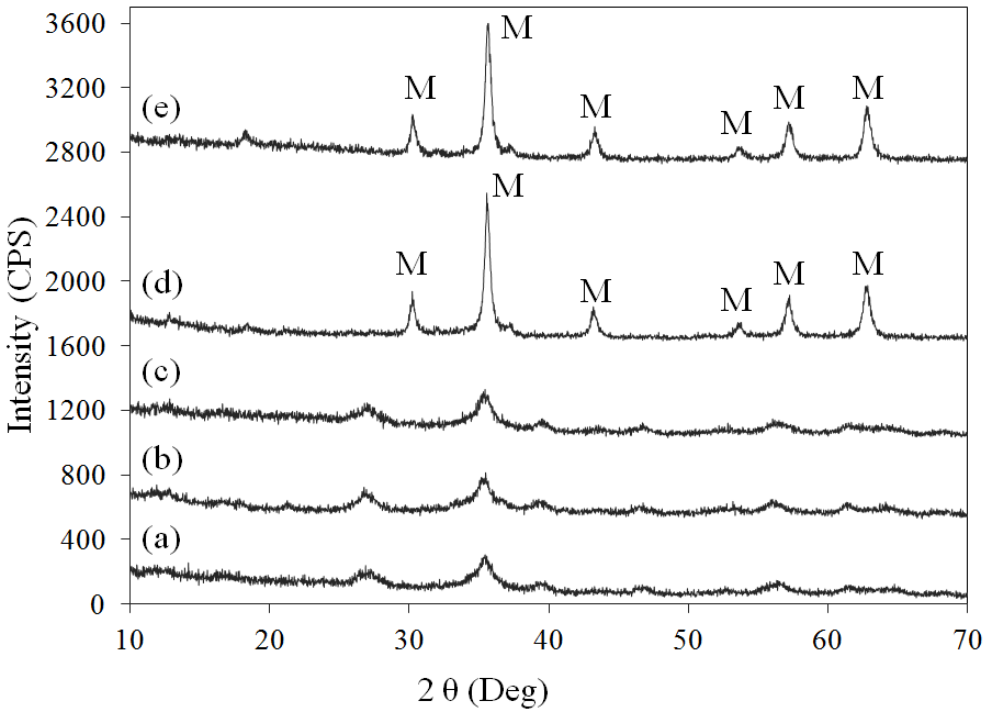

Figure 2.4. XRD spectra for initial ferrihydrite (a); solid products of ferrihydrite transformation when Fe^{2+} was added: at 3.13 mg of Fe^{2+}/hr for 4 days on the magnetic stir plate (b); at 3.13 mg of Fe^{2+}/hr for 4 days on the overhead stirrer (c); at 30.61 mg of Fe^{2+}/hr for 5 hr on the magnetic stir plate (d); and at 30.61 mg of Fe^{2+}/hr for 5 hr on the overhead stirrer (e).

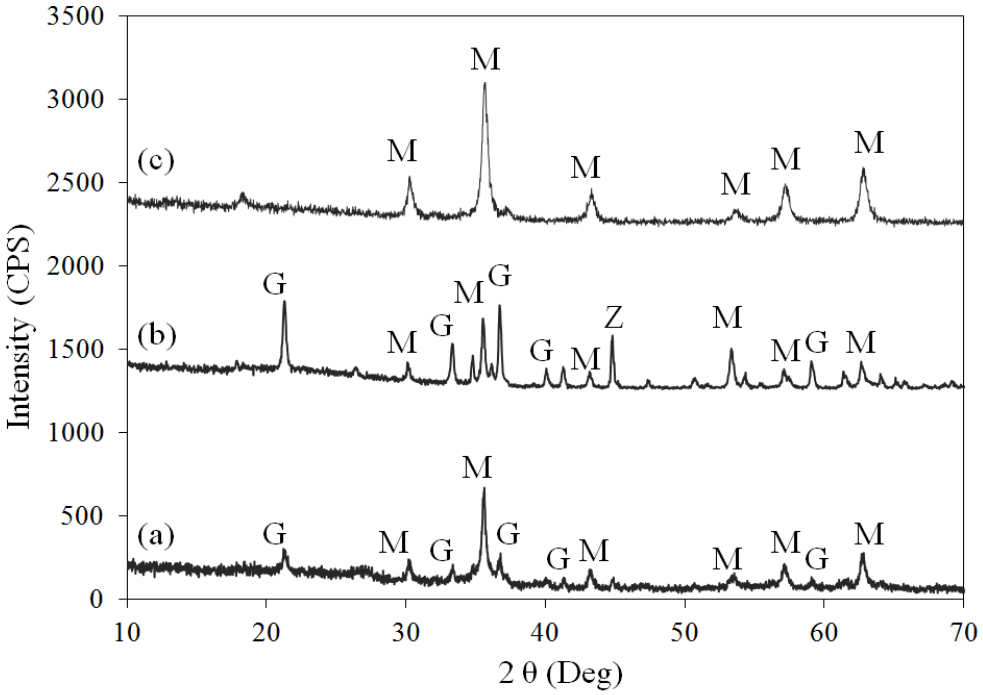

Figure 2.5. XRD spectra for solid products of ferrihydrite transformation in the presence of ZVI on: overhead stirrer with a magnetic bead attached to the propeller (a); overhead stirrer without any magnetic bead attached (b); and magnetic stir plate (c). All experiments were performed with an initial Fe (III):ZVI ratio of 1.0 and an initial pH of 6.8±0.2.

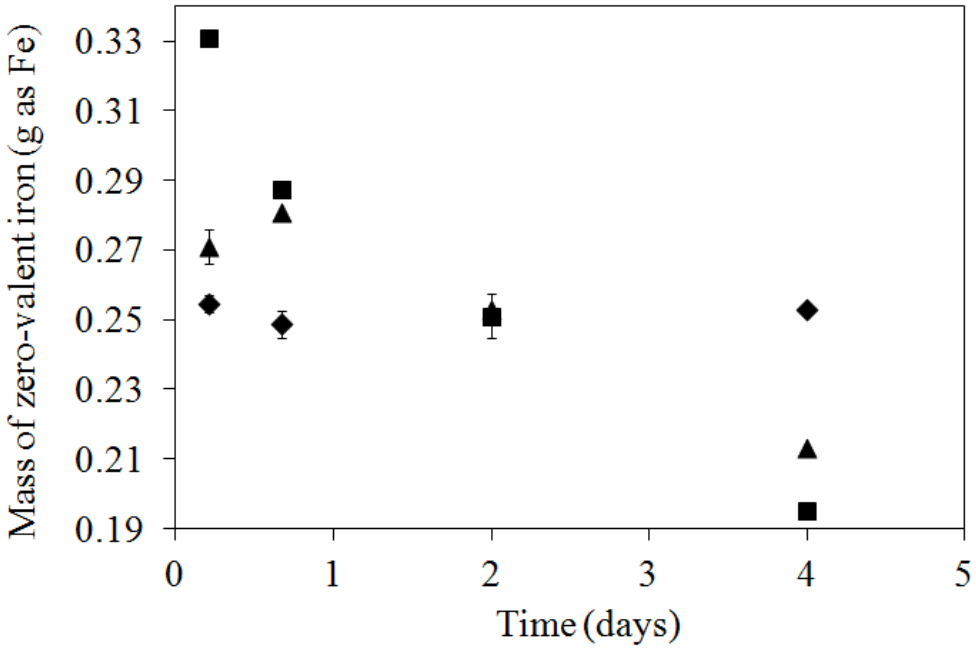

Figure 2.6. Zero-valent iron remaining as a function of time using a magnetic stirrer (♦), an overhead stirrer (■), and an overhead stirrer with a magnetic bead attached to the propeller shaft(▲). Initial amount of ZVI added to each system = 0.3g. The 2-day data points for all three systems overlap with each other. Error bars are standard errors from three replicates and were generated for 25% of the sampled data-points chosen randomly.

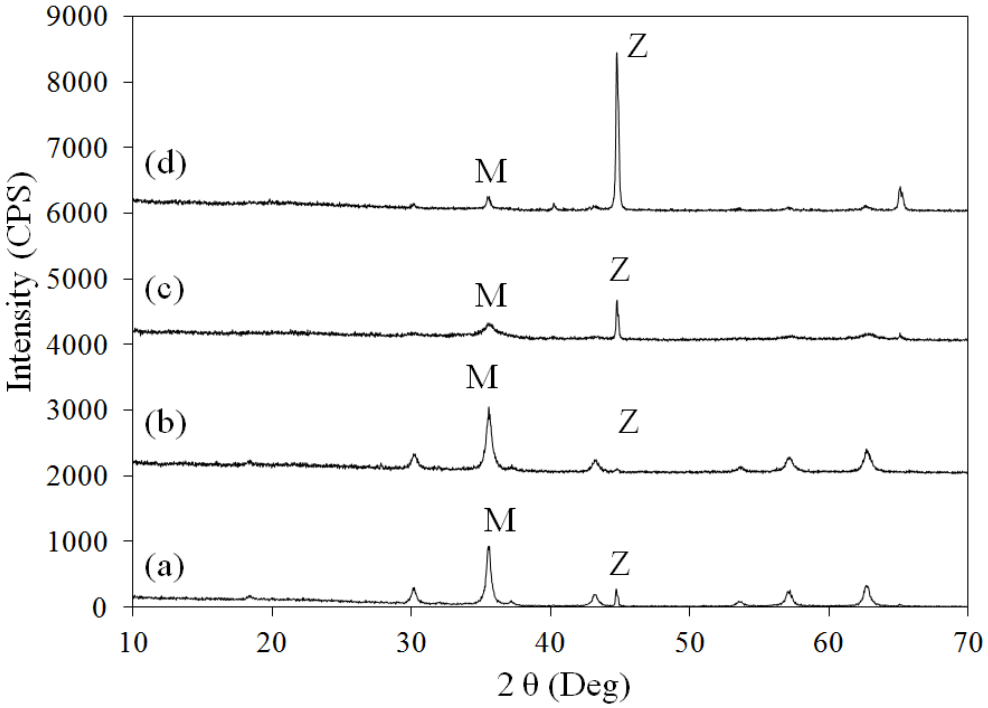

Figure 2.7. XRD spectra for solid products of iron-arsenic solid transformation in the presence of ZVI on the magnetic stirrer. Solids with the following Fe/As ratios were used: (a) ferrihydrite with no arsenic, (b) Fe/As=100, (c) Fe/As=20, and (d) Fe/As=5.7. All experiments were performed with an initial Fe (III):ZVI ratio of 1.0 and an initial pH of 6.8±0.2. M- 100% peak for magnetite, Z-100% peak for zero-valent iron.

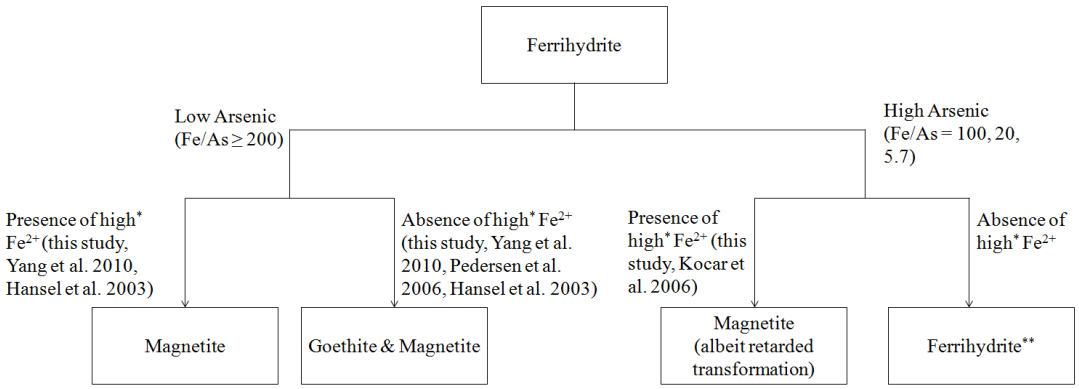

Figure 2.8. Summary of transformation pathways of amorphous ferric hydroxide under different arsenic loadings and presence/absence of high Fe (II) concentrations. *High Fe^{2+} concentrations can either be localized (this study) or uniformly distributed (other studies). Hansel et al. (2003) observed that a threshold Fe (II) concentration level of 0.3 mM is required for magnetite nucleation. **Suggested/ presumed short-term mineralogy (not confirmed in this study). Presence of high arsenic concentrations inhibit transformation of ferrihydrite to goethite by interfering with both the dissolution of ferrihydrite and the re-precipitation of goethite. Long-term arsenic sequestration/release will depend on the relative rates of ferrihydrite dissolution and re-precipitation as goethite in the presence of high concentrations of arsenic.

CHAPTER 3: SCOPING CANDIDATE MINERALS FOR STABILIZATION OF ARSENIC-BEARING SOLID RESIDUALS

Madhumitha Raghav[a], Jilei Shan[a, 1], A. Eduardo Sáez[a], and Wendell P. Ela[a,*]

[a] Department of Chemical and Environmental Engineering, The University of Arizona, Tucson, AZ 85641-0011, USA

[1]Present address: Los Angeles County Sanitation District, Whittier, CA, 90601, USA.

[*]Corresponding author. Tel.: (520) 626-9323; fax: (520) 621-6048; email address: wela@email.arizona.edu

ABSTRACT

Arsenic Crystallization Technology (ACT) is a potentially eco-friendly, effective technology for stabilization of arsenic-bearing solid residuals (ABSRs). The strategy is to convert ABSRs generated by water treatment facilities into minerals with a high arsenic capacity and long-term stability in mature, municipal solid waste landfills. Candidate minerals considered in this study include scorodite, arsenate hydroxyapatites, ferrous arsenates (symplesite-type minerals), tooeleite, and arsenated schwertmannite. These minerals were evaluated as to ease of synthesis, applicability to use of iron-based ABSR as a starting material, and arsenic leachability. The Toxicity Characteristic Leaching Procedure (TCLP) was used for preliminary assessment of candidate mineral leaching. Minerals that passed the TCLP and whose synthesis route was promising were subjected to a more aggressive leaching test using a simulated landfill leachate (SLL) solution.

Scorodite and arsenate hydroxyapatites were not considered further because their synthesis conditions were not found to be favorable for general application. Tooeleite and silica-amended tooeleite showed high TCLP arsenic leaching and were also not investigated further. The synthesis process and leaching of ferrous arsenate and arsenated schwertmannite were promising and of these, arsenated schwertmannite was most stable during SLL testing. The latter two candidate minerals warrant synthesis optimization and more extensive testing.

Keywords: Arsenic residuals; landfills; ferrous arsenate; schwertmannite; tooeleite.

Abbreviations: ACT – Arsenic Crystallization Technology, ABSR – Arsenic-bearing solid residuals, TCLP – Toxicity Characteristic Limit Procedure, SLL – Simulated Landfill Leachate, MSW – Municipal Solid Waste, ST-XRD – Synchrotron transmission X-ray diffraction, EDX spectroscopy – Energy Dispersive X-ray Spectroscopy, TC – Toxicity Characterisitic.

1. Introduction

EPA recommended Best Available Technologies (BATs) for arsenic removal from drinking water rely on precipitation/coagulation, adsorption and ion-exchange (USEPA 2001). All of these technologies generate large volumes of arsenic-bearing solid residuals (ABSRs) that must be safely disposed (Selvin et al. 2002; USEPA 2003). The regulatory leaching tests, the Toxicity Characteristic Limit Procedure (TCLP) and the California Waste Extraction Test (CA-WET), underestimate the leaching of arsenic from the residuals (Ghosh et al. 2004), and consequently arsenic is predicted to be released from ABSRs disposed in mature Municipal Solid Waste (MSW) landfills. Existing technologies for ABSR stabilization like cement encapsulation or vitrification are expensive and/or ineffective for ABSR stabilization (Shaw et al. 2008; USEPA 2000; Riveros et al. 2001). Polymeric encapsulation is promising, both technically and economically, but it is yet to be adopted commercially (Shaw et al. 2008).

The objective of this work is to conduct a scoping analysis of candidate minerals for an eco-friendly, effective Arsenic Crystallization Technology (ACT) for the stabilization of ABSRs under mature landfill conditions. The strategy is to convert ABSRs into minerals with a high arsenic capacity and long-term stability (meaning low arsenic solubility under disposal conditions), particularly those prevailing in MSW landfills. Ideal candidate minerals would be synthesized at ambient temperature and pressure from the original ABSRs, minimize use of expensive or hazardous reagents or complex processing, and exhibit minimal arsenic leaching under disposal conditions.

Five minerals were identified and examined in this study - scorodite, arsenate hydroxyapatite, tooeleite, ferrous arsenate (symplesite-type minerals), and arsenated schwertmannite. Scorodite ($FeAsO_4.2H_2O$) was considered due to its high arsenic capacity (25-30 % wt/wt) (Robins 1987; Harris and Krause 1993) and previous known synthesis procedures (Dove and Rimstidt 1985; Dutrizac and Jambor 1988; Le Berre et al. 2007; Le Berre et al. 2008; Fujita et al. 2012). Hydroxyapatites ($Ca_{10}(PO_4)_6(OH)_2$) are minerals with similar crystal structure but varying in exact composition. They are stable over a broad pH range and arsenate may substitute for phosphate in hydroxyapatite to form Johnbaumite ($Ca_{10}(AsO_4)_6(OH)_2$) (Mahapatra et al. 1989; Lee et al. 2009). Hydroxyapatite minerals have been studied for the immobilization of hazardous compounds containing lead, cadmium, nickel, copper, mercury and arsenic (Mahapatra et al. 1993; Bothe and Brown 1999; Radoicic and Raicevic 2008; Oliva et al. 2011).

Ferrous Arsenates (symplesite, parasymplesite and ferrisymplesite) belong to the vivianite group with the general formula $Y_3(XO_4)_2.8H_2O$, where Y^{2+} may be Co, Fe, Mg, Ni, or Zn, and X is As or P (Sturman 1976). Symplesite and parasymplesite both have the chemical formula $Fe_3(AsO_4)_2.8H_2O$, but differ in physical characteristics. Sadiq et al. (2002) determined that the arsenic solubility of Kelly Lake (Ontario) minerals, is controlled by the equilibrium of $Fe_3(AsO_4)_2.8H_2O(c)/Fe_4Fe_2(OH)_{12}.SO_4(c)$.

Previous studies have investigated arsenic immobilization by ferrous iron treatment, possibly leading to the formation of ferrous arsenate solids (Voigt 1996; Seidel et al. 2005). To our knowledge, there are only two studies on the synthesis and stability of ferrous arsenates (Khoe et al. 1991; Johnston and Singer 2007). Despite inconsistency in

the solubility products calculated in the studies, the solid synthesized showed low arsenic solubility.

In Schwertmannite, an iron (III)-oxyhydroxysulfate mineral [$(Fe_8O_8(OH)_x(SO_4)_y.nH_2O$, where $8 - x = y$ and $1.0 \leq y \leq 1.75$] arsenate can partially (up to 5.6 wt%) exchange for sulfate without significant disruption of the structure (Regenspurg and Peiffer 2005; Burton et al. 2009). In addition, arsenate can stabilize the schwertmannite structure and retard its Fe(II)-catalyzed transformation to goethite (Regenspurg and Peiffer 2005; Fukushi et al. 2003). The transformation would be expected to cause arsenic release due to a decrease in specific surface area between poorly-crystalline schwertmannite and more crystalline goethite. But Acero et al. (2006) reported no substantial decrease in the specific surface area and 99% arsenic retention after transformation of schwertmannite to goethite. Slightly alkaline conditions, such as those present in mature landfills, accelerate the transformation process (Regenspurg et al. 2004; Schwertmann and Carlson 2005; Knorr and Blodau 2007). Burton et al. (2010) showed that 1 mM As(III) or As(V) retarded this transformation and was accompanied by negligible release of arsenic.

Tooeleite, $Fe_6(AsO_3)_4SO_4(OH)_4.4H_2O$, is an iron arsenite oxyhydroxy-sulfate mineral, recently discovered in gold mines (Cesbron and Williams 1992; Marquez 1996) and acid mine waters (Morin et al. 2003; Morin et al. 2007; Egal et al. 2009). Tooeleite is an attractive candidate ACT mineral because of its high arsenic loading (~20-25% wt). As with other candidate minerals, the objective here was not to conduct a detailed parametric evaluation of tooeleite formation, but to get a first-cut idea of the effectiveness of tooeleite as an arsenic sink. Silica-coating of iron oxides such as magnetite, maghemite

and hematite has been studied to prevent metal leaching (Han et al. 2010; Li et al. 2010b; Yang et al. 2009), so this amendment was evaluated for the tooeleite solid.

2. Materials and Methods

Water was degassed by heating deionized water to 90±4 °C for 1 hour while bubbling nitrogen. The flask was then sealed tightly and stored in a Terra Universal Critical Environment Solutions glove box purged with nitrogen at room temperature (20-25 °C).

2.1. Ferrihydrite Preparation

Ferrihydrite was synthesized as a representative arsenic sorbent utilized for drinking water treatment. It was synthesized both without and with arsenic loading to mimic both a virgin sorbent and an ABSR ready for disposal. Synthesis followed a modified procedure by Mukiibi et al. (2008). Briefly, 1.00 M anhydrous ferric chloride solution was titrated with 10 M NaOH to a pH of 7.0 within 1 hour. The suspension settled and equilibrated for 48 hours with the pH maintained at 7 ± 0.3 by addition of 0.1 M HCl or 0.1 M NaOH as necessary. The pH of the suspension was monitored for an additional 48 hours more to ensure that the pH had stabilized at 7.0. The precipitate was vacuum filtered using 0.22 µm membrane filters to water content of approximately 75% wt and rinsed multiple times with deionized water to remove residual salts. The solid was sealed tightly and stored at 4°C.

Arsenic-loaded ferrihydrite (Fe/As molar ratio = 20:1) was prepared from equal volumes of 1.00 M anhydrous ferric chloride solution and 0.05 M sodium arsenate heptahydrate ($Na_2HAsO_4.7H_2O$, KR Grade, Sigma- Aldrich). The mixture was stirred and titrated with 10 M NaOH to pH 7.0 within 1 hour. All other steps were the same as those for ferrihydrite without arsenic.

2.2. Characterization and Analytical Methods

The iron and arsenic ratio of the synthesized arsenic-loaded ferrihydrite was determined as 20.5 and is referred to as such hereafter. Both ferrihydrite solids (Fe/As = 0.0 and 20.5) had water contents of 77.5±0.2% (wt/wt). Ferrihydrite samples (both Fe/As = 0.0 and 20.5) of 0.500 g were weighed and digested in 14.5 mL of concentrated nitric acid for 20 minutes using a CEM MDS 2100 Microwave Digestion System. Five replicates were run in each case. Digested samples were filtered using 0.22 μm cellulose nitrate filters (Millipore). The filtrate was analyzed for iron using the phenanthroline test (Clesceri et al. 1998) and for arsenic by Inductively Coupled Plasma Mass Spectrometer (ICPMS, Agilent 7500a).

Synthesized solids were subjected to the TCLP in accordance with EPA SW-846, Method 1311. The extraction solution consisted of 5.7 mL glacial acetic acid added to 64.3 mL of 1.0 M NaOH solution with the final volume brought to 1 L with DI water. The pH of this solution was adjusted to 4.93 ± 0.05 before adding the solids. 5.129 g of size reduced (< 1.4 mm) solid sample was added to 100 mL of leaching solution in a 120 mL bottle and

sealed. The sealed bottles were rotated end-over-end shaker (30 rpm) for 18 hours. For all tooeleite cases, the solids were dried and used on a dry weight basis in the TCLP.

In some cases a simulated landfill leachate (SLL) solution was used for more aggressive leach testing. This leachate solution was a modified version of SLL solutions used in a previous study on ABSR (Ghosh et al. 2004). The SLL composition was (mg/L): acetic acid (600.5), sodium citrate dihydrate (58,818), sodium bicarbonate (8,400), hydroquinone (110.1) and hydroxylamine hydrochloride (69.5). SLL pH was adjusted to 8.1±0.1 before addition of hydroxylamine hydrochloride, which was only added immediately prior to use due its short half life in an oxidizing environment. Similar to the TCLP, 5.129 g of size reduced (<1.4 mm) sample was added to 100 mL of the leaching solution in a 120 mL sealable bottle. In addition, the headspace of the bottle was purged vigorously with nitrogen prior to sealing and rotated end-over-end at 30 rpm for 48 hours. All leaching tests involved three replicate runs. After leaching, the bottles were removed from the shaker, the remaining solids settled, and aqueous samples taken through a 0.22 µm cellulose nitrate filters (Millipore).

Bulk sample crystalline phases were identified by XRD spectra (Bruker D8 ADVANCE diffractometer using Cu$K\alpha$ radiation). Samples were scanned from 5° to 90° for over 285 minutes. Peaks were matched against those in the International Centre for Diffraction Data (ICDD) database. Solids synthesized from the schwertmannite trials were analyzed using Synchrotron transmission X-ray diffraction (ST-XRD) collected at the Stanford

Synchrotron Radiation Lightsource (SSRL) on beamline 11-3 operating at 12735 eV (λ = 0.976 Å) with a focused spot size of 150 μm, using a 345 mm radius Mar detector image plate with a resolution of 100 μm^2 pixels, and calibrated to a LaB_6 standard. Approximately 50 mg of ground and homogenized sample was dispersed on, and sealed in, matte finish tape (Scotch Magic™) to obtain a uniform thin layer sample (<0.5 mm). Laue pattern images were collected while the sample was rastered over a 1 mm^2 area on an x-y stage. Laue ring pattern images were converted into 2-theta diffractograms using the Area Diffraction Machine software (Lande et al. 2007). The summed patterns were converted to conventional Cu Kα wavelength for comparison to known reference patterns. A Hitachi S-4800 II Field Emission Scanning Electron Microscope was used to obtain the SEM images and Energy Dispersive X-ray (EDX) spectroscopy was used for elemental composition.

2.3. Scorodite Synthesis

A natural scorodite ($FeAsO_4.2H_2O$) specimen purchased from Caldbeck Fells Mines, UK, was characterized using XRD analysis and used as a reference for scorodite synthesized in this study. Synthesis pH, temperature and Fe/As ratio for scorodite were independent study variables. Synthesis at pH 1.0, 3.0, 5.0 and 7.0 followed a procedure modified from Dutrizac and Jambor (1988): 0.300 M $Fe(NO_3)_3$ and 0.300 M NaH_2AsO_4 solutions were mixed to attain a Fe/As ratio of 1.0. The synthesis was conducted in an autoclave at 160 °C and 8.0 bar for 24 hours. The pH 1.0 experiment required no pH adjustment. For other trials pH was adjusted using 1.0 M NaOH. After 24 hours, the solids were 0.45 μm

filtered and washed thrice with 500 mL of hot water at 80-90 °C. Solids were dried at 60 °C for 4 days and then stored at room temperature.

Study on the effect of Fe/As ratio on scorodite synthesis again followed Dutrizac and Jambor (1988). 150 mL of 0.2 M, 0.500 M, or 1.00 M $Fe(NO_3)_3$ and 150 mL of 0.10 M NaH_2AsO_4 solutions were mixed in a 400 mL autoclave for Fe/As ratios of 2.0, 5.0, and 10.0, respectively. Initial pH was adjusted to 3.0 using 10.0 M NaOH and the solution was incubated for 24 hours at 160 °C and 8 bar. Solids were prepared for characterization as above.

Additionally, previously reported scorodite synthesis methods were evaluated with incubation temperatures of 60 °C, 95 °C, 150 °C and 230 °C (Dove and Rimstidt 1985; Dutrizac and Jambor 1988; Demopoulos 1995; Mambote et al. 2001). Summary synthesis conditions are shown in Table 1. In all cases solutions of 0.11 M $Fe(NO_3)_3$ and 0.10 M NaH_2AsO_4 were initially mixed. Following Demopoulos (1995) the mixture pH was brought to zero using 10.0 M HNO_3 and heated to 95 °C at 1 bar pressure. 10 M NaOH was then added gradually to bring the pH to 1.50. Following Dove and Rimstidt (1985), the resulting product was aged at 60 °C for 14 days without further pH adjustment. Finally, using a modified Mambote et al. (2001) procedure, the mixture was maintained at 150 °C and 8 bar or at 230 °C and 11 bar in an autoclave for 24 hours.

2.4. Arsenate Hydroxyapatite Synthesis

Apatite series compounds were synthesized using a procedure modified from Mahapatra et al. (1989). The first experiments involved synthesis of hydroxyapatite ($Ca_{10}(PO_4)_6(OH)_2$, arsenate phosphate hydroxyapatite, $Ca_{10}(As_xP_yO_4)_6(OH)_2$, with variable phosphate to arsenate ratios, and Johnbaumite, $Ca_{10}(AsO_4)_6(OH)_2$. In all cases, calcium, phosphate and arsenate were combined maintaining the Ca:(As+P) molar ratio at 5:3.The pH of the solution was adjusted to 11.0 using NaOH and the temperature held at 100 °C for 24 hours. The solids were rinsed with deionized water, filtered using a 0.45 µm filter and collected for XRD analysis. Different As/P ratios from 0 to 5 and a no phosphate case were studied.

Another set of experiments evaluated the effect of iron on synthesis of apatite-like compounds. The As/P ratio was fixed at 1.0 and different Fe/As ratios from 1 to 10 were studied. The initial pH was 12.0. All other experimental conditions were the same as above. All synthesized solids were 0.45 µm filtered, washed with deionized water, collected and dried at 100 °C for 24 hours before being characterized.

2.5. Tooeleite Synthesis

Tooeleite, $Fe_6(AsO_3)_4SO_4(OH)_4.4H_2O$, synthesis followed Nishimura and Robins (2008) with slight modifications: Equal volumes of 0.04 M ferric sulfate and 0.05 M sodium arsenite solutions were mixed for 2 hours. The pH at this point was 2.6±0.05. The beaker was incubated at 60 ºC for 2 days.

Synthesis of silica-coated tooeleite followed a modified version of the sol-gel coating procedure of Han et al. (2010) for Fe_2O_3 nanoparticles. Tooeleite prepared as described was dried and ground into fine particles. 0.45 g of dried and ground tooeleite was mixed vigorously with 20 mL of absolute ethanol for 45 minutes followed by addition of 7 mL of 98% tetraethoxysilane (TEOS). 3 mL of ammonium hydroxide (30%) were then added as a catalyst and the solution mixed for 6 hours to ensure maximum hydrolysis of the TEOS and formation of the monosilicic acid essential for condensation. Finally, the suspension was filtered and dried before being analyzed by XRD and SEM.

2.6. Ferrous Arsenate Synthesis

Ferrous arsenate $Fe_3(AsO_4)_2.8H_2O$ was synthesized from Fe(II) and As(V) according to Johnston and Singer (2007) to obtain a reference solid. Subsequently, ferrous arsenate synthesis started from arsenic loaded ferrihydrite (Fe/As molar ratio = 20.5) prepared in the laboratory. 1.2028 g of wet ferrihydrite in 250 mL of deoxygenated DI water was combined with zero-valent iron at a ZVI:Fe(III) molar ratio of 10.0 inside a glove box purged with nitrogen. The pH of the mixture was lowered to1.30. After 3 hours, complete dissolution and reduction of the Fe(III) to Fe(II) was observed. The remaining zero-valent iron was removed and 250 mL of 3.98 mM sodium arsenate heptahydrate, $NaH_2AsO_4.6H_2O$ was added. The pH of the solution was raised to 7.50 using NaOH. The resulting dark green precipitate was collected on a 0.22 µm filter and dried inside the glove box.

The synthesis procedure was repeated outside the glove box using deoxygenated DI water, although the synthesized solids were dried inside the glove box.

2.7. Arsenated-Schwertmannite Synthesis

Schwertmannite [$(Fe_8O_8(OH)_x(SO_4)_y$ .nH_2O, where 8 - x = y and $1.0 \leq y \leq 1.75$] was synthesized using the ferrihydrite prepared as previously described. The synthesis procedure was based on Bigham et al. (1990): 7.567 g of wet ferrihydrite solid, equivalent to 20 mmol of Fe(III) was added to 500 mL of 0.25 M HCl solution and mixed for 2 hours. The solution temperature was then raised to 60 ºC, sodium sulfate added to yield a 20 mM sulfate solution, and incubated for 12 minutes before cooling to room temperature. The solution was dialyzed using Fisherbrand regenerated cellulose dialysis tubing (Nominal Molecular Weight Cut-off = 12,000 -14,000 daltons) in ~ 12 L of deionized water. The pH was 2.6±0.05.The water was exchanged for fresh de-ionized water every day for 18 days. The specific conductance of the dialysis water was continuously <5 µS/cm for the last 5 days. Finally, the solids were 0.22 µm filtered, dried under flowing nitrogen, and collected.

The same procedure was repeated starting with lab-synthesized arsenic-loaded ferrihydrite (Fe/As = 20.5). This procedure was based on the method reported for synthesis of arsenated-schwertmannite starting from ferric, sulfate and arsenate solutions (at Fe/As = 22.22) (Carlson et al. 2002): 7.509 g of wet arsenic-loaded ferrihydrite, equivalent to 20 mmol Fe(III) and 0.96 mmol As(V) was added to 500 mL of 0.25 M

HCl solution and mixed for 2 hours, dissolving all ferrihydrite. Once the solid was completely dissolved, the solution was held at 60 ºC and sodium sulfate was added to yield a 22.4 mM sulfate solution. This solution was maintained at 60 ºC for an additional 12 minutes before being cooled to room temperature and dialyzed following the same steps as described above for the synthesis of schwertmannite from ferrihydrite solid.

3. Results and Discussion

Scorodite was synthesized at pH 1.0, 3.0, 5.0 and 7.0, at 160 °C and Fe/As ratio of 1.0 for 24 hours to evaluate if milder synthesis conditions were feasible than previously reported. The pH 1.0, 3.0, and 5.0 solids showed three primary XRD peaks for scorodite (Figure 1). However, as synthesis pH was increased unidentified peaks appeared (marked 1, 4, 5, and 6 in Figure 1) and the intensity of some secondary scorodite peaks (marked 2 and 3 in Figure 1) decreased. The solid from pH 7.0 synthesis was amorphous with no distinct scorodite peaks. This suggests synthesis at pH $\geq$ 3 leads to mixed solid phases with the crystalline scorodite contribution decreasing with increasing pH.

At pH $\leq$ 1.5 the scorodite synthesized at 95 °C, 150 °C, and 230 °C (Table1) was crystalline by XRD and SEM analysis (results not shown). The 60 °C solid was poorly crystalline scorodite of fine particle size. Particle size increased with increase in temperature up to 150 °C, but not thereafter. Scorodite was synthesized at pH 3.0, 160 °C and 8 bar, but different Fe/As ratios (1.0, 2.0, 5.0 and 10.0). The Fe/As ratio of 1.0 yielded only crystalline scorodite, whereas synthesis at a ratio of 2.0 yielded a poorly

crystalline scorodite and hematite mixture. Solid synthesized at Fe/As of 5.0 was amorphous and at Fe/As of 10.0 was only crystalline hematite with no evidence of scorodite (XRD not shown). Thus, increasing the Fe/As from 1.0 to 10.0 resulted in inhibition of scorodite formation.

Based on these results, scorodite synthesized at pH 1, Fe/As =1.1 and temperatures of 95°C, 160 °C and 230 °C was selected to evaluate leaching using the TCLP. The arsenic leaching observed was at least an order of magnitude less than the arsenic Toxicity Characteristic (TC) of 5 ppm (Figure 2).

In all phosphate/arsenate hydroxyapatite synthesis trials (100 °C and 1 bar), the solids obtained were found to lie structurally along the hydroxyapatite to johnbaumite mineralogic transition based on XRD analysis (Figure 3). Some weak peaks at 2θ angles of 22°, 26°, 34° and 49° were enhanced for As/P ratios > 1.0. As also seen in nature, substitution of the phosphate in hydroxyapatite by arsenate to form arsenate hydroxyapatite minerals causes no loss of structural and crystallographic integrity as the phosphate and arsenate tetrahedra readily interchange. Motivated by the ease of synthesis and insensitivity to As/P ratio, the leaching from these arsenate hydroxyapatite minerals was subjected to the TCLP. Only solids synthesized at As/P $\leq$ 0.2 showed As leachate concentrations below the TC (Figure 2).

Coagulation/microfiltration with iron salts and adsorption on ferric (hydr)oxides are EPA recommended Best Available Technologies for arsenic removal from drinking water. Hence, high iron content typifies ABSRs generated from water treatment facilities. Iron

arsenate hydroxyapatite synthesis trials showed iron can have an inhibitory effect on the formation of crystalline apatite minerals (Figure 4). At the lower Fe/As ratios studied (Fe/As = 1.0, 2.0) hematite and hydroxyapatite (both poorly crystalline) were formed. At higher ratios (Fe/As = 5.0, 10.0), crystalline hematite was the only solid identified. At these high Fe/As ratios, the iron content combined with high pH and high temperature synthesis - conditions known to favor hematite generation (Cornell and Schwertmann, 2003), disposes the system to crystallization of hematite at the expense of hydroxyapatite. Despite some apatite-type structure (at As/P ratio of < 0.2) showing arsenic leaching below the TC, because of the sensitivity of synthesis to low levels of iron, additional work on apatite-type arsenic minerals for arsenic residuals stabilization was not pursued.

Tooeleite synthesis with and without silica coating was confirmed by powder XRD (not shown here). To investigate whether the tooeleite surface was in fact coated with silica, SEM imaging and EDX spectroscopy were employed. Although the images obtained for the two solids using SEM (not shown here) looked different in terms of the surface morphology, this analysis was too crude to confirm that the tooeleite surface was coated with silica. When analyzing a solid sample using EDX, the accelerating voltage is directly proportional to the depth of X-ray penetration into the sample. Hence, at a higher accelerating voltage, the EDX elemental analysis will be influenced more by material deeper in the solid. Thus for one solid phase coated with a second solid of different elemental composition, it may be possible to detect the difference in composition with

depth using EDX analysis at different accelerating voltages. For silica-amended tooeleite it was observed that at 5 kV silicon and oxygen were the only elements detected (Table 2). Progressively increasing the accelerating voltage from 5 kV to 30 kV, progressively decreased the percent composition of silicon and oxygen, but iron and arsenic were not detected below a voltage of 30 kV (The carbon signal, due to the background carbon stub that was used to provide a conductive path for the electrons, became stronger as the accelerating voltage was increased). For tooeleite with no silica coating, iron and arsenic were detected at an accelerating voltage of 5 kV. This indicates that the tooeleite synthesis amended with silica did result in a core coated with silica, however, the technique does not allow for characterization of uniformity or thickness of the coating.

Tooeleite and silica-amended tooeleite were both tested for arsenic leachability using the TCLP. The arsenic leaching in both cases was at least an order of magnitude higher than the arsenic TC (Figure 2). The tooeleite and silica-amended tooeleite leached were completely dried prior to leaching. The process of drying often results in increased crystallinity of solid phases, which usually means increased stability of the solid. Hence, tooeleite solids would be expected to show equal or higher leaching if subjected to TCLP without prior drying. Although the silica-coating procedure resulted in an observable reduction in arsenic leaching (Figure 2), neither the pure nor the silica-amended tooeleite were considered for further ACT investigation due to the relatively high concentrations of As in the TCLP leachate.

A parasymplesite reference solid was synthesized from laboratory grade reagents and verified by powder XRD (Figure 5). Other solids synthesized for the ferrous arsenate trials used arsenic-loaded ferrihydrite as the starting material. Synthesis under anoxic conditions was important for the formation and stability of parasymplesite ($Fe(II)_3(As(V)O_4)_2.8H_2O$), because similar synthesis under oxic conditions outside the glove box generated a hydrated ferric arsenate, ferrisymplesite, ($Fe(III)_3(As(V)O_4)_2(OH)_3.5H_2O$) (Figure 5). It is known that parasymplesite can oxidize to form ferrisymplesite (http://www.mindat.org/min-1502.html last accessed on June 1st, 2013). The use of deoxygenated water for synthesis also seems to be important, since a similar ferrous arsenate synthesis trial performed outside the glove box with deionized water that was not deoxygenated yielded an amorphous product.

The ferrous arsenate solids synthesized inside and outside the glove box were acid-digested using 70% nitric acid to determine the iron and arsenic content in the solids (Table 3). All Fe/As ratios were higher than the theoretical symplesite ratio calculated from stoichiometry. We hypothesize that the synthesis process produces another amorphous mineral, such as a ferrous or ferric hydroxide, which results in a higher iron content than that calculated by assuming 100% parasymplesite or ferrisymplesite in the synthesized solids. Even though strong XRD peaks were detected for parasymplesite and ferrisymplesite (weaker peaks in the case of ferrisymplesite as compared to parasymplesite), because XRD is semi-quantitative with a minimum detection limit of

approximately 5% by weight, it cannot routinely quantify minor phases that may be present. If, as hypothesized, an iron hydroxide (ferric or ferrous) is co-precipitated with the symplesite phase, then this could easily affect the arsenic loading of the solid phase due to the high adsorption capacity of iron hydroxides for arsenic, and also the leachability of arsenic from the resulting solid mixture.

The arsenic leaching behaviors of parasymplesite and ferrisymplesite were tested using the TCLP. Even though synthesis under oxic and anoxic conditions resulted in different mineral phases by XRD characterization, not only was the level of arsenic loading similar (Table 3), but the two solids also displayed similar TCLP arsenic leaching behavior and both leached less than the TC (Figure 2).

Since both parasymplesite and ferrisymplesite passed the TCLP and a low temperature/pressure synthesis route from a ferrihydrite-type ABSR was demonstrated, further investigation of ferrous arsenate as a possible ACT was undertaken using the more aggressive SLL test. The conditions employed in this leaching test are more representative of the conditions in a mature, mixed-solid waste landfill. Hence, this test is expected to be a better indicator than the TCLP of the suitability of a candidate mineral to act as a sink for long-term arsenic immobilization under landfill conditions. It was observed again that the two solids displayed similar leaching behavior (Figure 6), but, as expected, the arsenic concentrations were significantly higher than those observed for the

TCLP. SLL arsenic leaching was approximately an order of magnitude higher than the Toxicity Characteristic value.

Solids obtained from Schwertmannite synthesis trials starting from ferrihydrite solid (Fe/As molar ratios of 0.0 and 20.46) after 18 days of dialysis were confirmed as Schwertmannite using synchrotron XRD analysis (Figure 7). The stability of the arsenated-schwertmannite synthesized from the arsenic-loaded ferrihydrite solid (Fe/As molar ratio = 20) was tested using the TCLP. Not only did this solid yield leach arsenic concentrations below the TC, but it also had the lowest level of arsenic leaching compared to the other candidate minerals in this study (Figure 2). Consequently, arsenated-schwertmannite was subjected to leaching using the SLL solution described earlier in the Materials and Methods section. SLL leaching was lower than that observed for the symplesite-type solids (Figure 6), although still higher than the arsenic TC (~2X) and significantly higher than the TCLP leaching results.

Schwertmannite, like other Fe(III) oxides is known to transform into more crystalline minerals such as goethite and magnetite with time (Burton et al. 2008; Jonsson et al. 2005; Paikaray and Peiffer 2010; Cutting et al. 2012). Such transformations can potentially release arsenic into the environment. But a recent schwertmannite transformation study by Cutting et al. (2012) with arsenic loadings of up to 4% by weight showed that only small quantities of arsenic were released into the aqueous phase (≤ 120 $\mu g L^{-1}$) due to sequestration in the transformation products.

4. Conclusions

Five candidate minerals – scorodite, arsenate hydroxyapatite, tooeleite symplesite-type phases, and arsenated schwertmannite – were considered in this study as candidate phases for arsenic stabilization. The suitability of the candidate phase was judged according to the simplicity of the synthesis route (e.g., temperature, pH, material requirements, duration of process), synthesis route compatability with an iron-based ABSR starting material, and stability with respect to arsenic leaching under TCLP and SLL conditions (Table 4).

Scorodite synthesis required relatively harsh and strict conditions ($T > 150$ °C, $P \sim 8$ bar, $pH \leq 1$, $Fe/As < 2$), but the arsenic leaching from the TCLP was below the arsenic TC. Apatite-series solids were synthesized under more moderate conditions ($T \sim 100$ °C, $P = 1$ bar, pH 12), but the inhibition of solid formation in the presence of iron precluded use of most ABSR as a starting material. TCLP leaching was slightly above that of scorodite. Tooeleite was synthesized under modest conditions ($T = 60$°C, $P = 1$ bar, $pH > 2$), but silica coating required additional time and reagents. Tooeleite leaching was poor and about 10X above the TC, both with and without silica amendment. Symplesite species (ferrous and ferric arsenate) were simple to synthesize (ambient T and P and no pH adjustment) and synthesis was achieved starting with a representative iron-based ABSR. TCLP leaching was lower than the arsenic TC, although SLL leaching was about 10X greater than the TC. Lastly, arsenated Schwertmannite synthesis required an involved and lengthy procedure (HCl dissolution, $T = 60$ °C, dialysis, $t \geq 18$ days), but was shown to be

amenable to an iron-based ABSR starting point. The Schwertmannite solids demonstrated the best arsenic leaching resistance (in both TCLP and SLL), although SLL was about 2X greater than the arsenic TC.

Based on these scoping results, symplesite-type phases and Schwertmannite showed the greatest promise for ABSR stabilization. In neither case, were the combination of synthesis conditions and leaching resistance completely satisfactory, yet both were shown to be amenable to an ABSR starting material. Since optimization of synthesis route and leaching resistance were beyond the immediate scope of this work, it is expected that with additional research and innovation, one or both of these solids may prove to be a stable, long-term repository for arsenic in ABSRs and might be synthesized through a relatively simple procedure amenable to use at a drinking water utility scale.

Acknowledgements

This work was supported by the National Institute of Environmental Health Sciences (NIEHS) Grant No. P42 ES04940. The authors declare no conflict of interest. This paper's contents are solely the responsibility of the authors and do not necessarily represent the official views of NIEHS. The authors thank Dr. Robert Downs' research group of the University of Arizona and Phil Anderson of the University Spectroscopic Imaging Facility at the University of Arizona for XRD analyses of solids and Mike Kopplin for early ICPMS arsenic analysis. The authors thank Dr.Jon Chorover and

Dr.Robert Root for Synchrotron XRD data for schwertmannite solids and sharing beam time at the Stanford Synchrotron Radiation LightSource. Arsenic analysis was performed by the Analytical Section of the Hazard Identification Core from our NIEHS-supported Superfund Basic Research Program Grant.

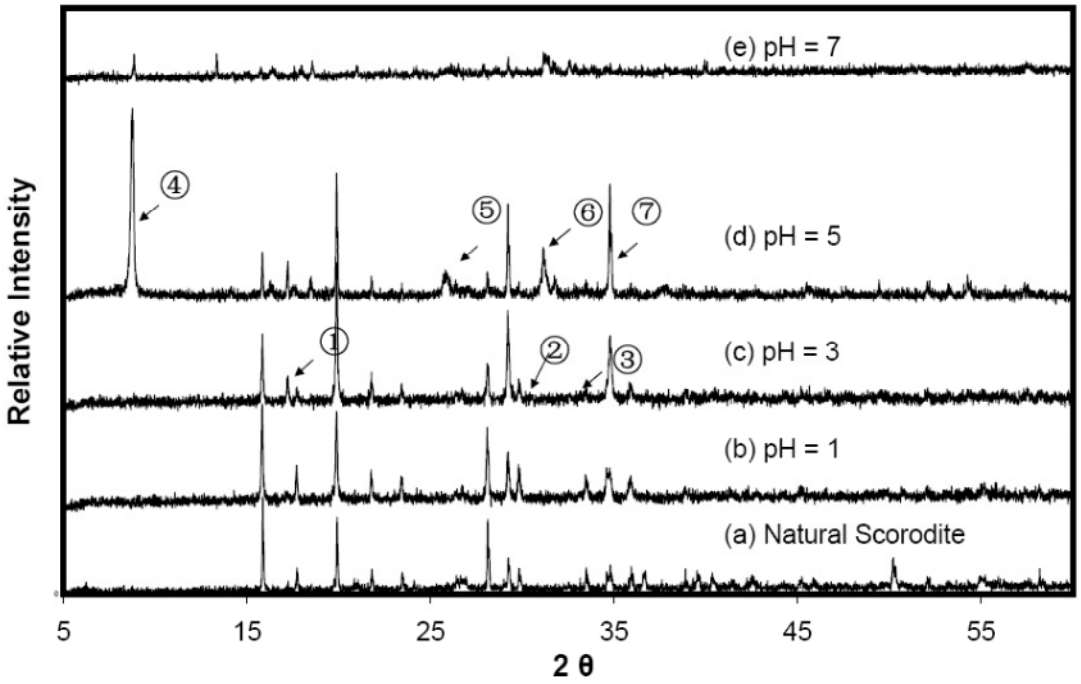

Figure 3.1. XRD spectra for solids generated from scorodite synthesis trials at 160 °C for 24 hours, a Fe/As molar ratio of 1.0, and initial pH as indicated.

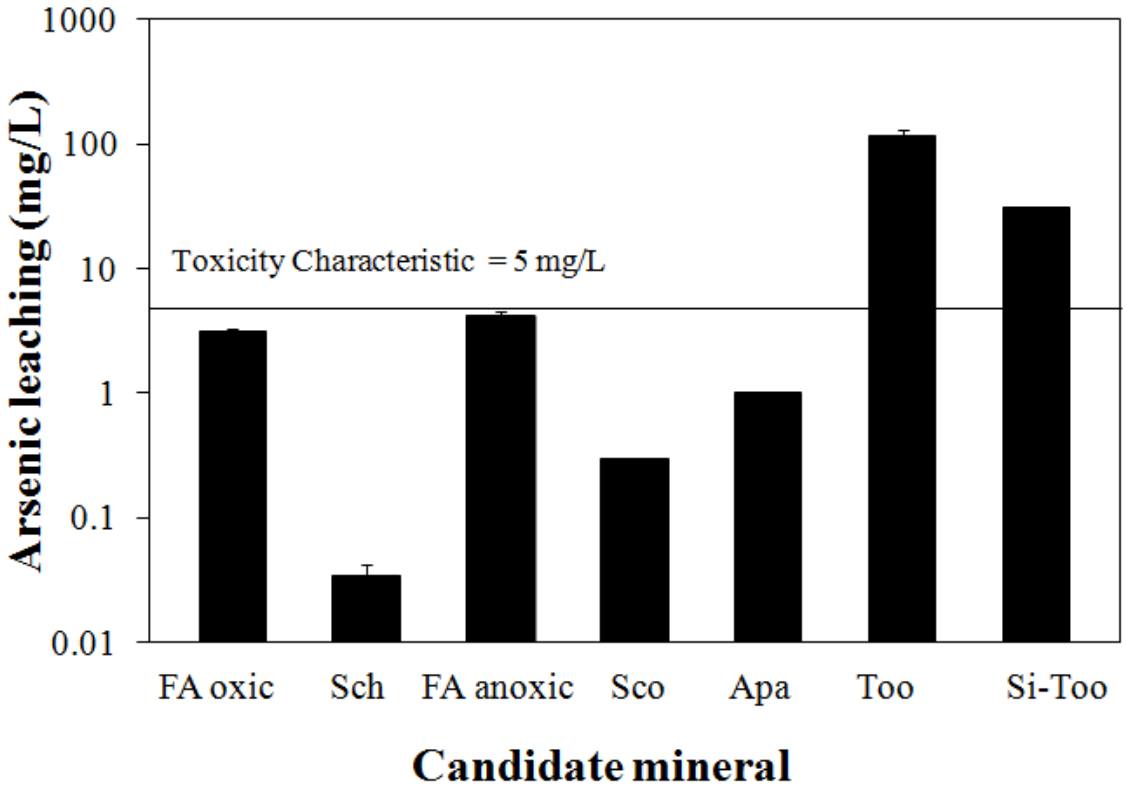

Figure 3.2. Arsenic concentration from Toxicity Characteristic Leaching Procedure for candidate minerals. FA oxic - Ferrisymplesite synthesized under oxic conditions, Sch - Arsenated-Schwertmannite, FA anoxic - Parasymplesite synthesized under anoxic conditions, Sco - Scorodite, Apa - Arsenate Hydroxyapatite (with no Fe and As/P < 0.2), Too - Tooeleite, Si-Too - Silica-amended Tooeleite. Note: Error bars were not be obtained for scorodite and arsenate-hydroxyapatite.

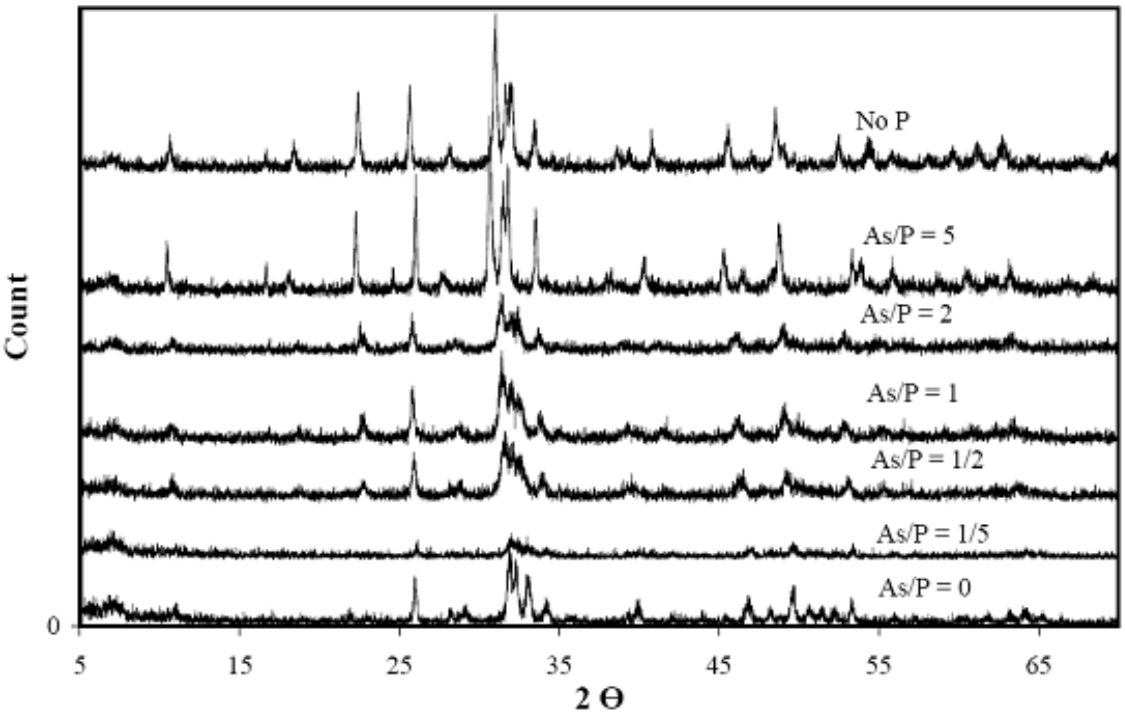

Figure 3.3. XRD spectra of solids generated from arsenate hydroxyapatite synthesis trials using different As/P ratios. All the solids were synthesized at 100 °C, an initial synthesis pH of 11 and reaction time of 24 hours.

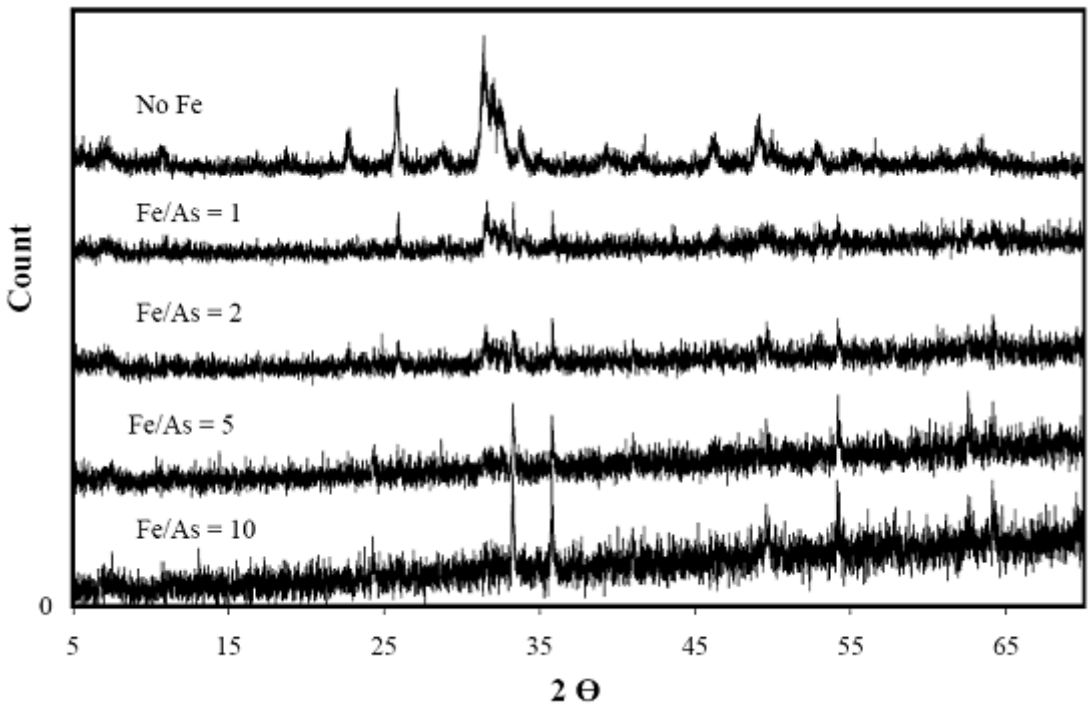

Figure 3.4. XRD spectra for solids obtained from the iron arsenate hydroxyapatite synthesis trials using different Fe/As ratios. All the solids were synthesized at 100 °C, Ca/(As+P) ratio of 5/3 and P/As ratio =1. The initial pH was 12 and the reaction time was 24 hours.

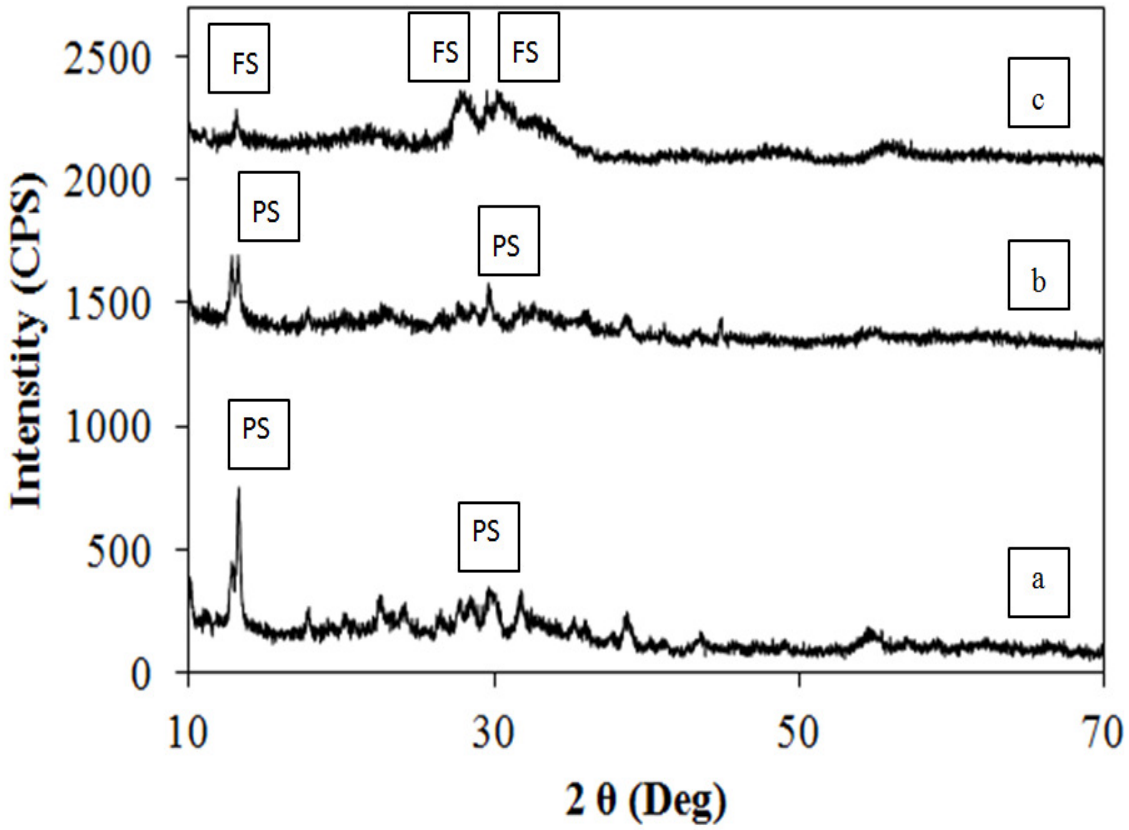

Figure 3.5. Solid synthesized from a.) pure Fe(II) and As(V) solutions following the procedure in Johnston and Singer (2007). b.) Fe/As = 20.46 solid, zero-valent iron [Fe(III)/ZVI = 10], at room temperature, inside the glove box purged with N_2. c.) Fe/As = 20 solid, zero-valent iron [Fe(III)/ZVI = 10], at room temperature, outside the glove box. Note: PS – Parasymplesite, FS – ferrisymplesite. There were no unidentified peaks. Only the major peaks have been labeled in all three cases.

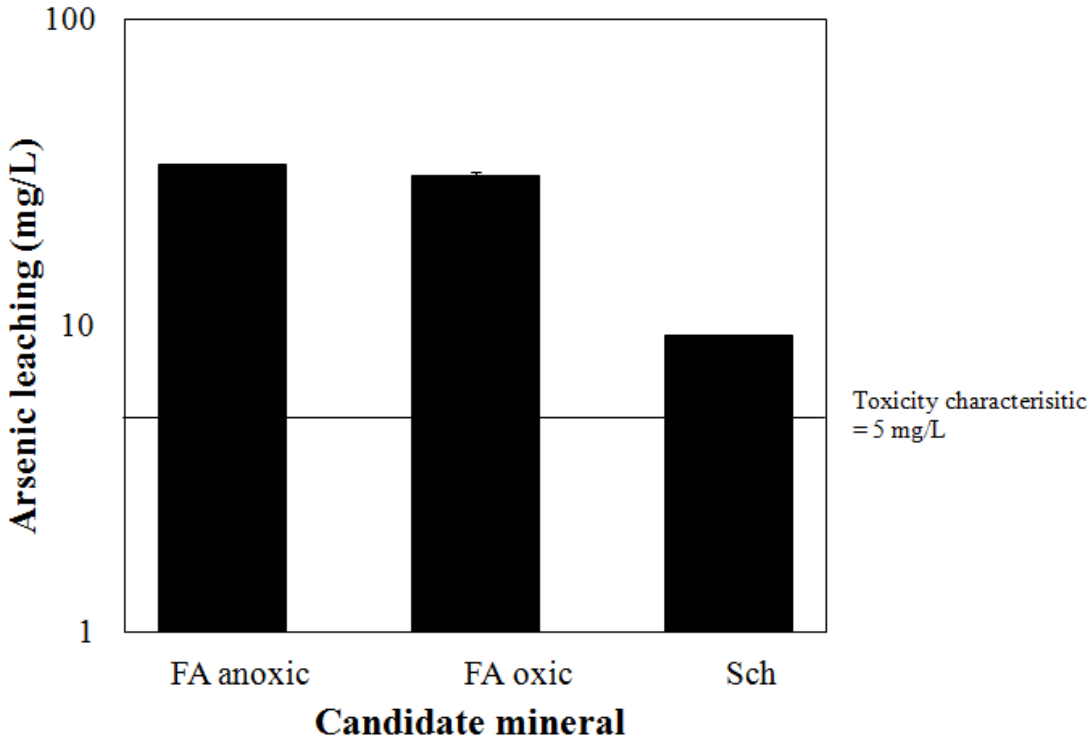

Figure 3.6. Arsenic leachate concentration from Simulated Landfill Leachate test on ferrous arsenate (FA) anoxic - Parasymplesite synthesized inside the glove box, FA oxic - Ferrisymplesite synthesized outside the glove box, and Sch - Arsenated-Schwertmannite.

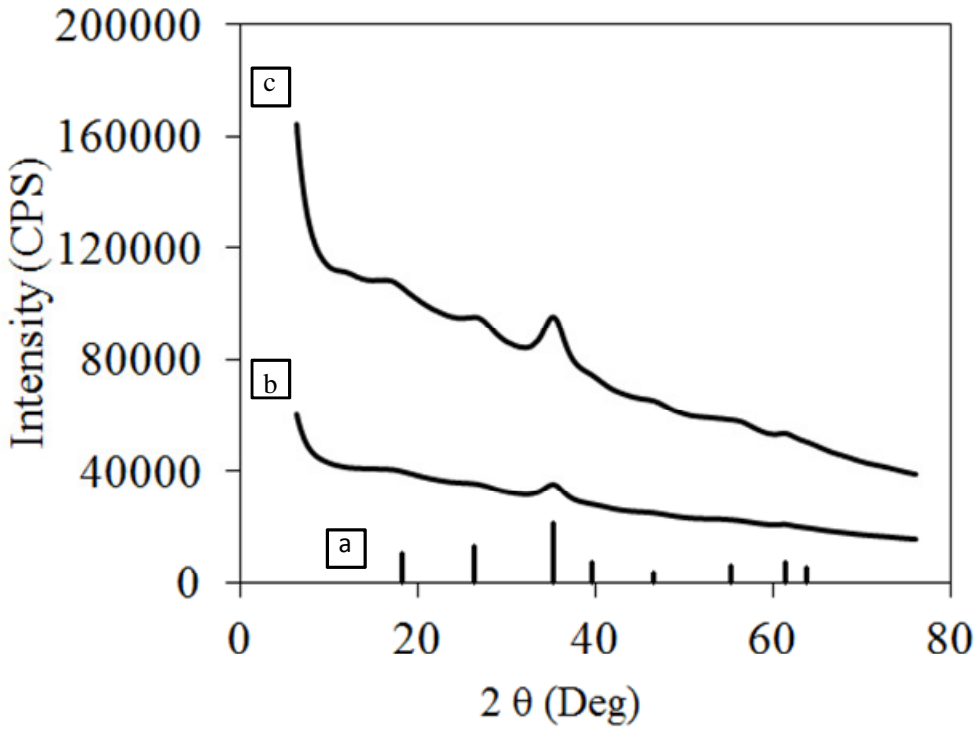

Figure 3.7. a.) XRD reference stick pattern for schwertmannite and Synchrotron XRD spectra for solid synthesized after 18 days from b.) lab synthesized arsenic-loaded ferrihydrite (Fe/As molar ratio = 20.46) following a procedure modified from Carlson et al. (2002) for arsenated-schwertmannite and b.) ferrihydrite following a procedure modified from Bigham et al. (1990) for schwertmannite synthesis.

Table 3.1. Summary of synthesis parameters for synthesis of scorodite under different temperatures

Temperature (°C)	Pressure (bar)	Initial pH	pH Control	Initial chemical composition			Method Reference
				$Fe(NO_3)_3$ (M)	NaH_2AsO_4 (M)	Fe/As molar ratio	
60	1	1.5	No	0.11	0.1	1.1	Dove and Rimstidt 1985
95	1	1.5	Yes	0.11	0.1	1.1	Demopoulos 1995
150	8	1	No	0.11	0.1	1.1	Dutrizac and Jambor 1988
230	11	1	No	0.11	0.1	1.1	Modified from Mambote et al. 2001

Table 3.2. Results of SEM-EDX analysis of tooeleite and solid synthesized from silica-coating of tooeleite

Sample	Accelerating voltage (kV)	Atom	Mean Atomic %*	Error (±σ)
Silica-amended Tooeleite	5	O Si	78.16 21.84	2.89 1.3
	10	O Si C	64.2 12.72 23.09	1.12 0.23 3.65
	15	O Si	61.18 7.38	0.94 0.11
	30	O Si Fe As	58.09 5.15 0.1 0.1	1.37 0.08 0.01 0.02
Tooeleite	5	O Fe As	56.3 13.37 10.08	1.48 1.56 0.27

* Mean atomic % values do not add up to a 100% because contribution from carbon (from the background carbon stub) and other trace impurities is not shown here.

Table 3.3. Characterization of ferrous arsenate (parasymplesite) synthesized from arsenic-loaded ferrihydrite

Mineral	mmole of Fe/g of wet solid*	mmole of As/g of wet solid*	Experimental Fe/As molar ratio	Theoretical Fe/As molar ratio (from stoichiometry)
Parasymplesite (anoxic synthesis in glove box)	0.04875	0.00936	5.2	1.5
Ferrisymplesite (oxic synthesis outside glove box)	0.0457	0.00756	6.04	1.5

* Water content of both solid was 99.15%.

Table 3.4. Summary of evaluation results of candidate minerals for Arsenic Crystallization Technology

Candidate mineral	Synthesis Conditions				Maximum expected As loading (wt/wt%) from stoichiometry or literature	% As loading observed in this study (wt/wt)	Advantages	Drawbacks
	T (°C)	Fe/As ratio	pH	Redox conditions				
Scorodite	>95	<2	<3	Oxidizing	~ 32%	NA	TCLP arsenic leaching below TC	High temperature, elevated pressure , low pH synthesis conditions
Arsenate apatite	4-90	<5	>11	Oxidizing	~ 35%	NA	TCLP arsenic leaching slightly below TC, simple synthesis conditions	Presence of Fe interferes with synthesis. Low arsenic capacity of arsenate. Tendency for hematite co-synthesis
Parasymplesite	25	1.5	7.5	Reducing	~ 25%	8.25%	Favorable synthesis conditions and TCLP arsenic leaching below TC	Relatively high arsenic leaching using SLL test

Ferrisymplesite	25	1.5	7.5	Oxidizing	~ 25%	6.67%	Favorable synthesis conditions and TCLP arsenic leaching below TC	Relatively high arsenic leaching using SLL test
Arsenated-Schwertmannite	60	20.46	2.6	Oxidizing	5.6	5.4-6.5%	Low arsenic leaching using TCLP and SLL test	Long duration of synthesis (atleast18 days)
Tooeleite	60	0.80	2.6	Oxidizing	~20-25%	~ 22%	High arsenic loading	High arsenic leaching using TCLP
Silica-amended Tooeleite	60	0.80	2.6	Oxidizing	NA	~ 21%	High arsenic loading	High arsenic leaching using TCLP

CHAPTER 4: MICROENCAPSULATION OF ARSENIC-BEARING SOLID RESIDUALS FOR LONG-TERM STABILIZATION UNDER LANDFILL CONDITIONS

Authors: Madhumitha Raghav, A. Eduardo Sáez, and Wendell P. Ela Department of Chemical and Environmental Engineering, The University of Arizona, Tucson, AZ 85641, USA

ABSTRACT

In this study, microencapsulation has been investigated as a technology for the long-term stabilization of iron-based arsenic-bearing solid residuals (ABSR) under mature, mixed solid waste landfill conditions. The strategy is to coat the ABSR with a mineral phase that isolates the arsenic in the ABSR and prevents its leaching. Previous studies have shown that ABSR subjected to simulated landfill conditions at laboratory scale release most of the arsenic on a time scale of one to two years. The arsenic that is retained is associated with secondary minerals formed during the time frame of the experiment. Powder X-ray diffraction (XRD) and X-ray Absorption Near Edge Structure (XANES) identified vivianite and siderite as the predominant secondary mineral phases that are stable at the end of the experiments. Hence, it was hypothesized that by coating the ABSRs with mineral phases like vivanite before landfill disposal, the stability of the ABSRs could be improved and the leaching of arsenic prevented or greatly reduced. Synthetic arsenic-loaded ferrihydrite (molar Fe/As ratio= 4) was used as the starting ABSR as it is representative of the ABSRs generated in water treatment facilities. Microencapsulation trials were performed in the presence of arsenic-loaded ferrihydrite and compared with

mixed system trials which involved mixing pre-formed vivianite with the arsenic-loaded ferrihydrite solid. PHREEQC modeling was performed to corroborate the experimental results. Synthesized solids were characterized using scanning electron microscopy (SEM) and X-ray Diffraction (XRD) analysis, and the most promising products evaluated using leaching trials. Aqueous arsenic concentrations before leaching for the microencapsulation trials showed a decrease in access to the arsenic-loaded ferrihydrite surface, indicating at least partial coating of the surface by vivianite and mass-transfer limited release. However, this advantage provided by the microencapsulation procedure was lost upon exposure to more stringent leaching conditions.

Keywords: Iron, arsenic, vivianite, encapsulation, landfills.

1. Introduction

Arsenic is a ubiquitous element that occurs in natural soils, sediments and rocks in the form of various arsenic-containing minerals. The dissolution of these minerals via slow geologic processes results in the introduction of arsenic into groundwater sources (Smedley and Kinniburgh 2002). Waste streams from some industrial processes, such as mining and wood preservation activities, also introduce arsenic into the environment (Smedley and Kinniburgh 2002).

The revised Arsenic Rule (USEPA) reduced the maximum contaminant level (MCL) for arsenic in drinking water from 50 mg/L to 10 mg/Lin 2006. It has been estimated that 10,000 tons of arsenic bearing solid residuals (ABSRs) are being generated every year as a result of this rule (Impellitteri and Scheckel 2006). Iron oxides are commonly used in water treatment processes for removing arsenic due to their high capacity and high affinity for arsenic (USEPA 2000; Jekel and Amy 2006) and consequently make up the greatest mass of ABSRs generated. It is well established that microbially induced reductive dissolution of iron oxides under landfill conditions can cause release of the associated arsenic (Pedersen et al. 2006; Ghosh et al. 2006a; Kocar et al. 2006).

Vitrification and solidification/stabilization are conventional technologies used for toxic waste stabilization (USEPA 2002). Vitrification is the Best Demonstrated Available Technology (BDAT) for stabilization of arsenic-bearing solids. It involves heating the arsenic-bearing solid to an extremely high temperature (2630-3330^{o}F) and then cooling

down to room temperature. But, it is not a viable technology for the stabilization of ABSRs because of the high temperature and high cost involved (USEPA 2000).

Solidification/stabilization involves mixing the toxic waste with binders such as Portland cement, concrete or fly ash and allowing time for curing into a solid form (Dutre and Vandecasteele 1998; Dawadi et al. 2004; Singh and Pant 2006; Chintalapati et al. 2009). The technology involves stabilizing the hazardous waste forms by both physical and chemical processes. The hazardous waste is physically bound/enclosed by the binders and also chemically converted to a solid with lower solubility, mobility and toxicity.

Polymer encapsulation has been investigated as a viable technology for the long-term stabilization of arsenic-bearing solid residuals (Carter et al. 1995; Shaw et al. 2008). It involves creating an epoxy resin/rubber matrix and mixing with a large mass of waste to form a solidified monolith. Testing of a polymeric encapsulation shows that it is promising, both technically and economically, but it is yet to be adopted commercially (Shaw et al. 2008).

Microencapsulation is a stabilization process that coats every grain/particle of the toxic waste with an impermeable, inert layer as opposed to coating a large block of solidified waste. Microencapsulation with ferric phosphate coatings has been used to protect pyrite surfaces in mining wastes from oxidation (Evangelou 1995). The ferric phosphate coatings were produced by leaching the pyrite surface with phosphate solution containing hydrogen peroxide. The H_2O_2 containing phosphate solution caused Fe^{3+} release by leaching of the pyrite, forming a passive coating of ferric phosphate on the pyrite surface.

The ferric phosphate coating reduced pyrite leaching to 20% (as opposed to 80% for uncoated pyrite) when exposed to 0.088 mol L^{-1} H_2O_2 for 800 minutes.

Scorodite ($FeAsO_4 \cdot 2H_2O$) microencapsulation by controlled deposition of aluminum phosphate coatings has been reported by Lagno et al. (2010). This encapsulation technique was found to stabilize the scorodite particles against pH and redox potential variations. Arsenic release from scorodite was reduced by more than one order of magnitude after encapsulation with aluminum hydroxide.

Vivianite is a ferrous phosphate mineral $Fe_3(PO_4)_2.8H_2O$ that is found in anoxic environments such as lakes and river sediments (Postma 1981; Fagel et al. 2005; Taylor and Boult 2007). Several studies have predicted ground waters in the Bengal delta and reduced aquifers from the Red river flood plain, Vietnam, to be supersaturated with respect to vivianite due to elevated concentrations of phosphate (Zheng et al. 2004; Ahmed et al. 2004; Postma et al. 2007). Vivianite precipitation controls phosphate concentration in anaerobic lake sediments and other natural soils (Nriagu and Dell 1974; Emerson 1976).

Vivianite has been successfully synthesized in the laboratory via both biotic and abiotic synthesis routes (Nriagu 1972; Fredrickson et al. 1998; Brown et al. 1999). Several studies have observed vivianite form as a secondary mineral from reductive transformation of Fe (III) hydroxides (Emerson and Widmer 1978; Zachara et al. 1998; Jorand et al. 2000; Glasauer et al. 2003). For instance, Glasauer et al. (2003) found that

vivianite was the stable end-product after reduction of hydrous ferric oxide by dissimilatory iron reducing bacteria in the presence of a medium containing 4.0 mmol/L P (inorganic phosphate). The released iron precipitates as secondary iron minerals such as vivianite, siderite and ferrous sulfide. These minerals were found to persist in biological columns under simulated landfill conditions for long durations. For instance, significant amounts of vivianite were found in biological columns operated for as long as 1-2 years under simulated landfill conditions as shown in Table 1 (Alday 2010; Root et al. under review; Fathordoobadi, unpublished results). XRF maps also showed evidence of some inaccessible arsenic that could possibly be coated by iron rich solids. This suggested that the arsenic-bearing solids were being coated/encapsulated by the secondary iron minerals precipitating inside the column, which makes them inaccessible to further reductive dissolution (Root et al. under review). These results were the motivation for the microencapsulation efforts in this study.

The objectives of this work were (i.) microencapsulation of lab-synthesized ABSR by vivianite, and (ii.) investigation of the efficiency of ABSR microencapsulation by vivianite.

A number of previously investigated Fe-As-P system interactions can potentially affect the vivianite microencapsulation of arsenate-loaded ferrihydrite: (i.) effect of sorbed ferrous ions on the reductive transformation of Fe(III) hydroxides (ii.) effect of sorbed or co-precipitated arsenic on such a transformation, (iii.) effect of phosphate sorption on such a transformation, (iv.) effect of competitive sorption processes between phosphate

and arsenate on ferrihydrite and vivianite, and (iv.) effect of vivianite uptake capacity for arsenic.

Although vivianite was investigated as an encapsulant and not as a sink for arsenic, there have been studies reporting the uptake of arsenic by biogenic vivianite (Islam et al. 2005; Thinnappan et al. 2008; Silva et al. 2012) and this could be an important mechanism of arsenic stabilization in the vivianite-ABSR system.

The competitive sorption behavior of phosphate resulting in the mobilization of arsenic from mineral surfaces has been well studied (Jackson and Miller 2000; Mohapatra et al. 2005; Violante and Pigna 2002; Zhao and Stanforth 2001; Ghosh et al. 2006b). Phosphate is known to have affinity for Fe and Al-oxide surfaces and, form inner-sphere complexes on mineral surfaces similar to arsenate (Arai and Sparks 2001; Gao and Mucci 2001). The acid dissociation constants for phosphate (pK_{a1} = 2.1, pK_{a2} = 7.2, pK_{a3} = 12.3) are also similar to those of arsenate (pK_{a1} = 2.2, pK_{a2} = 6.9, pK_{a3} = 11.4).

Phosphate has also been found to alter the surface reactivity of iron oxide surfaces (Borch et al. 2007). Borch et al. (2007) found that the presence of phosphate not only reduced the extent of Fe(III) reduction by *Shewanella putrefaciens* but also changed the bio-transformation pathway. The transformation of ferrihydrite to goethite was not observed in the presence of phosphate. This was due to the inhibition of ferrihydrite dissolution which is a critical step in the transformation (Galvez et al. 1999; Paige et al. 1997; Willett 1985). Phosphate influenced alterations to iron oxide transformation rates and pathways

have been observed in biotic as well as abiotic systems as evidenced in the aforementioned studies.

Fe (II) catalyzed transformation of iron oxides and fate of the associated arsenic has also been widely studied in literature (Pedersen et al. 2006; Hansel et al. 2003; Yee et al. 2006; Burton et al. 2010; Mukiibi et al. 2008). Fe(II) produced by microbial reduction of Fe(III) oxides or added as ferrous chloride can accelerate the transformation of iron oxides like ferrihydrite and schwertmannite to more stable oxides such as magnetite and goethite. The fate of the associated arsenic would depend on the product of such transformations.

2. Materials and Methods

2.1. Preparation of Synthetic Arsenic-loaded Ferrihydrite

Arsenic-loaded ferrihydrite solid (with Fe/As molar ratio = 4:1) was synthesized to mimic the arsenic bearing solid residuals (ABSRs) generated from water treatment processes to remove arsenic (e.g.; co-precipitation with ferric salts; adsorption of granular ferric hydroxide, activated carbon, activated alumina; ion exchange; nanofiltration). The solid was prepared by mixing equal volumes of 1.00 M anhydrous ferric chloride and 0.0500 M sodium arsenate heptahydrate ($Na_2HAsO_4.7H_2O$, KR Grade, Sigma- Aldrich). The mixture was stirred using an overhead stirrer (Arrow 1750) and titrated with 10 M NaOH to obtain a pH of 7.0 within 1 hour. The suspension was allowed to settle and equilibrate

for 48 hours. The pH fluctuated by ± 0.3 during this period and was adjusted back to 7 as necessary using 0.1 M HCl or 0.1 M NaOH. The pH of the suspension was monitored for another 48 hours to ensure that it had stabilized at 7.0, but no further pH adjustment was required in the second 48 hour period. The precipitate was then vacuum filtered using 0.22 µm filters to achieve a water content of approximately 75% wt and rinsed multiple times with deionized water to remove residual salts. The solid thus obtained was transferred to high density polyethylene storage jars, sealed tightly using parafilm, and stored at 4°C for later use.

2.2. Characterization and Analytical Methods

The total iron and arsenic contents of the synthesized arsenic-loaded ferrihydrite (Fe/As = 4) were determined after microwave digestion of known amounts of the solid. Solid samples of 0.5 g each were carefully weighed and digested in 14.5 mL of concentrated nitric acid for 20 minutes using a CEM MDS 2100 Microwave Digestion System. Three replicates were run in each case. Digested samples were diluted and analyzed for iron content using the phenanthroline test (Clesceri et al. 1998) and for arsenic content using an Inductively Coupled Plasma Mass Spectrometer (ICPMS, Agilent 7500a). The Fe/As molar ratio of the arsenic-loaded ferrihydrite was confirmed to be 3.97 and the water content was 78.1%.

Aqueous samples were filtered using 0.22 µm cellulose nitrate filters (Millipore) before analyzing for iron, arsenic and phosphorus concentrations. To 1 mL of sample (original or diluted with deionized water depending on the initial concentrations of the analyte),

0.5 mL of 1% acetic acid and 0.5 mL of 3.42 mM EDTA were added to preserve samples for total arsenic and phosphorus analysis. The samples were kept frozen until ICPMS analysis.

The crystalline phases in the bulk samples were identified using XRD spectra collected on a Bruker D8 ADVANCE diffractometer using Cu$K\alpha$ radiation. The samples were scanned from 5° to 90° for over 285 minutes. Peaks were matched against those in the International Centre for Diffraction Data (ICDD) database. A Hitachi S-4800 II Field Emission Scanning Electron Microscope was used to obtain the SEM images of the solid phases. Energy Dispersive X-ray (EDX) spectroscopy analysis was performed to obtain elemental composition of the synthesized solids using a Thermo Scientific Si(Li) detector equipped with Noran System Six.

Elemental X-ray mapping, Transmission Electron Microscopy (TEM) imaging, and Fourier Transform Infrared Spectroscopy (FTIR) were also used to characterize the synthesized solids. More information about characterization efforts can be found in Appendix A.

An acetic acid leaching procedure was used for evaluation of the stability of the solids synthesized in this study. This test is a modified version of the standard TCLP using extended duration of leaching (50 hours as opposed to 18 hours) under anoxic conditions. The anoxic conditions used in this test better simulate the conditions in a mature landfill. The supernatant was removed to obtain 40 mL of wet slurry, which was transferred to a

120 mL plastic bottle. 10 mL of 0.5 M acetic acid was added and the pH was raised to 4.85± 0.15 using less than 1 mL of 5 M NaOH. Three replicates were run for all samples. One batch of synthesized solid was used for one replicate of the leaching test. The plastic bottles were placed in an end-to-end shaker for 50 hours inside a glove box (Terra Universal Critical Environment Solutions) purged with nitrogen. The pH was measured and found to remain at 4.9 ± 0.2 at the end of the 50 hours.

2.3. PHREEQC Modeling

The geochemical software PHREEQC-2 (Parkhurst and Appelo 1999) was used to predict the aqueous arsenic and phosphorus concentrations before and after leaching (using the acetic acid leaching procedure described above). Thermodynamic data for modeling were obtained from the wateq4 database. The generalized two-layer, surface complexation model of Dzombak and Morel (1990) was used to simulate the sorption equilibria between aqueous species and the ferrihydrite surface. Two types of sorption sites were used, ≡(s)FeOH and ≡(w)FeOH, to indicate strong and weak sites, respectively. Literature values for the surface area and site densities of ferrihydrite (600 m^2/g, 0.005 mol/mol Fe for ≡(s)FeOH, and 0.2 mol/mol Fe for ≡(w)FeOH) were used (Dzombak and Morel 1990). Some studies have used a weak site density of 0.4 mol/mol Fe in the case of high As/Fe loading experiments (Dixit and Hering 2006; Burnol et al. 2007). A weak site density of 0.3 mol/mol Fe worked well for our system and was used throughout.

2.4. Experimental Setup

2.4.1.Vivianite Synthesis Trials - Instantaneous Addition vs. Continuous Dosing

Experiments were conducted at different total phosphorus to Fe(II) ratios [TOTP/Fe(II)] and different absolute concentrations of total phosphorus and Fe(II) (Table 2). Sodium phosphate (Na_2HPO_4) and ferrous chloride tetrahydrate ($FeCl_2.4H_2O$) solutions were mixed to reach the desired concentrations and 2.00M NaOH was added to adjust the synthesis pH to be in the range 7 ± 0.4. The concentrations (Table 2) are not final concentrations of total phosphate and ferrous iron measured after precipitation of solids, but concentrations assuming only dilution of the stock solutions.

Another set of trials was performed with continuous addition of ferrous and phosphate solutions using a syringe pump as opposed to instantaneous addition. A molar TOTP/Fe(II) ratio of 3 was used in these trials. 180 mL of 0.30 M sodium phosphate (Na_2HPO_4) solution and 180 mL of 0.10 M ferrous chloride tetrahydrate ($FeCl_2.4H_2O$) solution were simultaneously fed using a syringe pump into a 1000 mL beaker filled with 400 mL of deionized, deoxygenated water and mixed with an overhead stirrer. The feed rates of the two solutions were varied at 180 mL/hr, 90 mL/hr, 36 mL/hr, 15 mL/hr and 7.5mL/hr, to feed the entire volume of each solution within 1, 2, 5, 12 and 24 hours, respectively, in five separate trials.

After each trial, the beaker was transferred to a glove box purged with nitrogen and the suspension allowed to settle for 48 hours after which aqueous samples were collected for

total arsenic and phosphorus concentrations. More details on the analytical procedure for aqueous sampling are given in the Characterization and Analytical Methods section.

2.4.2. Mixed System Synthesis Trials (Pre-formed Vivianite and ABSR)

180 mL of 0.3 M sodium phosphate (Na_2HPO_4) solution and 180 mL of 0.1 M ferrous chloride tetrahydrate ($FeCl_2.4H_2O$) solution were simultaneously fed using a syringe pump into a 1000 mL beaker filled with 400 mL of deionized, deoxygenated water and mixed with an overhead stirrer. The feed rates of the two solutions were maintained at 180 mL/hr, 90 mL/hr and 36 mL/hr to feed the entire volume of each solution within 1, 2 and 5 hours, respectively.

4.566 g of wet Fe/As = 4 solid (1±0.05 g dry solid) was added to 50 mL of deionized, deoxygenated water and homogenized using an overhead stirrer for 30 minutes. At the end of the 2 hour dosing period this suspension was added to the 760 mL from before and mixed for an additional 20 minutes.

2.4.3. Microencapsulation Trials

Encapsulation trials were performed using continuous addition of ferrous and phosphate solutions to a solution containing 1±0.05 g of dry arsenic-loaded ferrihydrite (Fe/As = 4). 180 mL of 0.3 M sodium phosphate (Na_2HPO_4) solution and 180 mL of 0.1 M ferrous chloride tetrahydrate ($FeCl_2.4H_2O$) solution were simultaneously fed using a syringe

pump into a 1000 mL beaker filled with 400 mL of deionized, deoxygenated water and mixed with an overhead stirrer. A feed rate of 90 mL/hr was used to feed the entire volume of each solution within 2 hours.

3. Results and Discussion

The total phosphorus to ferrous iron ratio [TOTP/Fe(II)] ratio, absolute ferrous iron and phosphate concentrations, and pH for the vivanite synthesis trials using instantaneous addition are reported in Table 2 along with the observed pH and supersaturation indices calculated using PHREEQC. A clear correlation was observed between the formation of crystalline vivianite and the supersaturation index. It was found that the experimental conditions resulting in supersaturation indices less than or equal to 9.02 yielded an amorphous product. The conditions resulting in supersaturation indices greater than or equal to 9.87 yielded crystalline vivianite. It was also observed that the XRD peaks for vivianite were stronger with increasing supersaturation index values (Figure 1).

Mixed system trials and microencapsulation trials were also performed using instantaneous addition of all chemicals. In case of the microencapsulation trials, Fe(II) and phosphate solutions were added to a suspension containing the arsenic-loaded ferrihydrite (Fe/As = 4) solid. Arsenic-loaded ferrihydrite was mixed with pre-formed vivianite generated by continuous addition of Fe(II) and phosphate solutions in the case of the mixed system trials. The mixed system trials were used as a reference against which to check if vivianite particles were coating the ferrihydrite surface in the

microencapsulation trials. The experimental conditions of TOTP/Fe(II) = 3 (molar ratio), 0.02845 M phosphate and 9.483 mM Fe(II) were selected because they yielded the most crystalline vivianite solid at near neutral pH conditions (Figure 1). The final solids generated in both set of trials were characterized using XRD, SEM, and SEM-EDX elemental mapping to confirm vivianite presence and provide evidence regarding encapsulation. The goal was to understand whether the vivianite particles were nucleating on the surface of existing ferrihydrite particles (heterogeneous nucleation) and causing encapsulation or nucleating independently (homogeneous nucleation) and subsequently growing on the freshly nucleated vivianite without causing encapsulation. It was hypothesized that if the vivianite particles nucleated and grew on the surface of the existing ferrihydrite particles, they could coat and possibly render the associated arsenic recalcitrant to leaching.

The SEM images and elemental maps in both set of trials were not conclusive but there was some indication of vivianite particles nucleating independent of the ferrihydrite particles (Appendix A). However using SEM, it was not possible to clearly discern whether the vivianite particles were nucleating and growing on the ferrihydrite surface in addition to homogeneous nucleation and crystal growth. Since evidence for homogeneous nucleation was observed, it was decided that the conditions used were probably not ideal for microencapsulation of the ferrihydrite particles. A likely reason for this was the high supersaturation index created in this trial. Homogeneous nucleation is favored under high supersaturation conditions since the activation energy barrier to form stable nuclei can be exceeded under such conditions. The presence of a seed crystal with good structural

compatibility with the precipitating solid lowers the activation barrier and favors heterogeneous nucleation on the seed crystal surface at a lower supersaturation index. We did not undertake detailed research into the structural compatibility of the ferrihydrite and vivianite solids as it was outside the scope of this work.

In order to favor heterogeneous nucleation of vivianite, continuous dosing of the ferrous chloride and sodium phosphate was implemented using a syringe pump. First, vivianite synthesis (without any arsenic-loaded ferrihydrite solid) was evaluated at different dosing rates. Feed rates of the ferrous and phosphate solutions were varied at 180 mL/hr, 90 mL/hr, 36 mL/hr, 15 mL/hr and 7.5mL/hr in separate trials in order to feed the ferrous and phosphate solutions within 1, 2, 5, 12 and 24 hours respectively. It was found that the trials at feed rates of 180 mL/hr, 90 mL/hr, 36 mL/hr, all generated crystalline vivianite as detected by XRD (Figure 2). Comparison of the SEM images for the solid obtained from the vivianite synthesis trials under these conditions suggested that the local crystal structure was being lost on decreasing the feed rate of the ferrous and phosphate solutions (Figure 3). But comparison of the XRD spectra did not show any significant difference in the peak location or intensity for solids generated at these three rates of addition. Hence, it is possible that the vivianite particles forming at lower rates of addition were smaller and their crystal habitat could not be observed at the resolution achieved using the SEM instrument employed in this study.

A feed rate of 90 mL/hr (feed duration of 2 hours) was selected for further microencapsulation trials and mixed system trials. Figure 4 shows the SEM image and

elemental information from EDX analysis for the final solid obtained from the microencapsulation trials using continuous dosing. Two different types of particles can be clearly seen. From EDX spectroscopy, the Fe/P and Fe/As ratios of particles 1 and 3 are similar and quite different from those of particle 2. Particles 1 and 3 look like ferrihydrite particles whereas the morphology of particle 2 looks like that of crystalline vivianite. This suggests that vivianite particles are nucleating independently even when continuous, slow dosing of ferrous and phosphate solutions was used. But this does not rule out the possibility of vivianite also coating the ferrihydrite surface. Hence, it was decided to evaluate the effectiveness of the microencapsulation procedure using other techniques such as elemental maps, TEM images, FTIR spectra, total aqueous arsenic and phosphorus concentrations in equilibrium with the solids after 48 hours and after leaching with acetic acid. Results from TEM imaging, elemental mapping and FTIR analysis were all inconclusive in that it was not possible to observe any significant differences between the two trials. More details on these efforts are provided in Appendix A.

PHREEQC modeling was used to predict the total aqueous arsenic and phosphorus concentrations before and after leaching in the different systems studied here except for the microencapsulation system. PHREEQC modeling of microencapsulation must a priori assume that the ferrihydrite is completely encapsulated by vivianite in which it would play no role in the equilibrium model or that the ferrihydrite is not completely encapsulated (in other words it acts as a separate solid phase in what is now a two solid phase system). The former case is the modeling of the vivianite only system, whereas the latter case is the vivianite plus ferrihydrite mixed solid system. There is one additional

possible equilibrium case: where a portion of the ferrihydrite is fully encapsulated (inaccessible to solution equilibria) and the balance of the ferrihydrite is only partially encapsulated (subject to solution-solid equilibria). This case was not considered because neither the fraction encapsulated is measurable nor can the program calculate the transitory state concentrations prior to equilibria.The total arsenate and phosphate balances are as follows:

$$\text{Total Arsenic (mg)} = As_{aq} + As_{ferrihydrite} + As_{vivianite} \quad \text{Eq1}$$

where,

As_{aq} = aqueous arsenic (mg)

$As_{ferrihydrite}$ = arsenic associated with ferrihydrite (mg)

$As_{vivianite}$ = arsenic associated with vivianite (mg)

Or,

$$\text{Total As (mg)} = (C_{As,aq})(V) + (K_{,dferr})(C_{As,aq})(m_{ferr}) + (K_{d,viv})(C_{As,aq})(m_{viv}) \quad \text{Eq2}$$

where,

$C_{As,aq}$ = aqueous arsenic concentration in mg/L

V = volume of solution in L

$K_{d,ferr}$ = [mg As/ kg ferrihydrite] / [mg As/ L water]

$K_{d,viv}$ = [mg As/ kg vivianite] / [mg As/ L water]

m_{ferr} = mass of ferrihydrite in kg

m_{viv} = mass of vivianite in kg

Although, vivianite was intended to be an encapsulant around the arsenic-loaded ferrihydrite and not a sink for arsenic, significant uptake of arsenate by vivianite has been

reported in literature (Islam et al. 2005; Thinnappan et al. 2008) and hence cannot be ignored in the modeling efforts. In modeling the mixed system trials and microencapsulation trials, both vivianite and ferrihydrite were assumed to be present at equilibrium (with supersaturation index = 0). But, the PHREEQC model used did not include arsenate sorption on vivianite due to lack of information on vivianite surface site densities and other surface properties. Hence, PHREEQC predicted arsenic concentrations both before and after leaching only assumed sorption on the ferrihydrite surface as follows:

$$\text{Total Arsenic (mg)} = (As_{aq})(V) + (K_{,dferr})\,(C_{As,aq})(m_{ferr}) \qquad \text{Eq3}$$

An iterative, trial and error method as shown below was used to arrive at the arsenic concentration (before and after leaching) in equilibrium with both the ferrihydrite and vivianite solids at the conditions employed in this study:

Step 1: Assume total arsenic (in mg) lower than the actual arsenic used in the experiment.

Step 2: Predict arsenic partitioning into solution (water or acetic acid leaching solution) and ferrihydrite surface using PHREEQC.

Step 3: Use the aqueous arsenic concentration ($C_{As,aq}$) predicted from Step 2 and $K_{d,viv}$ of 180 [mg As/ kg vivianite] / [mg As/ L water] from literature (Thinnappan et al. 2008), calculate total arsenic (in mg) accounting for arsenate sorption on vivianite as well (according to Eq2).

Step 4: Check if total arsenic calculated from Step 3 equals experimental total arsenic. If yes, the arsenic concentration predicted in step 2 is the aqueous arsenic concentration in

equilibrium with both the ferrihydrite and vivianite solids. If no, then adjust assumption for total arsenic and repeat the above steps.

Phosphate balance is the system is as follows:

Total Phosphorus (in mg) = $P_{aq} + P_{ferrihydrite} + P_{vivianite}$ Eq4

where,

P_{aq}= aqueous phosphorus (mg)

$P_{ferrihydrite}$ = phosphorus associated with ferrihydrite (mg)

$P_{vivianite}$ = phosphorus associated with vivianite (mg)

The total phosphorous concentrations at equilibrium in the vivianite system and the mixed system were predicted by PHREEQC modeling (Figure 5). The total phosphorus concentrations in the two cases were comparable and also agreed well with their corresponding observed concentrations and the observed concentration in the microencapsulation trial. These results not only indicate that the PHREEQC model simulated the systems well, but also that vivianite precipitation controlled the total phosphorus concentration at equilibrium in all three systems (vivianite, mixed and microencapsulation trials).

Aqueous arsenic concentrations before leaching were predicted for the pure arsenic loaded ferrihydrite (Fe/As = 4) and the mixed system using PHREEQC modeling. Aqueous arsenic concentration was also predicted for arsenic-loaded ferrihydrite in the presence of 1718.5 mg/L P (total phosphorus concentration at equilibrium with vivianite, see Figure 6). This was done to understand the effect of phosphate sorption and the

subsequent release of some previously sorbed arsenate from the arsenic-loaded ferrihydrite. These predicted concentrations along with the observed concentrations for the mixed system and the microencapsulation system are shown in Figure 6.

The observed aqueous arsenic concentration in the microencapsulation trials was lower than that observed in the mixed system by around a factor of two. The observed aqueous arsenic concentration in the microencapsulation trial was also lower than the concentrations predicted for the arsenic loaded ferrihydrite (Fe/As = 4) solid, the mixed system, and arsenic-loaded ferrihydrite in the presence of 1718.5 mg/L P.

The lower aqueous arsenic concentration observed in the microencapsulation trials indicates decreased accessibility of the arsenic-loaded ferrihydrite particles. These results are consistent with at least a partial coating of the arsenic-loaded ferrihydrite particles by the vivianite leading to a kinetic or mass transfer limited release of arsenic within the time-frame of the experiments. The total arsenic concentration in the mixed system trials is higher than that for the arsenic loaded ferrihydrite and the microencapsulation systems possibly due to competitive desorption of arsenate from the ferrihydrite surface by the phosphate ions added. These results showed some promise for using microencapsulation as an arsenic stabilization technique. Hence, the solids were subjected to acetic acid leaching to evaluate their stability under more aggressive conditions.

The equilibrium aqueous arsenic concentrations after leaching were predicted using PHREEQC for the arsenic-loaded ferrihydrite and the solids from the mixed system trials. These predicted concentrations were compared with their corresponding observed concentrations and the observed concentrations in the microencapsulation trial (Figure 7).

The arsenic concentration in the microencapsulation trials after exposure to the acetic acid leaching solution was comparable to that observed in the mixed system trials. The arsenic concentration for arsenic-loaded ferrihydrite (Fe/As = 4) was lower than that observed in the other two systems indicating better stability of the arsenic-loaded ferrihydrite (Fe/As = 4) solid under these conditions. These results suggest that the apparent advantage provided by the microencapsulation procedure (decrease in accessibility to the arsenic-loaded ferrihydrite) is lost when the solids are exposed to the more aggressive acetic acid leaching solution. In fact, there is an increase in arsenic leaching as compared to that of the arsenic-loaded ferrihydrite, possibly due to competitive desorption of arsenate on the exposed ferrihydrite surface by phosphate in solution. This is consistent with the arsenic in the mixed and the microencapsulation systems being equal.

PHREEQC modeling does not indicate any dissolution of the vivianite solid under the conditions of the acetic acid leaching test. The mechanism behind this increased leaching in the microencapsulation system is not clear. It is possible that any vivianite coating formed during the encapsulation procedure was detached from the ferrihydrite surface and exposed it to the leaching solution causing an increase in the aqueous arsenic concentration.

4. Conclusions

In this study microencapsulation was studied as an arsenic stabilization technology. Vivianite was studied as an encapsulant for arsenic-loaded ferrihydrite. The observed aqueous arsenic concentration in the microencapsulation trials indicated a decrease in accessibility to the arsenic-loaded ferrihydrite, which was consistent with at least a partial coating of the ferrihydrite surface and mass transfer limited release of arsenic. But this advantage (reduction in aqueous arsenic concentration) was lost upon exposure to the leaching solution, where an increase in arsenic leaching was observed. Results from this study seem to suggest that the phosphate system might not be a good option for encapsulation due to its significant competition with arsenate for sorption sites on ferrihydrite. This may also be the case with other anions such as carbonate that are known to compete with arsenate for sorption sites on ferrihydrite.

For the microencapsulation procedure, success would be defined by a decrease in accessibility of the arsenic-bearing solid core that is maintained even under conditions of an aggressive leaching solution. Results indicate that success of the microencapsulation procedure depends not only on the stability of the encapsulant under conditions of the leaching test, but also on the type and strength of association between the core and the encapsulant. Hence, more research is needed to select candidate encapsulants that would be stable under landfill conditions and also form strong associations/bonds with the arsenic-loaded ferrihydrite surface. Once a candidate mineral is selected, synthesis

conditions such as dosage rate and core:encapsulant ratio (molar) should be optimized in order to form a uniform coating around the arsenic core and improve stability of the solid. Spectroscopic tools (e.g.; extended X-Ray Absorption Fine Structure, EXAFS) can be used to study the effect of synthesis conditions on the coating effectiveness (e.g., thickness, uniformity of coating etc.) and mechanisms of arsenic stabilization in the encapsulated solid.

Acknowledgements

This work was supported by the National Institute of Environmental Health Sciences (NIEHS) Grant No. P42 ES04940. The authors declare no conflict of interest. This paper's contents are solely the responsibility of the authors and do not necessarily represent the official views of NIEHS. The authors thank Phil Anderson and Steven Hernandez of the University Spectroscopic Imaging Facility at the University of Arizona for XRD and SEM analyses of solids respectively and Mary Kay Amistadi for the arsenic and phosphorus analyses. The analyses for total arsenic and phosphorus concentrations were performed by the Arizona Laboratory for Emerging Contaminants (ALEC) at the University of Arizona from our NIEHS-supported Superfund Research Program Grant.

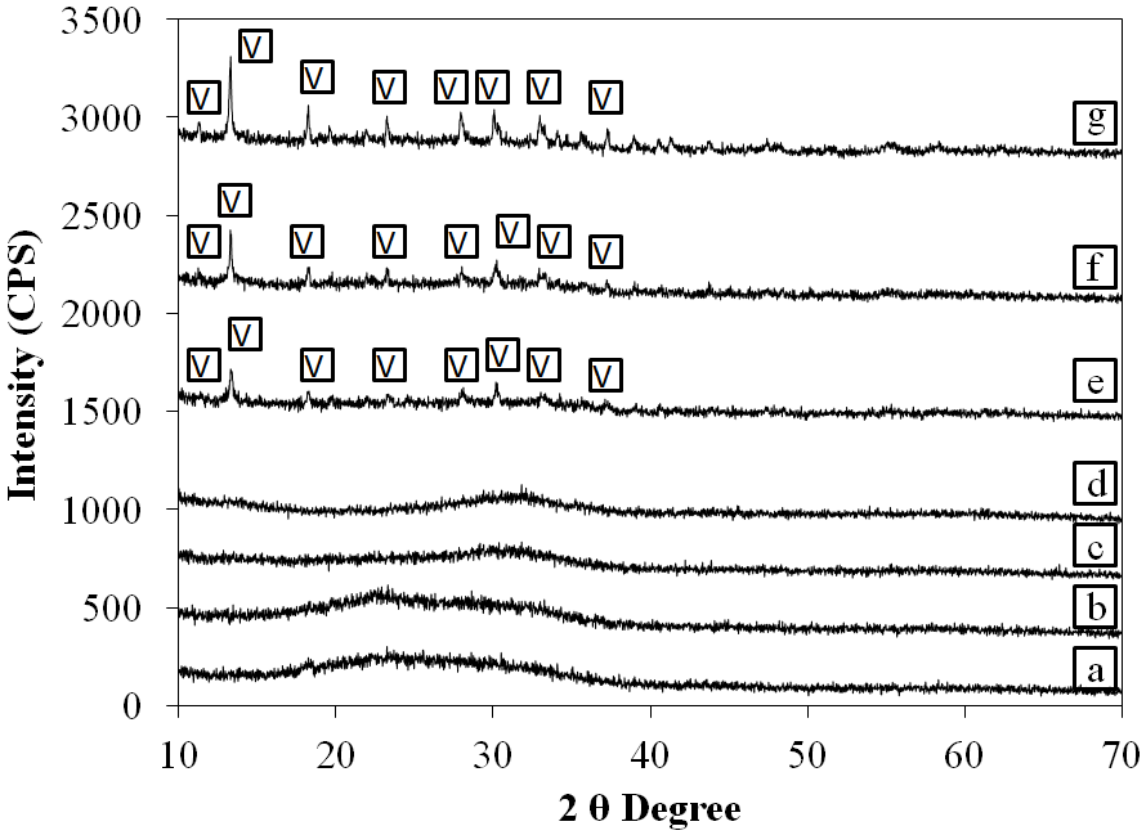

Figure 4.1. XRD spectra for final solid in vivianite synthesis trials using instantaneous addition of ferrous and phosphate solutions and total phosphorus to Fe(II) molar ratios of: a.) TOTP/Fe(II) = 333.33, b.) TOTP/Fe(II) = 190.47, c.) TOTP/Fe(II) = 82.67, d.) TOTP/Fe(II) =15, e.) TOTP/Fe(II) = 5, f.) TOTP/Fe(II) = 4, g.) TOTP/Fe(II) = 3.

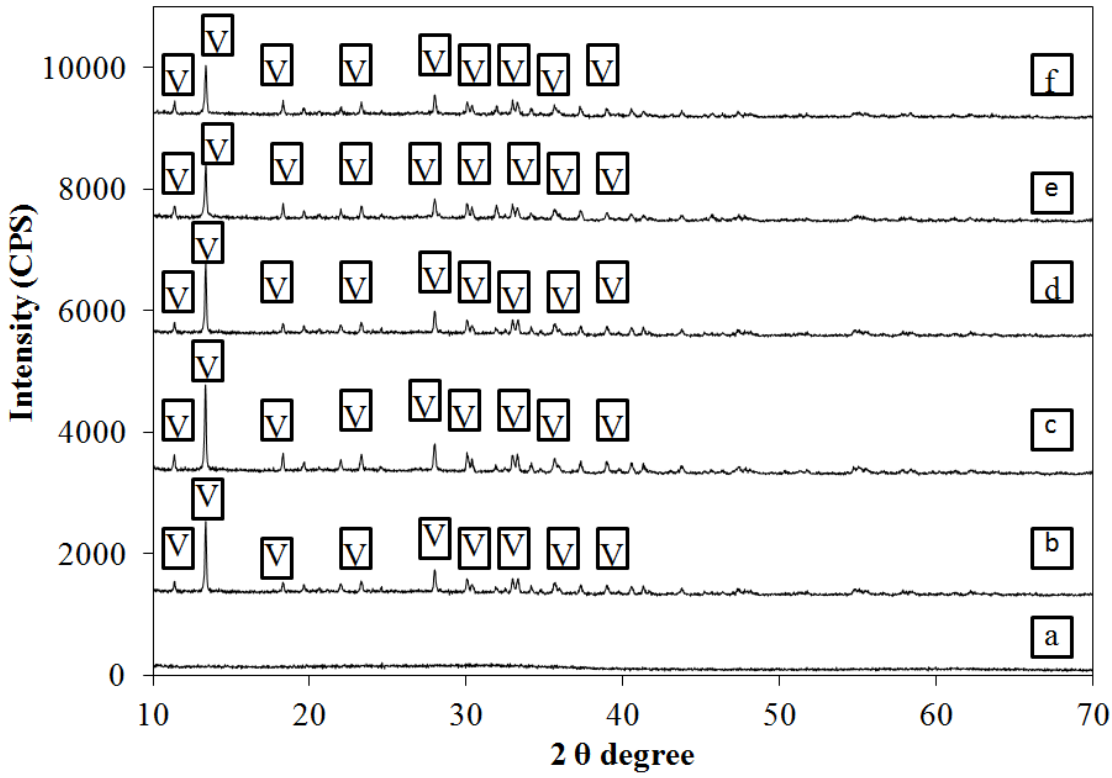

Figure 4.2. XRD spectra of a.) arsenic loaded ferrihydrite (Fe/As = 4) and final solids from synthesis trials under continuous dosing conditions for vivianite (b-d) and the mixed system (arsenic-loaded ferrihydrite solid mixed with pre-formed vivianite) (e, f). The feed rates used in each case for the Fe(II) and phosphorus solutions are: b.) 180 mL/hr, c.) 90 mL/hr d.) 36 mL/hr e.) 90 mL/hr and f.) 36 mL/hr.

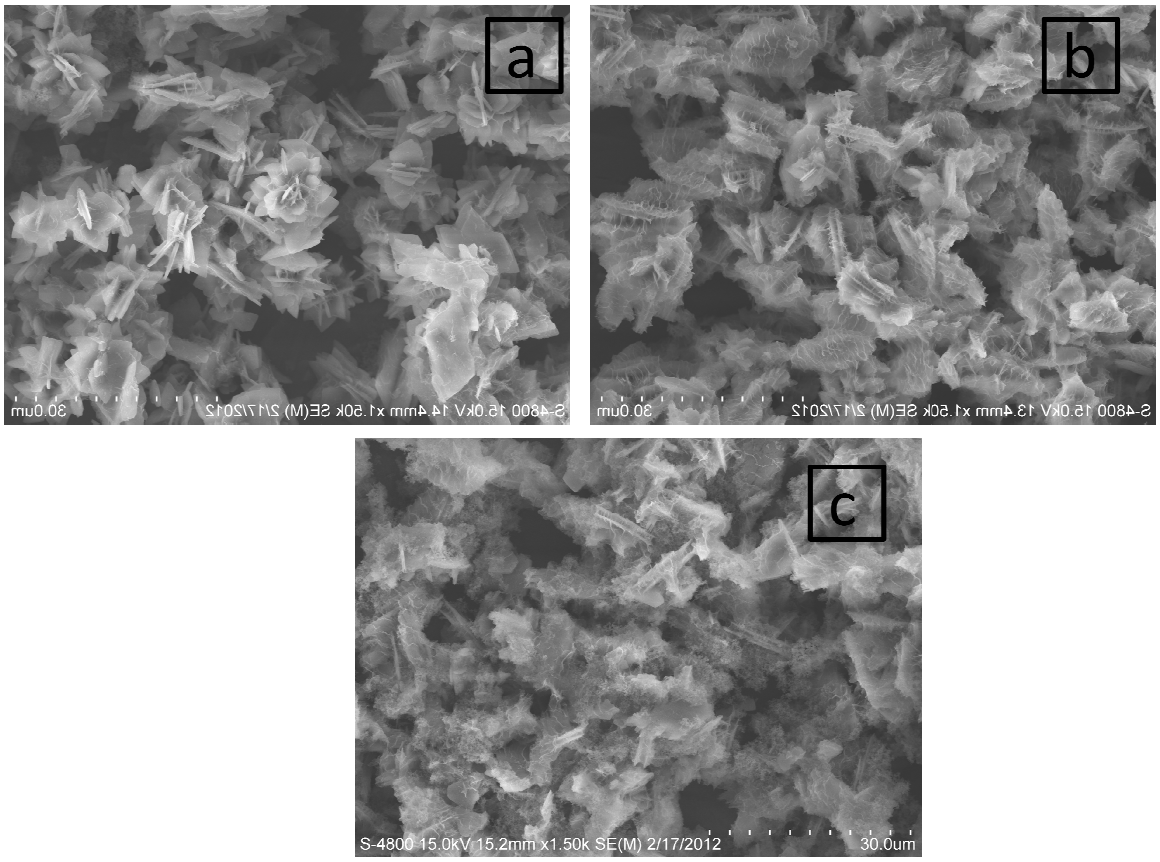

Figure 4.3. SEM images of solid synthesized from pure vivianite synthesis trial with continuous dosing of ferrous and phosphate solutions at a.) 180mL/hr (duration = 1 hour), b.) 90 mL/hr (duration = 2 hour) and c.) 36 mL/hr (duration = 5 hour).

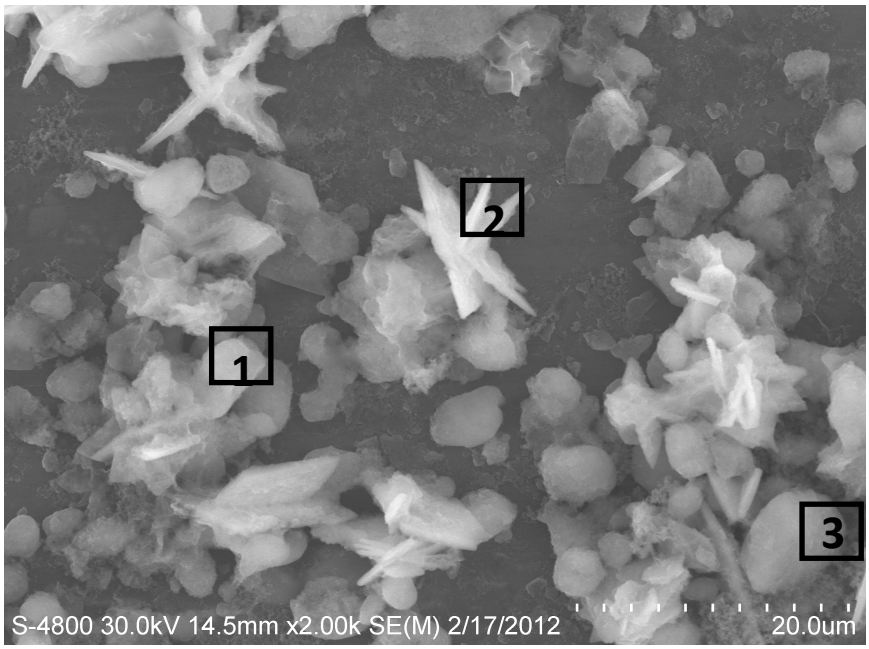

	O (molar %)	P (molar %)	Fe (molar %)	As (molar %)	Fe/P ratio	Fe/As ratio
Point 1	65.29	7.29	1.58	0.32	0.22	4.9
Point 2	66.48	5.53	3.62	0.15	0.65	24.1
Point 3	62.19	9.74	3	0.61	0.3	4.9

Figure 4.4. SEM image and Energy Dispersive X-Ray (EDX) elemental analysis results for final solids obtained from microencapsulation trials using simultaneous continuous dosing of Fe(II) and phosphorus solutions at feed rates of 90 mL/hr each.

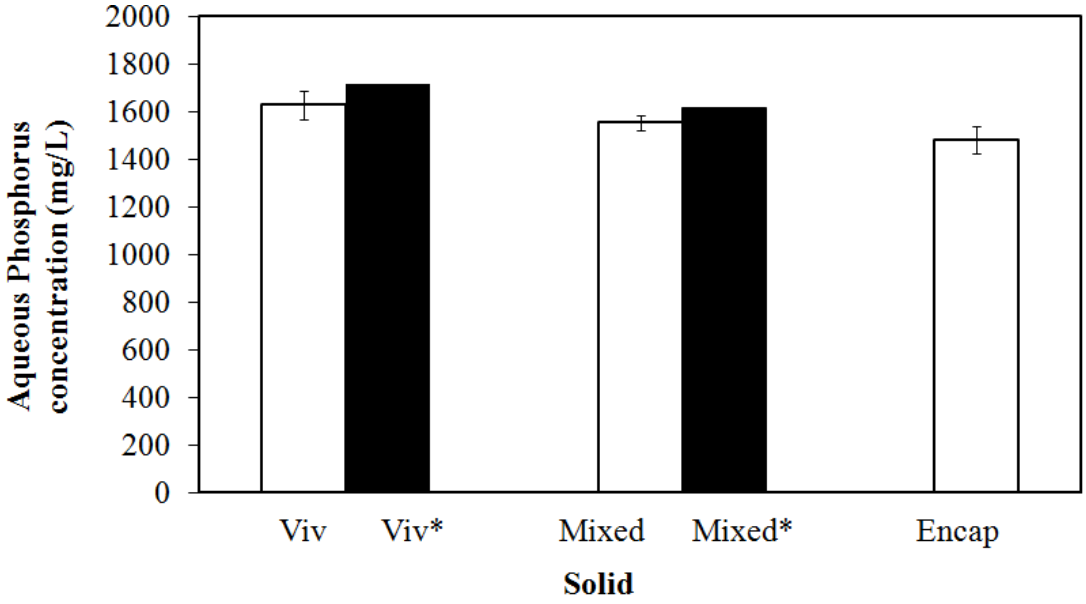

Figure 4.5. Aqueous phosphorus concentrations at equilibrium for different solids included in this study. Note: PHREEQC predicted values are reported for all solids marked with an *. Experimentally observed values for aqueous phosphorus concentrations are reported in all other cases. Final pH was 7.2 ± 0.1. Viv – vivianite solid, Mixed - arsenic loaded ferrihydrite mixed with pre-formed vivianite, Encap - solid obtained from the microencapsulation trial.

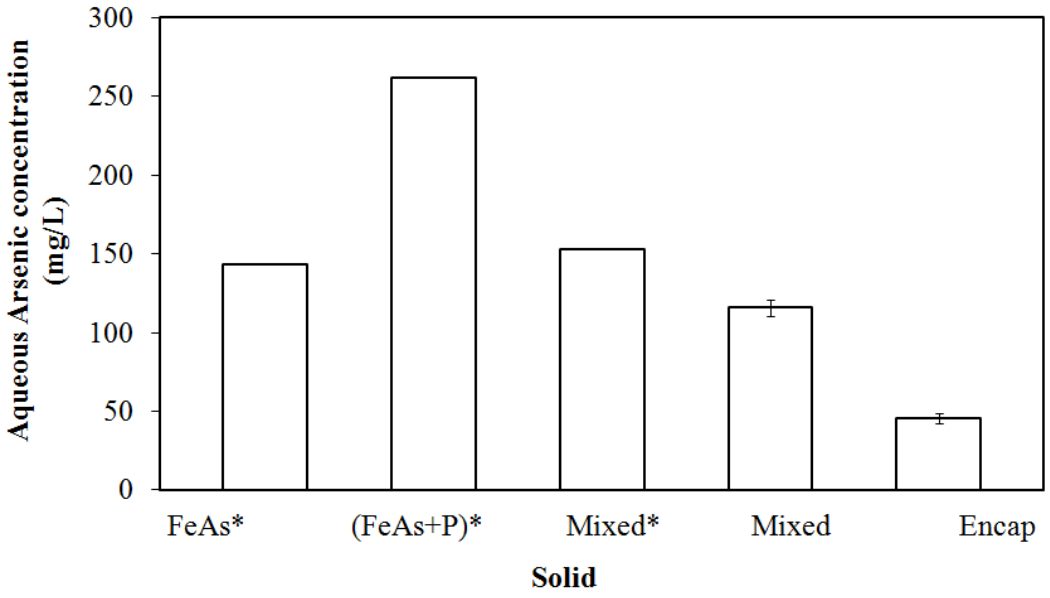

Figure 4.6. Aqueous arsenic concentrations at equilibrium for different solids included in this study. Note: PHREEQC predicted values are reported for all solids marked with an *. Experimentally observed values for aqueous arsenic concentrations are reported in all other cases. A total suspension volume of 760 mL was assumed for all PHREEQC calculations. All cases contained 1±0.05 g of arsenic loaded ferrihydrite (equivalent to approx 200 mg of arsenic). Final pH was 7.2 ± 0.1. FeAs* - arsenic loaded ferrihydrite in deionized water, FeAs+P* - arsenic loaded ferrihydrite in 1718 mg/L phosphorus solution (this is the total phosphorus concentration in equilibrium with vivianite solid as determined by PHREEQC), Mixed - arsenic loaded ferrihydrite mixed with pre-formed vivianite, Encap – solid obtained at equilibrium from the microencapsulation trial described in this study.

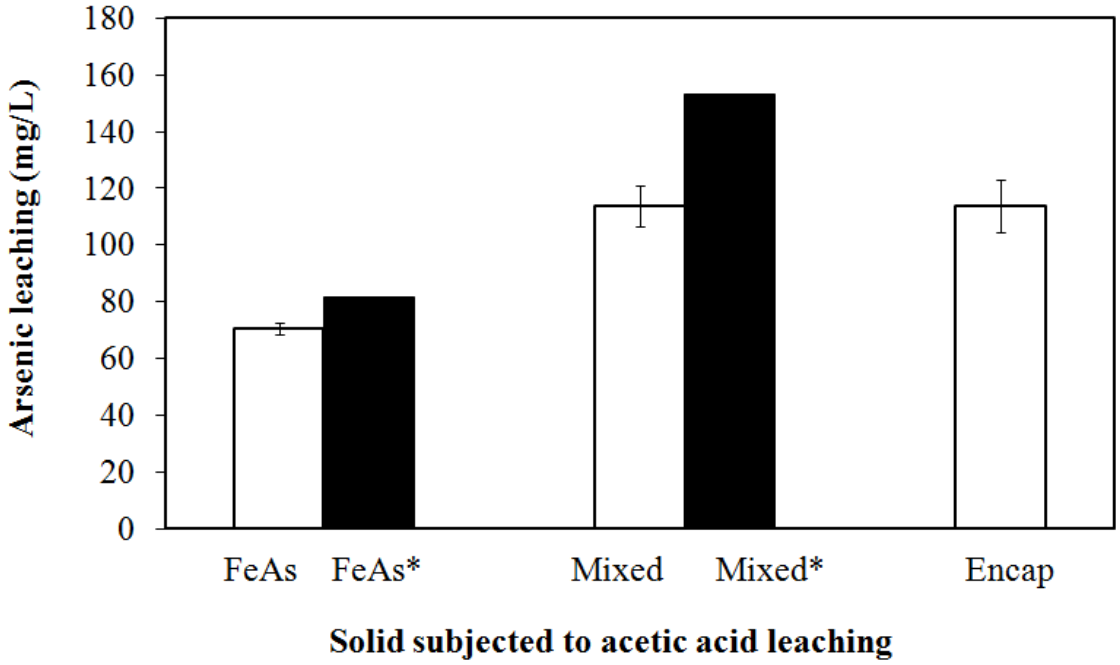

Figure 4.7. Aqueous arsenic concentrations after 50 hours of exposure to acetic acid leaching for solids included in this study. Note: PHREEQC predicted values are reported for all solids marked with a *. Experimentally observed values for aqueous arsenic concentrations are reported in all other cases. Final pH was 4.9 ± 0.2. FeAs - arsenic loaded ferrihydrite, Mixed - arsenic loaded ferrihydrite mixed with pre-formed vivianite, Encap – solid obtained from the microencapsulation trial.

Table 4.1. Compilation of arsenic leaching and final transformation products in biological columns operated under simulated landfill conditions

Column Description	Number of days	% Fe leached out	%As leached out	Major solid phase mineralogy
No sulfate[a]	665	<1%	~72%	**Vivianite**, siderite
0.064 mM sulfate[b]	432	~6.7%	~81.4%	**Vivianite**, siderite, goetite (weak peaks)
0.064 mM sulfate, methanogen inhibition[b]	300	~3.3%	~84%	**Vivianite**, siderite, goethite
0.064 mM sulfate, SRB inhibition[b]	300	~5.21%	~37.65%	**Vivianite**, siderite, goethite
2.08 mM sulfate[c]	331	<1%	~26%	**Vivianite**, siderite, FeS, goethite, realgar
20.08 mM sulfate[a]	523	<1%	~56%	**Vivianite**, goethite, elemental sulfur

[a] Fathordoobadi, unpublished results

[b] Alday 2010

[c] Root et al. under review

Table 4.2. PHREEQC calculated supersaturation indices for vivianite in synthesis trials using instantaneous addition of ferrous and phosphate solutions (Note: TOTP and Fe(II) concentrations are initial concentrations after dilution of the stock solutions)

TOTP/Fe(II)	TOTP (M)	Fe(II) (mM)	pH observed at the end of synthesis trial	Saturation Index for vivianite (calculated using PHREEQC software, version 2, wateq4 database)	Final Solid phase (detected by XRD analysis)
600	0.27	0.45	7.303	6.47	Amorphous
333.33	0.27	0.81	7.326	7.36	Amorphous
190.47	0.27	1.417	7.193	7.83	Amorphous
82.67	0.27	3.266	7.157	8.95	Amorphous
15	0.27	18	7.135	8.94	Amorphous
5	0.0282	5.64	7.47	8.92	Amorphous
15	0.0582	3.88	6.844	9.02	Amorphous
2	0.0282	14.1	6.69	9.87	Vivianite
15	0.1132	7.547	6.97	9.98	Vivianite

5	0.0564	11.28	7.48	10.71	Vivianite
5	0.1132	22.64	6.86	11.47	Vivianite
2	0.0565	28.25	6.83	11.82	Vivianite
4	0.0564	14.1	7.37	12.77	Vivianite
3	0.02845	9.483	7.15	14.50	Vivianite

CHAPTER 5: CONCLUSIONS

It has been well-established that arsenic-bearing solid residuals (ABSRs) will leach arsenic under long-term municipal solid waste (MSW) landfill conditions.The main objective of this study was to develop technologies for arsenic stabilization under mature MSW landfill conditions.

Since knowledge of the fate of ABSRs under such conditions is crucial to the development of such technologies, one component of the doctoral effort was directed towards studying the same as well. This research effort was focused specifically on one parameter - the effect of local Fe(II) concentrations on iron oxide transformation pathways and subsequently fate of the associated arsenic.

Ferrous ion is known to influence the secondary mineralization pathways of iron oxides and hence the release of associated contaminants. Mature landfills are heterogeneous, anoxic systems rich in a diverse microbial community. Hence, localized build-up of Fe(II) due to microbial reduction of Fe(III) is a significant phenomenon in landfills. In our study, we looked at ferrihydrite transformations influenced by high local Fe(II) concentrations generated oxidation of zero-valent iron held on the magnetic bead used for mixing the system. The presence of high local Fe(II) concentrations was found to dispose the ferrihydrite system to form magnetite, whereas in the absence of the same, goethite was the major transformation product with minor amounts of magnetite formed. These results have implications for the fate of the arsenic-loaded ferrihydrite solids disposed in MSW landfills (at low to moderate arsenic loadings, for e.g.; Fe/As (molar) =100 to 20).

Goethite and magnetite have different capacities and association mechanisms for the uptake of arsenic.Hence, the presence of high local Fe(II) concentrations can influence the transformations that arsenic-loaded ferrihydrite (a synthetic surrogate for arsenic-bearing solid residuals (ABSRs) generated from water treatment) can undergo, and subsequently affect the fate and mobility of the associated arsenic under landfill conditions.

Two technologies for arsenic stabilization under landfill conditions were investigated as part of this doctoral study - Arsenic Crystallization Technology (ACT) and microencapsulation. The objective of ACT was to convert iron-based ABSRs to crystalline minerals with high arsenic capacity and low solubility under landfill conditions. Arsenated-schwertmannite, ferrous arsenate, tooeleite and silica-amended tooeleite were considered as candidate minerals for ACT. Although schwertmannite is only poorly-crystalline, it was considered as an ACT candidate because several studies have reported its ability to structurally incorporate arsenate. Scorodite and arsenate apatite were evaluated in a previous study and were included here for comparison with other ACT candidates considered in this study.

Both scorodite and arsenate apatite were not considered for further investigation – scorodite due to the extreme synthesis conditions (low pH and elevated temperature) involved and arsenate apatite due to the fact that the presence of iron interfered with its synthesis. Although high arsenic loadings (20-22% wt/wt) were achieved with tooeleite and silica-amended tooeleite, the arsenic leaching was high even under TCLP conditions,

which are known to underestimate the aggressiveness of landfill conditions. Hence, neither tooeleite nor silica-amended tooeleite were considered suitable candidates for long-term arsenic stabilization under landfill conditions.

Arsenated-schwertmannite and ferrous arsenate showed the most promise in terms of low arsenic leaching in TCLP. Arsenate-schwertmannite solid demonstrated relatively low leaching even in the more aggressive SLL (Simulated Landfill Leachate) solution. But, in the case of schwertmannite not only was the duration of synthesis long (18 days) but the arsenic loading obtained was also low (approximately 5.6% wt/wt). The arsenic loading obtained for the solids synthesized from the ferrous arsenate trials in this study was also much lower than that expected from stoichiometry. A likely explanation is that the synthesis procedure used in this study resulted in the formation of an additional iron-based solid, such as an iron oxide. This could result in decreased arsenic sorption capacity and increased arsenic leaching of the resulting solid mixture. Hence, synthesis conditions need to be optimized to maximize yield of ferrous arsenate before any conclusions can be reached on its effectiveness as a stable arsenic sink. Results from our initial scoping tests are promising and warrant further optimization of both ferrous arsenate and arsenated schwertmannite synthesis conditions.

Results from our microencapsulation trials suggest that this technique could be a potentially promising solution for ABSR stabilization although the efforts here were not completely successful. One of the problems faced in this work was finding a suitable characterization technique to confirm the formation of a coating or encapsulating layer of

vivianite around the arsenic-loaded ferrihydrite. Various techniques were investigated such as SEM imaging, elemental mapping, EDX analysis, FTIR and TEM, but none of the techniques was found to be appropriate in order to conclusively confirm the presence of an encapsulating layer of vivianite. Aqueous arsenic concentrations in the microencapsulation trial indicated a decrease in accessibility to the arsenic-loaded ferrihydrite, which is consistent with at least a partial coating of the ABSR surface with vivianite and mass-transfer limited release of arsenic. But, the advantage provided by the microencapsulation procedure was lost on exposure to a leaching solution. A modified version of the TCLP was used to evaluate the stability of the final product of the encapsulation trials. The vivianite solid itself was stable in the presence of the leaching solution i.e., vivianite dissolution was insignificant on exposure to the leaching solution. Hence, it is not clear why increased arsenic leaching was observed when the solid obtained from the microencapsulation trial was subjected to leaching. The results of the microencapsulation trials performed in this study suggest that the success of this technique would depend on the type of association or bonds formed between the core and the encapsulant surface. Hence, further research is needed to identify encapsulant solids, which would not only be stable under landfill conditions but also form strong associations with the core ABSR surface.

The TCLP, modified TCLP and simulated landfill leachate tests used throughout this study only provide a preliminary evaluation of the effectiveness of a particular stabilization technology. They should be followed with other characterization tools such as synchrotron-based spectroscopic techniques and finally biological columns operated

under simulated landfill conditions, before proof-of-concept is validated. Since, column studies are time intensive, leaching tests such as ones used in this study were used as quick, initial scoping tests to narrow the field of potential ACT candidates.

Future research efforts should also focus on investigating other avenues for long-term stabilization of iron-based ABSRs under landfill conditions. One such avenue that has received a lot of attention recently for the remediation of heavy metals and radionuclides is biomineralization (Warren et al. 2001; Roden et al. 2002; Cheng et al. 2012; Dong and Lu 2012; Lauchnor et al. 2013; Li et al. 2013). Many studies have established that biomineralization is a dominant mechanism for the formation of minerals that play an important role in contaminant cycling via various processes such as sorption, coprecipitation, oxidation/reduction, etc. (Zhang et al. 2009; Benzerara et al. 2011; Brookshaw et al. 2012). Mineral-microbial interactions are of utmost importance in nature. Microbial activity can alter mineral solubility and surface reactivity in ways not possible in a purely abiotic system. Advances in synchrotron-based spectroscopic techniques such as X-ray Absorption Spectroscopy (XAS) and X-ray Fluorescence (XRF) have allowed researchers to study the association mechanisms of contaminants such as arsenic, cadmium and uranium with mineral surfaces (Sharp et al. 2011; Rennert et al. 2012; Salome et al. 2013). Future work should explore arsenic sequestration in biogenic arsenic-bearing phases and encapsulated arsenic-bearing solids synthesized from ABSRs by exploiting microbial metabolic pathways.

Biological columns with synthetic arsenic-loaded ferrihydrite (or actual spent water treatment sorbents) operated under simulated landfill conditions provide useful insights into secondary mineralization pathways and arsenic release and sequestration under landfill conditions. Information about arsenic partitioning into solid phases under landfill conditions can then be used to develop stabilization technologies which dispose the ABSRs towards mineralization pathways and Fe-As associations that result in arsenic stabilization under these conditions.

Further research is also needed to evaluate the current scenario with regard to the fate of arsenic residuals in actual landfill sites. There have been studies in the past that have established that landfill leachate can mobilize arsenic from natural sediments into groundwater. With the enforcement of the Arsenic Rule in 2006, the volume of arsenic waste disposed into landfills has increased tremendously. Hence, efforts need to be directed towards collecting aqueous samples and solid core samples at different depths from representative mixed solid waste landfills that have been accepting significant volumes of ABSR for the past few years. Reference levels need to be established for the arsenic concentrations in soil, surface and groundwater in the vicinity of landfills and/or impacted by landfill leachate. This would give us a real sense of the gravity of the problem and whether results from biological columns accurately simulate arsenic release and sequestration phenomena under actual landfill conditions.

APPENDIX A: CHARACTERIZATION TECHNIQUES FOR ANALYSIS OF SOLIDS FROM MICROENCAPSULATION PROCEDURE

METHODS

Elemental X-ray mapping was performed to obtain spatial compositional information about synthesized solids. A Hitachi S-4800 II Field Emission Scanning Electron Microscope was used to obtain the SEM images of the solid phases. Energy Dispersive X-ray (EDX) spectroscopy analysis was performed to obtain elemental composition of the synthesized solids using a Thermo Scientific Si(Li) detector equipped with Noran System Six.

Initial preparation techniques included placing the dried sample in the bottom of a 1-inch diameter epoxy mold. Once cured, the epoxy pucks were polished with increasing grit SiC paper, and a final polish of colloidal silica. The particles were assumed to be spherical, so the strategy was to polish part way through the particles so as to have a polished cross section. The problem with this technique was that the epoxy was not hard enough to keep the particles in place, so rather than polishing, they were displaced from the puck. Final preparation techniques involved suspending the powder samples in 18.0 M-Ohm water, and drop casting them on polished Al SEM mounts. Only a few selected maps from our elemental mapping efforts are shown here.

FTIR spectra were obtained using a Magna-IR 560 Nicolet spectrometer (Madison, WI) equipped with a purge gas generator and a DTGS detector. All samples were first dried inside a glove box (Terra Universal Critical Environment Solutions) purged with nitrogen

and ground to a fine powder. All spectra were acquired at room temperature with 4.0 cm^{-1} resolution and 400 scans over the spectral range of 4000 - 600 cm^{-1} using the autogain function and aperture set at 100. Samples were purged with CO_2 free air for 15 minutes and a final background spectrum was collected when no further changes in the spectra were observed. A final sample spectrum was obtained by subtracting the appropriate background spectrum from the sample spectrum. All data collection and spectral processing, including background subtraction and baseline correction, were performed using the OMNIC program (Thermo Nicolet, Co.).

A 200 kEV Hitachi H-8100 transmission electron microscope using a LaB6 filament (with a point to point resolution of 2 Å for the high resolution pole piece and 2.3 Å for the analytical pole piece) was used to obtain the TEM images. The Hitachi H-8100 ultra high resolution objective lens was used.

RESULTS AND DISCUSSION

Elemental maps were used to check for any patterns in the Fe, P and As concentrations in the solids synthesized as part of the vivianite microencapsulation efforts described in Chapter 4. The elemental maps for vivianite solid synthesized by instantaneous addition of ferrous and phosphate solutions are shown in Figure A1. The Fe/P ratio was determined to be 1.14 ± 0.1 by bulk Energy Dispersive X-ray analysis of these solid particles. No specific pattern for arsenic was detected in the elemental maps for pure arsenic-loaded ferrihydrite particles with Fe/As molar ratio = 20 (not shown here). The arsenic signal was not localized on the particles but rather dispersed everywhere and

blended in with the background noise. This is possibly due to the low arsenic concentration when compared to the iron concentration in the solid.

It was decided to use ferrihydrite solid with higher arsenic loading (Fe/As = 4), in order to improve resolution of the arsenic patterns during elemental mapping. Microencapsulation of an ABSR with high arsenic loading (low Fe/As ratio) is advantageous as compared to one with a low arsenic loading (high Fe/As ratio) because it significantly reduces the volume of hazardous waste that needs to be handled and disposed. There is also the accompanying risk of the solid releasing high concentrations of arsenic when exposed to aggressive leaching environments. Hence, it would be important to evaluate the leachability of the final encapsulated solid under aggressive leaching conditions.

Elemental mapping of the pure Fe/As = 4 solid showed regions of high arsenic concentrations co-located with regions of high iron concentrations (Figure A2). But, the solids obtained from the vivianite microencapsulation experiment did not show any specific patterns for arsenic (Figure A3). The arsenic signal was dispersed and blended in with the background noise. But, the problem with understanding these results is that the arsenic signal would look like this even for the case where arsenic-loaded ferrihydrite particles are completely coated with vivianite. The successful case for this study (complete encapsulation of ABSR) would show the same elemental map as the completely unsuccessful case for this study (e.g. significant release of arsenic resulting in uniform detection of arsenic throughout the mapped area). These results suggest that

elemental mapping may not be an appropriate technique to study microencapsulation of arsenic-loaded ferrihydrite by vivianite. Hence, this technique was not used to analyze the solids obtained from microencapsulation trials using continuous addition of Fe(II) and phosphate solutions.

Powder Fourier Transform Infrared (FTIR) spectroscopy was used as a preliminary scoping tool to look for any indication of a vivianite coating on the arsenic-loaded ferrihydrite surface. The authors were aware that the steps involved in the sample preparation procedure for the powder FTIR analysis such as drying and grinding of the samples could possibly introduce artifacts that would interfere with interpretation of the results (e.g. destroy an existing coating). But, the powder FTIR analysis could still give us some useful insights as a scoping tool to decide if further analyses with Attenuated Total Reflectance Fourier Transform Infrared (ATR-FTIR) spectroscopy would provide any evidence for vivianite encapsulation of arsenic-loaded ferrihydrite.

Powder FTIR spectra were obtained for the arsenic-loaded ferrihydrite (Fe/As = 4) solid, vivianite solid, arsenic-loaded ferrihydrite (Fe/As = 4) solid with phosphate sorbed on the surface, mixed solid (arsenic-loaded ferrihydrite and pre-formed vivianite), and solid obtained from the microencapsulation trial (Figure A4). Spectra were also obtained for the arsenic-loaded ferrihydrite (Fe/As = 4) and vivianite solids mixed in different ratios (weight of Fe/As = 4 solid: weight of vivanite = 0, 0.25, 0.5, 0.75, 1) (Figure A5).

The spectra for vivianite, mixed solid (arsenic loaded ferrihydrite mixed with pre-formed vivianite), and solid obtained from the microencapsulation trial showed no difference in

peaks. It was observed that the peaks for vivianite dominated the spectra. This is also evident from Figure B4, where the peaks for vivianite dominated the spectra in the case of solids obtained by mixing vivianite and arsenic-loaded ferrihydrite in different ratios (for ratios studied from 0.25 to 1). These results suggested that powder FTIR analysis cannot be used to confirm if vivianite particles are coating the arsenic-loaded ferrihydrite particles as opposed to just nucleating independently. It was decided not to pursue further investigation with ATR-FTIR analysis due to the same issue.

Results from TEM imaging showed that it is not an appropriate technique to confirm coating of the arsenic-loaded ferrihydrite surface by vivianite. The morphologies of the two solids could not be clearly distinguished (see Figures A6 – A10).

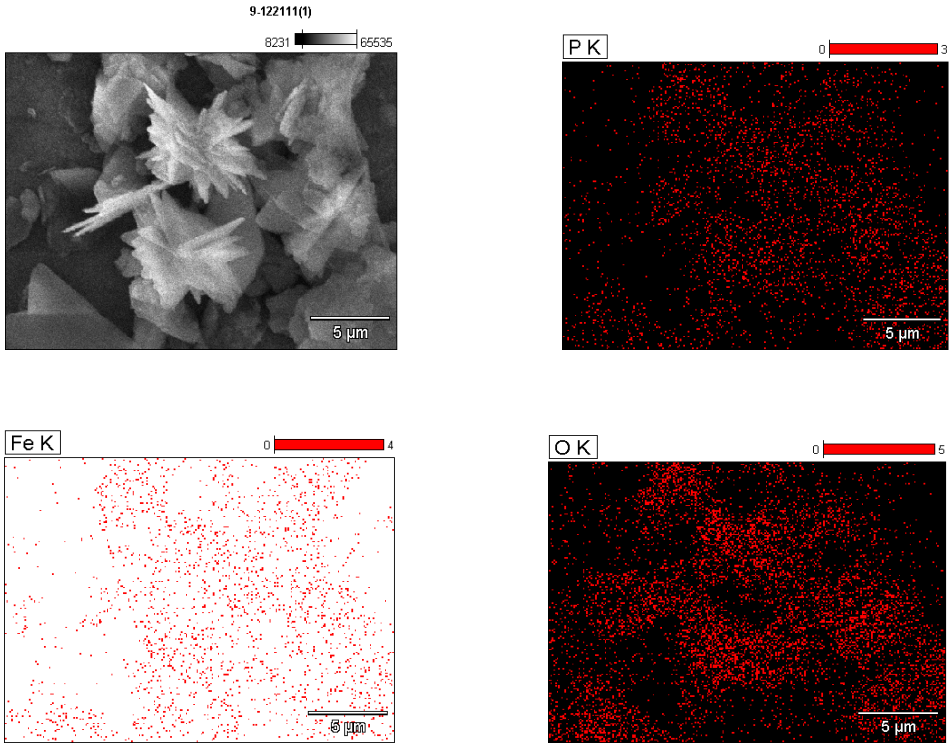

Figure A1. Vivianite solid synthesized using instantaneous addition of 50 mL of 0.07 M sodium phosphate (Na_2HPO_4) solution and 50 mL of 0.02325 M ferrous chloride tetrahydrate ($FeCl_2.4H_2O$) solution to 23 mL of deionized water (TOTPO4/Fe(II) = 3), without any arsenic-loaded ferrihydrite solid added. Note: Final pH observed = 7.15. For SEM elemental mapping, accelerating voltage used: 15 kV and magnification used: 5030.

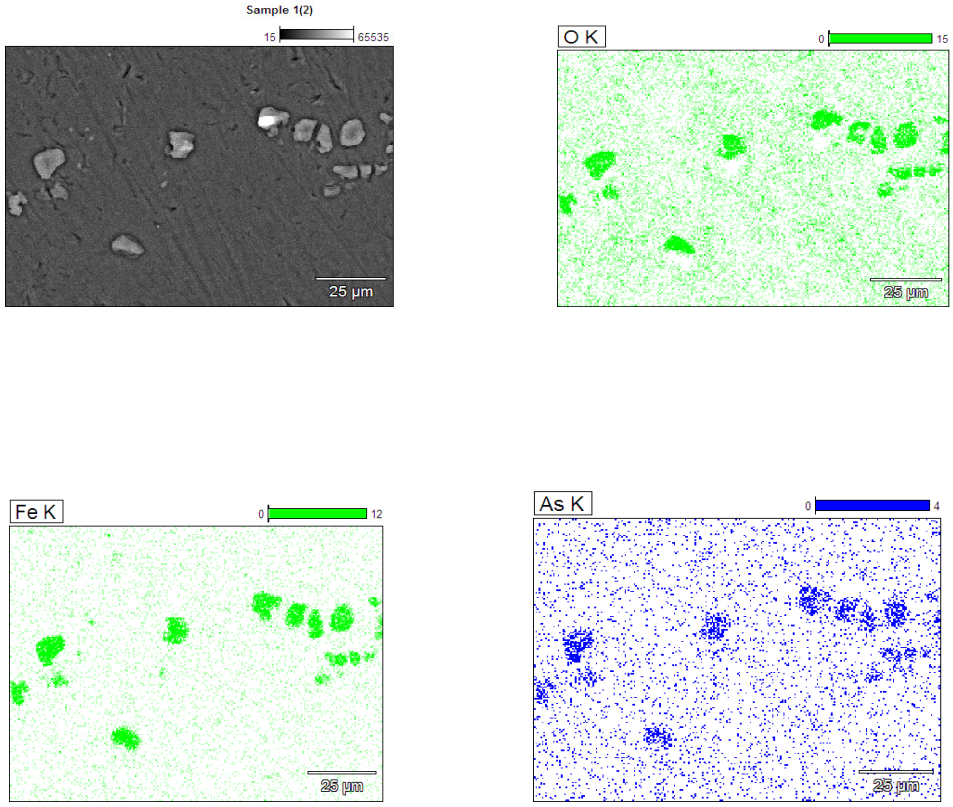

Figure A2. Arsenic-loaded ferrihydrite (Fe/As molar ratio = 4) solid. Note: SEM accelerating voltage: 20 kV, magnification: 900.

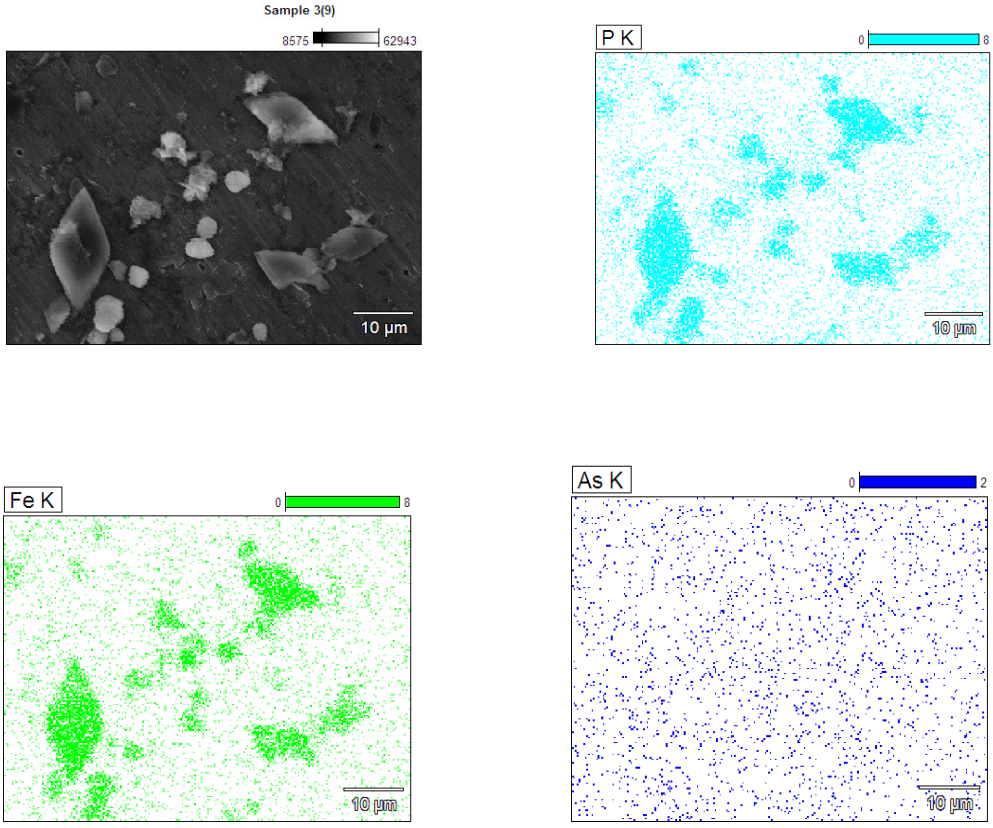

Figure A3. Solid from microencapsulation trial using instantaneous addition of ferrous and phosphate solutions to a suspension containing the arsenic-loaded ferrihydrite solid (Fe/As = 4). 17 ml of 0.3 M sodium phosphate and 17 ml of 0.1 M ferrous chloride were added to 0.2 g of arsenic-loaded ferrihydrite suspended in 100 ml. Two such doses of Fe (II) and phosphate solutions followed at 20 minute intervals of each other. Final pH observed = 7.2. Note: SEM accelerating voltage: 20 kV, magnification: 1800.

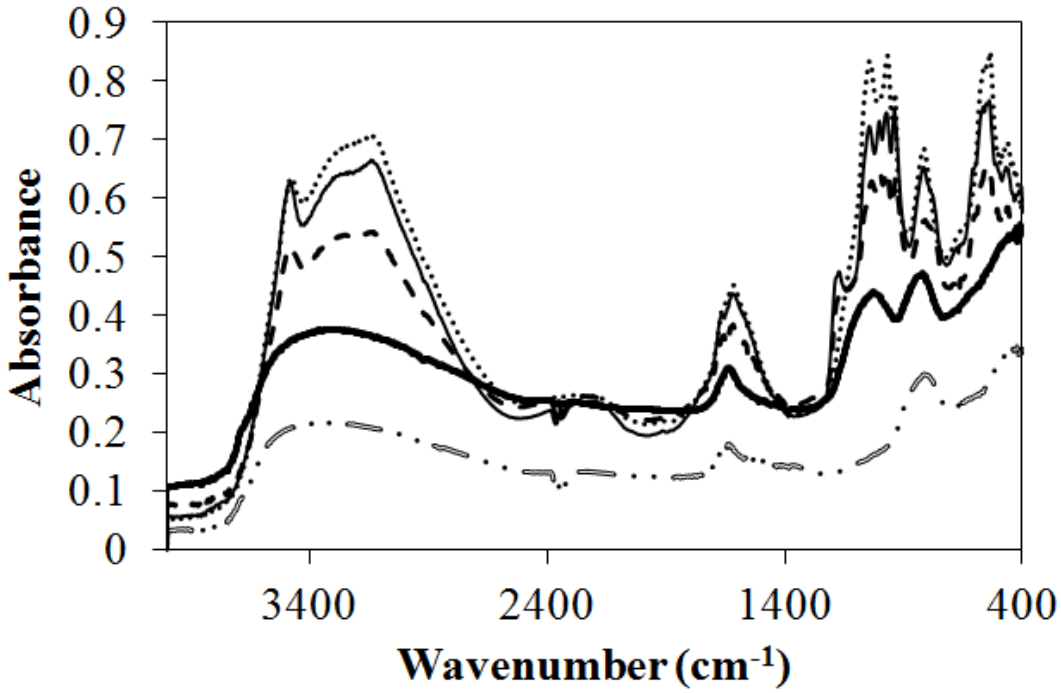

Figure A4. FTIR spectra of different solids synthesized as part of vivianite microencapsulation efforts

Fe/As = 4 solid with phosphate sorbed on the surface

Mixed Fe/As = 4 solid and pre-formed vivianite

Vivianite solid using continuous dosing

Solid from encapsulation experiment using continuous dosing

Fe/As = 4 solid

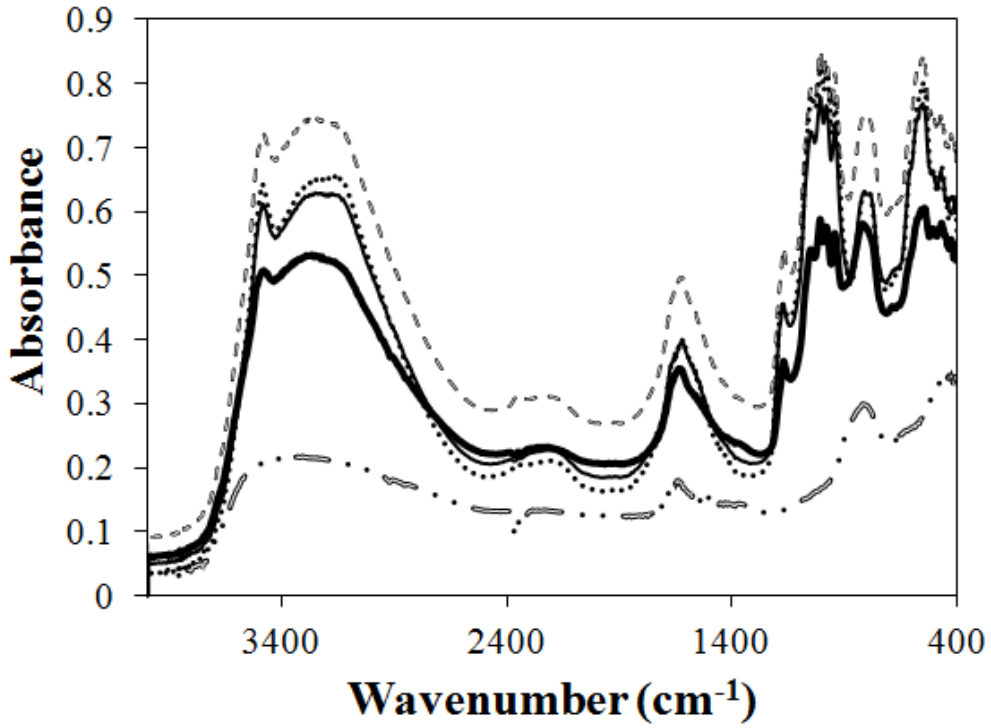

Figure A5. FTIR spectra of arsenic loaded ferrihydrite (Fe/As = 4) and vivianite mixed in the different ratios:

100% Fe/As = 4 solid

75% Fe/As = 4 solid, 25% vivianite

50% Fe/As = 4 solid, 50% vivianite

25% Fe/As = 4 solid, 75% vivianite

100% vivianite

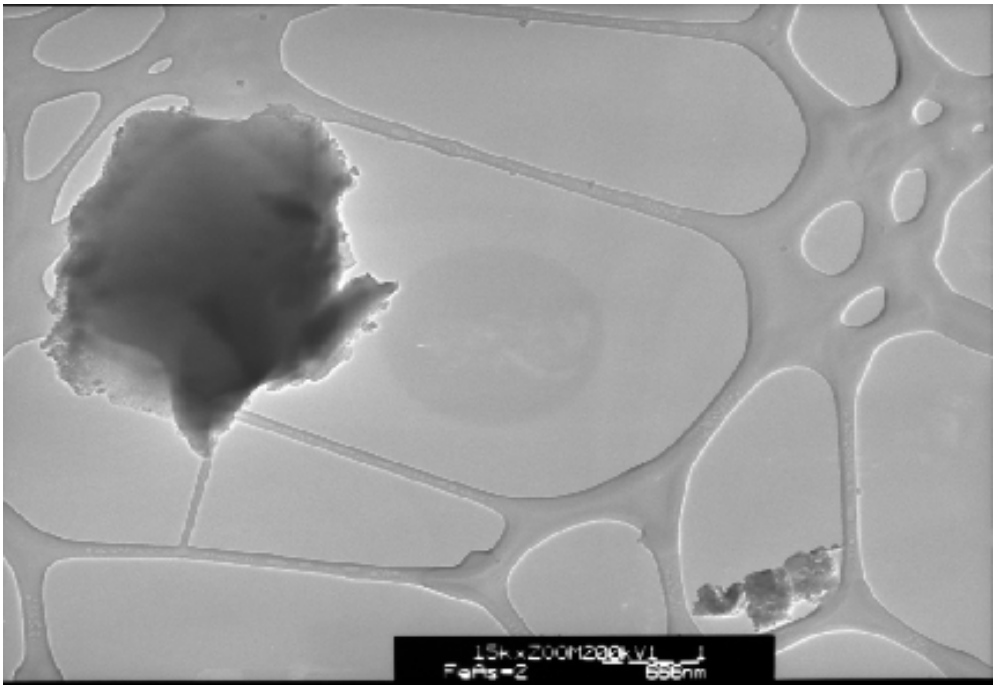

Figure A6. TEM image of arsenic-loaded ferrihydrite (Fe/As = 4).

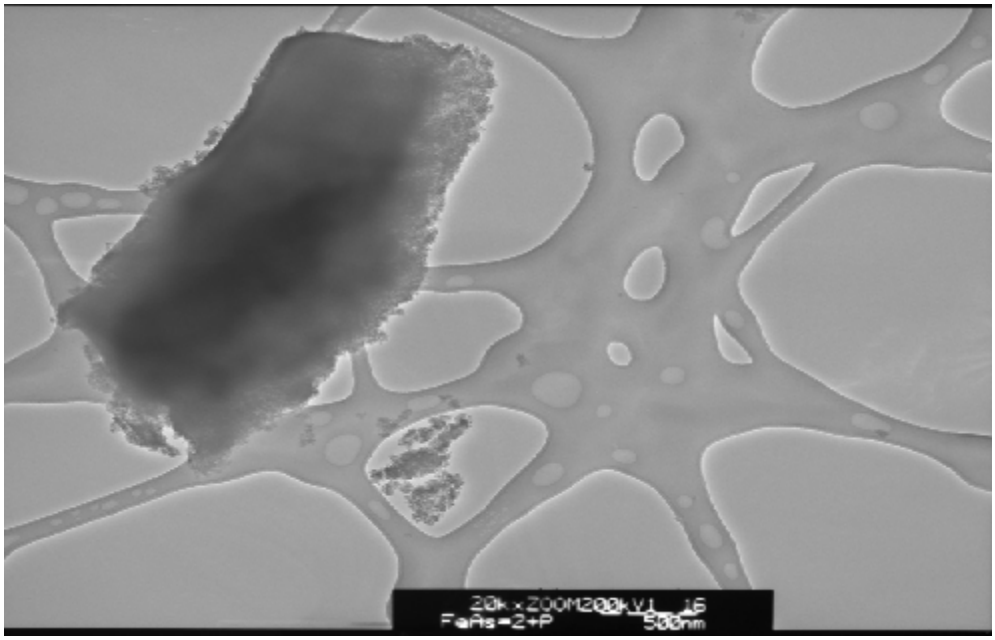

Figure A7. TEM image of arsenic loaded ferrihydrite (Fe/As = 4) with 0.3M phosphate added.

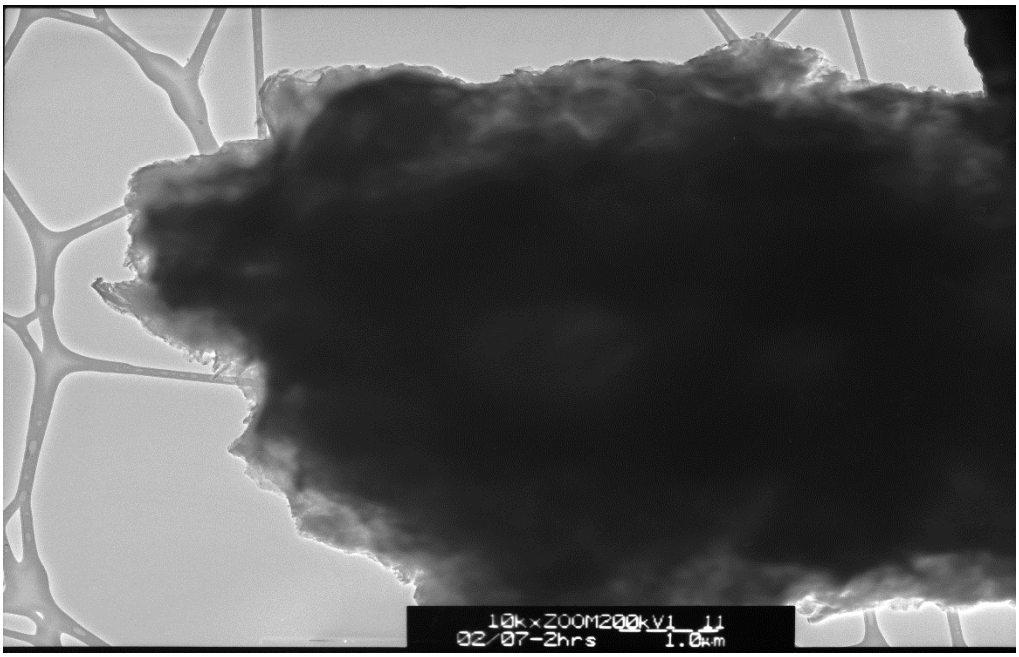

Figure A8. TEM image of vivianite solid synthesized using continuous dosing of Fe(II) and phosphate solutions fed simultaneously at 90 mL/hr each.

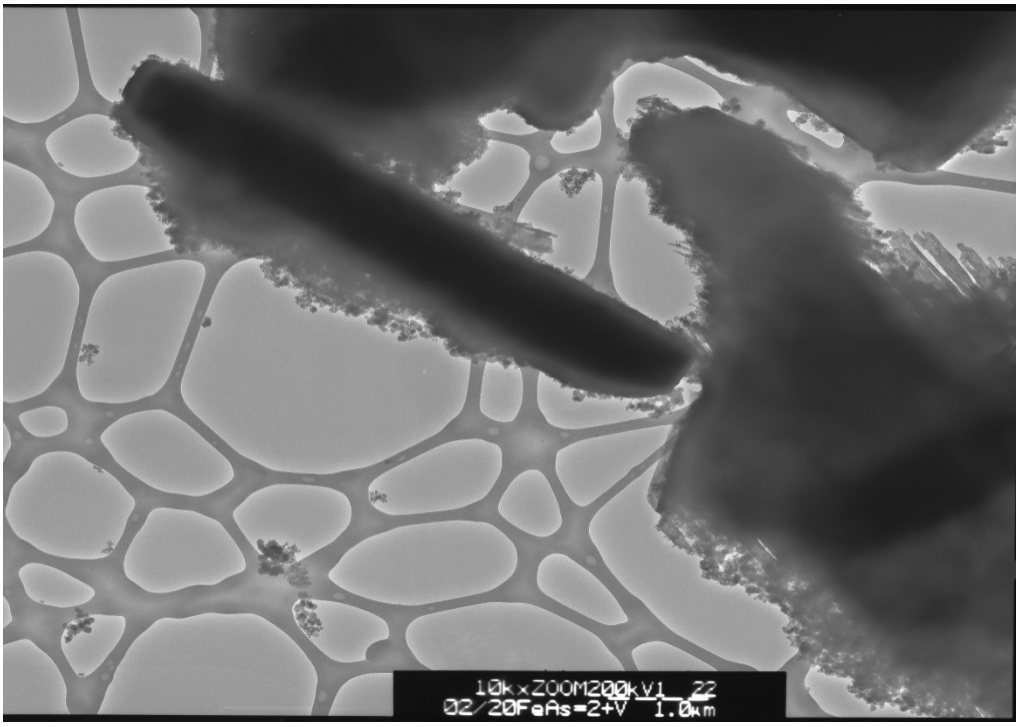

Figure A9. TEM image of mixed solid (arsenic-loaded ferrihydrite Fe/As = 4 and pre-formed vivianite) synthesized under continuous dosing at a feed rate of 90 mL/hr for Fe(II) and phosphate solutions.

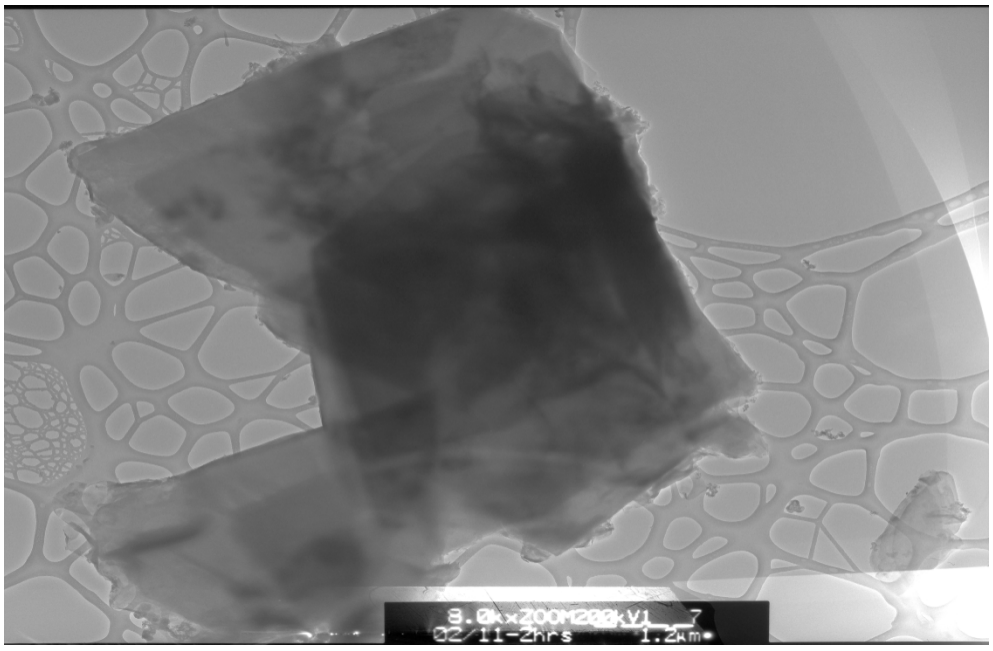

Figure A10. TEM image of solid obtained from microencapsulation trial under continuous dosing at a feed rate of 90 mL/hr for Fe(II) and phosphate solutions.

APPENDIX B: MICROENCAPSULATION TRIALS USING ALUMINUM HYDROXIDE

HYPOTHESIS

Aluminum is known to be stable both under oxidizing and reducing conditions. Results from vivianite encapsulation trials seemed to suggest that the phosphate system might not work well for encapsulation trials using arsenate loaded ferrihydrite due to significant competition between the two anions for sorption sites on ferrihydrite. Hence, microencapsulation of arsenic-loaded ferrihydrite (Fe/As = 4) solid was attempted using aluminum hydroxide as the encapsulant.

MATERIALS AND METHODS

Aluminum hydroxide synthesis

100 mL of 0.5 M aluminium chloride hexahydrate ($AlCl_3.6H_2O$) and 100 mL of 1.35 M NaOH were simultaneously fed using a syringe pump into a 500 mL beaker filled with 100 mL of deionized water and mixed with an overhead stirrer. The feed rates of the two solutions were maintained at 50 mL/hr.

Encapsulation trials with aluminum hydroxide

Encapsulation trials were performed with continuous addition of aluminum chloride and sodium hydroxide solutions in the presence of 1.3 ± 0.05 g (dry weight) of arsenic loaded ferrihydrite (Fe/As = 4) solid. 100 mL of 0.5 M aluminium chloride hexahydrate

($AlCl_3.6H_2O$) and 100 mL of 1.35 M NaOH were simultaneously fed using a syringe pump into a 500 mL beaker filled with 100 mL of deionized water and mixed with an overhead stirrer. The arsenic loaded ferrihydrite solid was added to the 100 mL of water before addition of the ferrous and phosphate solutions. The feed rates of the two solutions were maintained at 50 mL/hr.

A mixed system with the arsenic-loaded ferrihydrite (Fe/As = 4) and pre-formed aluminum hydroxide (as described above) was used as a reference to check whether the aluminum hydroxide particles were coating the ferrihydrite particles or nucleating independently. First, aluminum hydroxide was prepared as described above. Then, 1.3 ± 0.05 g (dry weight) of arsenic-loaded ferrihydrite suspended in 50 mL of deionized water was added and mixed for 20 minutes.

Aqueous samples for total arsenic and aluminum analysis using ICPMS were taken after 48 hours in all cases after filtering through a 0.22 μm filter. The acetic acid leaching procedure described in Chapter 4 was used to evaluate the stability of the solids generated from the microencapsulation procedure.

RESULTS AND DISCUSSION

The final solid from the aluminum hydroxide synthesis trials was found to be amorphous by powder XRD analysis (not shown here). It is possible that the solid was amorphous aluminum hydroxide. The aqueous arsenic concentrations before leaching were near detection limits (detection limit = 0.5 mg/L) and in all cases <8 mg/L (Figure B1). The aqueous arsenic concentrations after leaching were < 60 mg/L in all replicates of both the

microencapsulation and mixed (Fe/As = 4 solid and pre-formed aluminum hydroxide) trials (Figure B2). The aqueous arsenic concentrations in the two trials were within a factor of two of each other both before and after leaching. Since there is no significant difference in the aqueous arsenic concentrations between the microencapsulation and mixed (Fe/As = 4 solid and pre-formed aluminum hydroxide) trials both before and after leaching, there is no indication of a protective aluminum hydroxide coating formed on the ferrihydrite surface. The PHREEQC predicted aqueous arsenic concentration in the pure arsenic loaded ferrihydrite system under similar conditions before and after leaching were 288 ppm and 135 ppm respectively. The aqueous arsenic concentrations in the mixed system and microencapsulation trials using aluminum hydroxide were significantly lower compared to the PHREEQC predicted concentrations for the arsenic loaded ferrihydrite. This is possibly due to the significant arsenate sorption capacity of amorphous aluminum hydroxide.

The aqueous aluminum concentrations after leaching are significantly higher than the concentrations before leaching (about 2-3 orders of magnitude), which indicate dissolution of the aluminum hydroxide solid (Figures B3 and B4). But, this dissolution does not seem be significant based on the fraction of total aluminum released into solution (<0.3%).

CONCLUSIONS

In microencapsulation trials using aluminum hydroxide as an encapsulant, arsenic concentrations fell by several orders of magnitude as compared to the arsenic-loaded ferrihydrite system. But, this decrease in arsenic concentration seemed to be due to the high arsenic sorption capacity of aluminum hydroxide as opposed to the formation of an aluminum hydroxide coating on the ferrihydrite surface. These preliminary results seem to suggest that research efforts should be directed towards studying amorphous aluminum hydroxide as a potential sorbent for arsenic rather than an encapsulant for arsenic-loaded ferrihydrite.

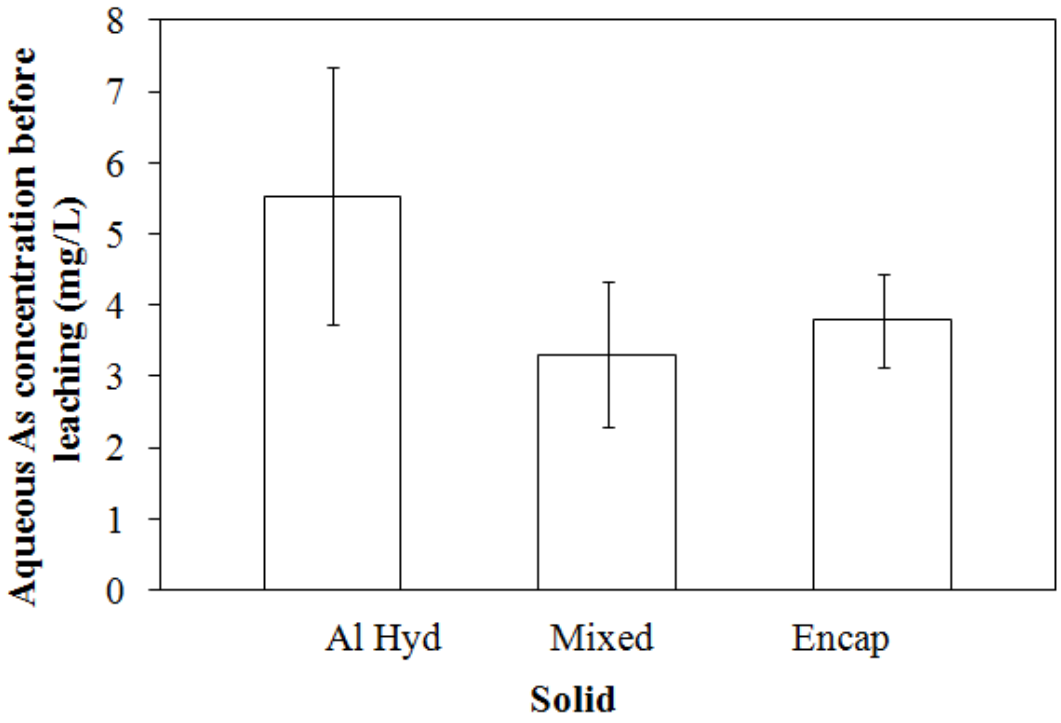

Figure B1: Aqueous total arsenic concentrations before leaching in the 'Al Hyd'- aluminum hydroxide system, 'Mixed'- mixed system (Fe/As = 4 solid and pre-formed aluminum hydroxide solid) and 'Encap' - microencapsulation system. Note: The final pH in all systems was 6.8 ±.1. The arsenic detected in the pure aluminum hydroxide system was probably because the concentrations were close to detection limit for arsenic.

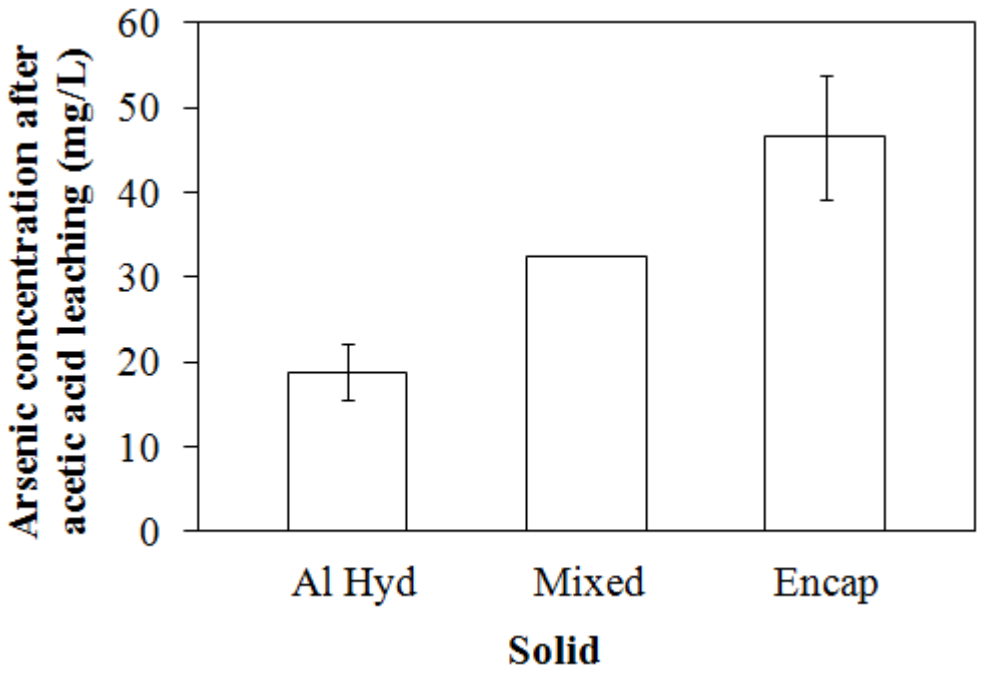

Figure B2: Aqueous total arsenic concentrations after leaching in the 'Al Hyd' - aluminum hydroxide system, 'Mixed' - mixed system (Fe/As = 4 solid and pre-formed aluminum hydroxide solid) and 'Encap' - microencapsulation system. Note: The final pH in all systems was 4.85 ± 0.15. Arsenic detected in the pure aluminum hydroxide system indicates low levels of contamination. If this contamination was present in the mixed and microencapsulation systems as well that would only mean that the actual arsenic concentrations in the system are lower. Hence, this observation does not change the interpretation of our results.

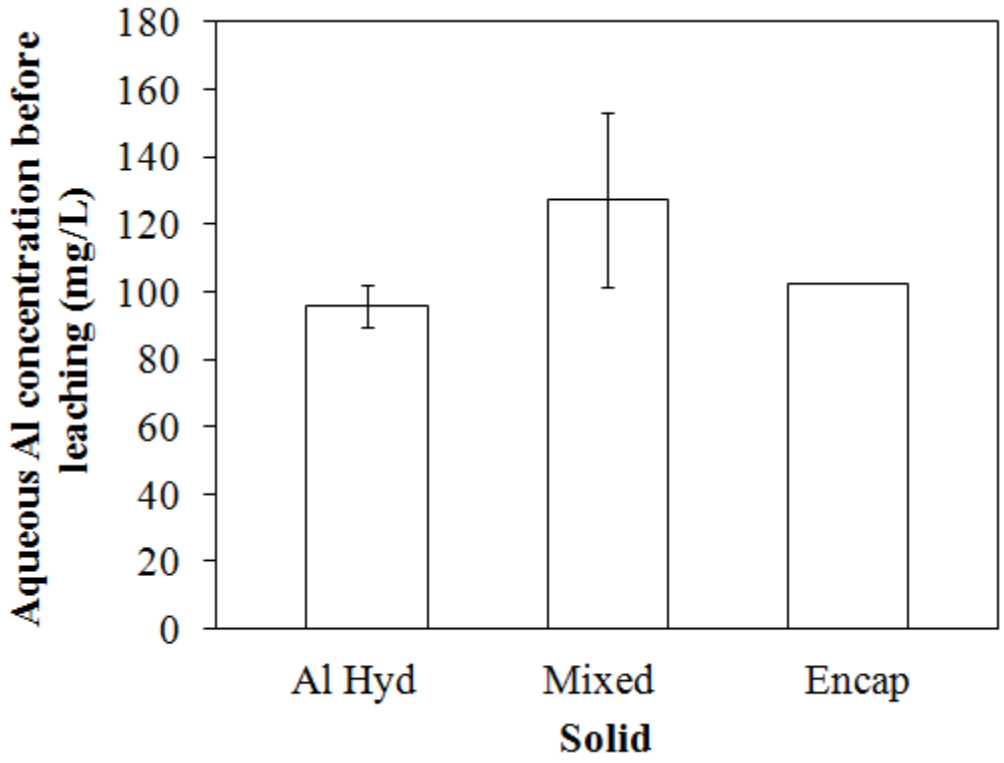

Figure B3: Aqueous total aluminum concentrations before leaching in the 'Al Hyd' - aluminum hydroxide system, 'Mixed' - mixed system (Fe/As = 4 solid and pre-formed aluminum hydroxide solid) and 'Encap' - microencapsulation system. Note: The final pH in all systems was 6.8 ±.1.

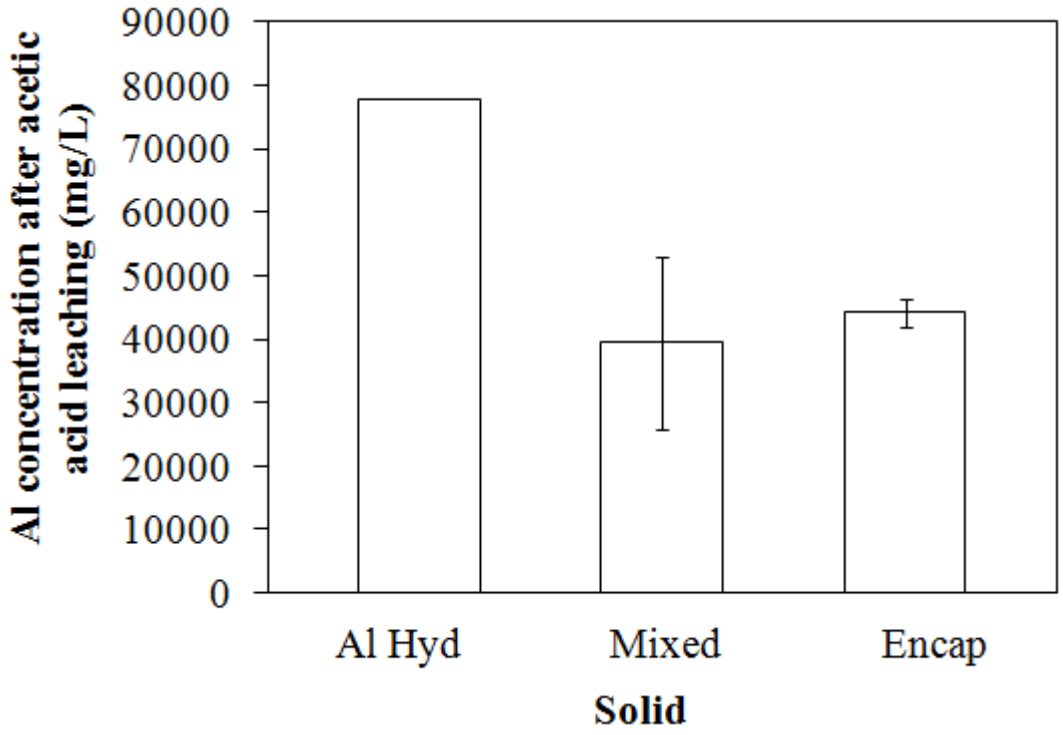

Figure B4: Aqueous total aluminum concentrations after leaching in the 'Al Hyd' - aluminum hydroxide system, 'Mixed' - mixed system (Fe/As = 4 solid and pre-formed aluminum hydroxide solid) and 'Encap' - microencapsulation system. Note: The final pH in all systems was 4.85 ± 0.15.

REFERENCES

Acero, P., Ayora, C., Torrento, C., Nieto, J. (2006). "The Behavior of Trace Elements during Schwertmannite Precipitation and Subsequent Transformation into Goethite and Jarosite." *Geochim. Cosmochim. Acta,* 70(16), 4130-4139.

Ahmed, K., Bhattacharya, P., Hasan, M., Akhter, S., Alam, S., Bhuyian, M., Imam, M., Khan, A., Sracek, O. (2004). "Arsenic Enrichment in Groundwater of the Alluvial Aquifers in Bangladesh: An Overview." *Appl. Geochem.,* 19(2), 181-200.

Alday, F. (2010) "Iron Biomineralization: Implications on the Fate of Arsenic in Landfills." Doctoral Dissertation, The University of Arizona, Tucson, AZ.

Arai, Y., and Sparks, D. (2001). "ATR-FTIR Spectroscopic Investigation on Phosphate Adsorption Mechanisms at the Ferrihydrite-Water Interface." *J. Colloid Interface Sci.,* 241(2), 317-326.

Bai, M., and Roegiers, J. (1997). "Triple-Porosity Analysis of Solute Transport." *J. Contam. Hydrol.,* 28(3), 247-266.

Benner, S., Hansel, C., Wielinga, B., Barber, T., Fendorf, S. (2002). "Reductive Dissolution and Biomineralization of Iron Hydroxide Under Dynamic Flow Conditions." *Environ. Sci. Technol.,* 36(8), 1705-1711.

Benzerara, K., Miot, J., Morin, G., Ona-Nguema, G., Skouri-Panet, F., Ferard, C. (2011). "Significance, Mechanisms and Environmental Implications of Microbial Biomineralization." *Comptes Rendus Geoscience,* 343(2-3), 160-167.

Bigham, J., Schwertmann, U., Carlson, L., Murad, E. (1990). "A Poorly Crystallized Oxyhydroxysulfate of Iron Formed by Bacterial Oxidation of Fe(Ii) in Acid-Mine Waters." *Geochim. Cosmochim. Acta,* 54(10), 2743-2758.

Borch, T., Masue, Y., Kukkadapu, R. K., Fendorf, S. (2007). "Phosphate Imposed Limitations on Biological Reduction and Alteration of Ferrihydrite." *Environ. Sci. Technol.,* 41(1), 166-172.

Bose, P., and Sharma, A. (2002). "Role of Iron in Controlling Speciation and Mobilization of Arsenic in Subsurface Environment." *Water Res.,* 36(19), 4916-4926.

Bostick, B., Fendorf, S., Brown, G. (2005). "In Situ Analysis of Thioarsenite Complexes in Neutral to Alkaline Arsenic Sulphide Solutions." *Mineralogical Magazine,* 69(5), 781-795.

Bostick, B., and Fendorf, S. (2003). "Arsenite Sorption on Troilite (FeS) and Pyrite (FeS2)." *Geochim. Cosmochim. Acta,* 67(5), 909-921.

Bothe, J., and Brown, P. (1999). "Arsenic Immobilization by Calcium Arsenate Formation." *Environ. Sci. Technol.,* 33(21), 3806-3811.

Bowell, R. (1994). "Sorption of Arsenic by Iron-Oxides and Oxyhydroxides in Soils." *Appl. Geochem.,* 9(3), 279-286.

Bozkurt, S., Moreno, L., Neretnieks, I. (2000). "Long-Term Processes in Waste Deposits." *Sci. Total Environ.,* 250(1-3), 101-121.

Brookshaw, D. R., Pattrick, R. A. D., Lloyd, J. R., Vaughan, D. J. (2012). "Microbial Effects on Mineral-Radionuclide Interactions and Radionuclide Solid-Phase Capture Processes." *Mineralogical Magazine,* 76(3), 777-806.

Brown, D. A., Sherriff, B. L., Sawicki, J. A., Sparling, R. (1999). "Precipitation of Iron Minerals by a Natural Microbial Consortium." *Geochim. Cosmochim. Acta,* 63(15), 2163-2169.

Burgess, W., and Pinto, L. (2005). "Preliminary Observations on the Release of Arsenic to Groundwater in the Presence of Hydrocarbon Contaminants in UK Aquifers." *Mineralogical Magazine,* 69(5), 887-896.

Burnol, A., Garrido, F., Baranger, P., Joulian, C., Dictor, M., Bodenan, F., Morin, G., Charlet, L. (2007). "Decoupling of Arsenic and Iron Release from Ferrihydrite Suspension Under Reducing Conditions: A Biogeochemical Model." *Geochemical Transactions,* 8, 12.

Burton, E. D., Bush, R. T., Sullivan, L. A., Mitchell, D. R. G. (2008). "Schwertmannite Transformation to Goethite Via the Fe(II) Pathway: Reaction Rates and Implications for Iron-Sulfide Formation." *Geochim. Cosmochim. Acta,* 72(18), 4551-4564.

Burton, E. D., Johnston, S. G., Bush, R. T. (2011). "Microbial Sulfidogenesis in Ferrihydrite-Rich Environments: Effects on Iron Mineralogy and Arsenic Mobility." *Geochim. Cosmochim. Acta,* 75(11), 3072-3087.

Burton, E. D., Johnston, S. G., Watling, K., Bush, R. T., Keene, A. F., Sullivan, L. A. (2010). "Arsenic Effects and Behavior in Association with the Fe(II)-Catalyzed Transformation of Schwertmannite." *Environ. Sci. Technol.,* 44(6), 2016-2021.

Burton, E. D., Bush, R. T., Johnston, S. G., Watling, K. M., Hocking, R. K., Sullivan, L. A., Parker, G. K. (2009). "Sorption of Arsenic(V) and Arsenic(III) to Schwertmannite." *Environ. Sci. Technol.,* 43(24), 9202-9207.

Carlson, L., Bigham, J., Schwertmann, U., Kyek, A., Wagner, F. (2002). "Scavenging of as from Acid Mine Drainage by Schwertmannite and Ferrihydrite: A Comparison with Synthetic Analogues." *Environ. Sci. Technol.,* 36(8), 1712-1719.

Carter, M., Baker, N., Burford, R. (1995). "Polymer Encapsulation of Arsenic-Containing Waste." *J Appl Polym Sci,* 58(11), 2039-2046.

Cesbron, F., and Williams, S. (1992). "Tooeleite, a New Mineral from the United-States Mine, Tooele County, Utah." *Mineral. Mag.,* 56(382), 71-73.

Clesceri, L.S., Greenberg, A.E., Eaton, A.D. (1998). *Standard Methods for the Examination of Water and Wastewater*, APHA, Washington DC.

Cheng, Y., Holman, H., Lin, Z. (2012). "Remediation of Chromium and Uranium Contamination by Microbial Activity." *Elements,* 8(2), 107-112.

Chintalapati, P. K., Davis, A. D., Hansen, M. R., Sorensen, J. L., Dixon, D. (2009). "Encapsulation of Limestone Waste in Concrete After Arsenic Removal from Drinking Water." *Environ. Earth Sci.,* 59(1), 185-190.

Christensen, T.H., and Kjeldsen, P. (1995). "Landfill emissions and environmental impact: An introduction." T.H.Christensen, R. Cossu, R. Stegmann, eds., *SARDINIA '95, Fifth International Landfill Symposium, Proceedings, Volume III,* CISA, Cagliari, Italy, pp. 3-12.

Coker, V. S., Gault, A. G., Pearce, C. I., van der Laan, G., Telling, N. D., Charnock, J. M., Polya, D. A., Lloyd, J. R. (2006). "XAS and XMCD Evidence for Species-Dependent Partitioning of Arsenic during Microbial Reduction of Ferrihydrite to Magnetite." *Environ. Sci. Technol.,* 40(24), 7745-7750.

Cornell, R. (1988). "The Influence of some Divalent-Cations on the Transformation of Ferrihydrite to More Crystalline Products." *Clay Miner.,* 23(3), 329-332.

Cornell, R.M., and Schwertmann, U. (2003). *The Iron Oxides: Structure, Properties, Reactions, Occurences and Uses,* 2nd Ed. Wiley VCH, Weinheim.

Cortinas, I., Sierra-Alvarez, R., Field, J. A. (2008). "Biologically Mediated Mobilization of Arsenic from Granular Ferric Hydroxide in Anaerobic Columns Fed Landfill Leachate." *Biotechnol. Bioeng.,* 101(6), 1205-1213.

Couture, R., and Van Cappellen, P. (2011). "Reassessing the Role of Sulfur Geochemistry on Arsenic Speciation in Reducing Environments." *J. Hazard. Mater.,* 189(3), 647-652.

Cullen, W., and Reimer, K. (1989). "Arsenic Speciation in the Environment." *Chem. Rev.,* 89(4), 713-764.

Cummings, D., Caccavo, F., Fendorf, S., Rosenzweig, R. (1999). "Arsenic Mobilization by the Dissimilatory Fe(III)-Reducing Bacterium Shewanella Alga BrY." *Environ. Sci. Technol.,* 33(5), 723-729.

Cutting, R. S., Coker, V. S., Telling, N. D., Kimber, R. L., van der Laan, G., Pattrick, R. A. D., Vaughan, D. J., Arenholz, E., Lloydt, J. R. (2012). "Microbial Reduction of Arsenic-Doped Schwertmannite by Geobacter Sulfurreducens." *Environ. Sci. Technol.,* 46(22), 12591-12599.

Dawadi, S., Hansen, M., Berdanier, B. (2004). "Encapsulation of Contaminated Soil in Concrete Mortar." *ACI Mater. J.,* 101(5), 347-352.

Demopoulos, G.P. (1995). “Precipitation of crystalline scorodite ($FeAsO_4.2H_2O$) from chloride solution.” *Hydrometallurgy* 38(3), 245-261.

Dixit, S., and Hering, J. (2006). "Sorption of Fe(II) and as(III) on Goethite in Single- and Dual-Sorbate Systems." *Chem. Geol.,* 228(1-3), 6-15.

Dixit, S., and Hering, J. (2003). "Comparison of Arsenic(V) and Arsenic(III) Sorption Onto Iron Oxide Minerals: Implications for Arsenic Mobility." *Environ. Sci. Technol.,* 37(18), 4182-4189.

Dong, H., and Lu, A. (2012). "Mineral-Microbe Interactions and Implications for Remediation." *Elements,* 8(2), 95-100.

Dove, P., and Rimstidt, J. (1985). "The Solubility and Stability of Scorodite, $FeAsO_4.2H_2O$." *Am. Mineral.,* 70(7-8), 838-844.

Dowling, C., Poreda, R., Basu, A., Peters, S., Aggarwal, P. (2002). "Geochemical Study of Arsenic Release Mechanisms in the Bengal Basin Groundwater." *Water Resour. Res.,* 38(9), 1173.

Dutre, V., and Vandecasteele, C. (1998). "Immobilization Mechanism of Arsenic in Waste Solidified using Cement and Lime." *Environ. Sci. Technol.,* 32(18), 2782-2787.

Dutrizac, J., and Jambor, J. (1988). "The Synthesis of Crystalline Scorodite, $FeAsO_4.2H_2O$." *Hydrometallurgy,* 19(3), 377-384.

Dzombak, D.A., and Morel, F.M.M. (1990). *Surface complexation modeling: hydrous ferric oxide*, John Wiley & Sons, New York.

Egal, M., Casiot, C., Morin, G., Parmentier, M., Bruneel, O., Lebrun, S., Elbaz-Poulichet, F. (2009). "Kinetic Control on the Formation of Tooeleite, Schwertmannite and Jarosite by Acidithiobacillus Ferrooxidans Strains in an As(III)-Rich Acid Mine Water." *Chem. Geol.,* 265(3-4), 432-441.

Emerson, S., and Widmer, G. (1978). "Early Diagenesis in Anaerobic Lake-Sediments .2. Thermodynamic and Kinetic Factors Controlling Formation of Iron Phosphate." *Geochim. Cosmochim. Acta,* 42(9), 1307-1316.

Emerson, S. (1976). "Early Diagenesis in Anaerobic Lake-Sediments - Chemical-Equilibria in Interstitial Waters." *Geochim. Cosmochim. Acta,* 40(8), 925-934.

Evangelou, V. (1995). "Potential Microencapsulation of Pyrite by Artificial Inducement of Ferric Phosphate Coatings." *J. Environ. Qual.,* 24(3), 535-542.

Fagel, N., Alleman, L., Granina, L., Hatert, F., Thamo-Bozso, E., Cloots, R., Andre, L. (2005). "Vivianite Formation and Distribution in Lake Baikal Sediments." *Global Planet. Change,* 46(1-4), 315-336.

Farquhar, M., Charnock, J., Livens, F., Vaughan, D. (2002). "Mechanisms of Arsenic Uptake from Aqueous Solution by Interaction with Goethite, Lepidocrocite, Mackinawite, and Pyrite: An X-Ray Absorption Spectroscopy Study." *Environ. Sci. Technol.,* 36(8), 1757-1762.

Fredrickson, J., Zachara, J., Kennedy, D., Dong, H., Onstott, T., Hinman, N., Li, S. (1998). "Biogenic Iron Mineralization Accompanying the Dissimilatory Reduction of Hydrous Ferric Oxide by a Groundwater Bacterium." *Geochim. Cosmochim. Acta,* 62(19-20), 3239-3257.

Fujita, T., Fujieda, S., Shinoda, K., Suzuki, S. (2012). "Environmental Leaching Characteristics of Scorodite Synthesized with Fe(II) Ions." *Hydrometallurgy,* 111, 87-102.

Fukushi, K., Sato, T., Yanase, N. (2003). "Solid-Solution Reactions in As(V) Sorption by Schwertmannite." *Environ. Sci. Technol.,* 37(16), 3581-3586.

Fuller, C., and Davis, J. (1989). "Kinetics of Arsenate Interactions with Iron Oxyhydroxides." *Abstr. Pap. Am. Chem. Soc.,* 198, 41-GEOC.

Galvez, N., Barron, V., Torrent, J. (1999). "Effect of Phosphate on the Crystallization of Hematite, Goethite, and Lepidocrocite from Ferrihydrite." *Clays Clay Miner.,* 47(3), 304-311.

Gao, Y., and Mucci, A. (2001). "Acid Base Reactions, Phosphate and Arsenate Complexation, and their Competitive Adsorption at the Surface of Goethite in 0.7 M NaCl Solution." *Geochim. Cosmochim. Acta,* 65(14), 2361-2378.

Ghosh, A., Saez, A., Ela, W. (2006b). "Effect of pH, Competitive Anions and NOM on the Leaching of Arsenic from Solid Residuals." *Sci. Total Environ.,* 363(1-3), 46-59.

Ghosh, A., Mukiibi, M., Ela, W. (2004). "TCLP Underestimates Leaching of Arsenic from Solid Residuals Under Landfill Conditions." *Environ. Sci. Technol.,* 38(17), 4677-4682.

Ghosh, A., Mukiibi, M., Saez, A. E., Ela, W. P. (2006a). "Leaching of Arsenic from Granular Ferric Hydroxide Residuals Under Mature Landfill Conditions." *Environ. Sci. Technol.,* 40(19), 6070-6075.

Glasauer, S., Weidler, P., Langley, S., Beveridge, T. (2003). "Controls on Fe Reduction and Mineral Formation by a Subsurface Bacterium." *Geochim. Cosmochim. Acta,* 67(7), 1277-1288.

Goldberg, S., and Johnston, C. (2001). "Mechanisms of Arsenic Adsorption on Amorphous Oxides Evaluated using Macroscopic Measurements, Vibrational Spectroscopy, and Surface Complexation Modeling." *J. Colloid Interface Sci.,* 234(1), 204-216.

Guo, H., Stueben, D., Berner, Z. (2007). "Adsorption of Arsenic(III) and Arsenic(V) from Groundwater using Natural Siderite as the Adsorbent." *J. Colloid Interface Sci.,* 315(1), 47-53.

Han, H., Johnson, A., Kaczor, J., Kaur, M., Paszczynski, A., Qiang, Y. (2010). "Silica Coated Magnetic Nanoparticles for Separation of Nuclear Acidic Waste." *J. Appl. Phys.,* 107(9), 09B520.

Hansel, C. M., Benner, S. G., Neiss, J., Dohnalkova, A., Kukkadapu, R. K., Fendorf, S. (2003). "Secondary Mineralization Pathways Induced by Dissimilatory Iron Reduction of Ferrihydrite Under Advective Flow." *Geochim. Cosmochim. Acta,* 67(16), 2977-2992.

Hansel, C., Benner, S., Fendorf, S. (2005). "Competing Fe(II)-Induced Mineralization Pathways of Ferrihydrite." *Environ. Sci. Technol.,* 39(18), 7147-7153.

Herbel, M., and Fendorf, S. (2006). "Biogeochemical Processes Controlling the Speciation and Transport of Arsenic within Iron Coated Sands." *Chem. Geol.,* 228(1-3), 16-32.

Horneman, A., Van Geen, A., Kent, D. V., Mathe, P. E., Zheng, Y., Dhar, R. K., O'Connell, S., Hoque, M. A., Aziz, Z., Shamsudduha, M., Seddique, A. A., Ahmed, K. M. (2004). "Decoupling of As and Fe Release to Bangladesh Groundwater Under Reducing Conditions. Part 1: Evidence from Sediment Profiles." *Geochim. Cosmochim. Acta,* 68(17), 3459-3473.

Huang, J. -., Ilgen, G., Vogel, D., Michalzik, B., Hantsch, S., Tennhardt, L., Bilitewski, B. (2009). "Emissions of Inorganic and Organic Arsenic Compounds Via the Leachate Pathway from Pretreated Municipal Waste Materials: A Landfill Reactor Study." *Environ. Sci. Technol.,* 43(18), 7092-7097.

Huang, J., and Matzner, E. (2006). "Dynamics of Organic and Inorganic Arsenic in the Solution Phase of an Acidic Fen in Germany." *Geochim. Cosmochim. Acta,* 70(8), 2023-2033.

Impellitteri, C. A., and Scheckel, K. G. (2006). "The Distribution, Solid-Phase Speciation, and desorption/dissolution of as in Waste Iron-Based Drinking Water Treatment Residuals." *Chemosphere,* 64(6), 875-880.

Islam, F., Pederick, R., Gault, A., Adams, L., Polya, D., Charnock, J., Lloyd, J. (2005). "Interactions between the Fe(III)-Reducing Bacterium Geobacter Sulfurreducens and Arsenate, and Capture of the Metalloid by Biogenic Fe(II)." *Appl. Environ. Microbiol.,* 71(12), 8642-8648.

Islam, F., Gault, A., Boothman, C., Polya, D., Charnock, J., Chatterjee, D., Lloyd, J. (2004). "Role of Metal-Reducing Bacteria in Arsenic Release from Bengal Delta Sediments." *Nature,* 430(6995), 68-71.

Jackson, B. P., and Miller, W. P. (2000). "Effectiveness of Phosphate and Hydroxide for Desorption of Arsenic and Selenium Species from Iron Oxides." *Soil Sci. Soc. Am. J.,* 64(5), 1616-1622.

Jekel, M., and Amy, J.L. (2006). “Chapter 11: Arsenic removal during drinking water treatment.” *Interface Science in Drinking Water Treatment,* G. Newcombe and D. Dixon, eds., 1st ed., Elsevier Ltd.

Johnston, R. B., and Singer, P. C. (2007). "Solubility of Symplesite (Ferrous Arsenate): Implications for Reduced Groundwaters and Other Geochemical Environments." *Soil Sci. Soc. Am. J.,* 71(1), 101-107.

Jonsson, J., Persson, P., Sjoberg, S., Lovgren, L. (2005). "Schwertmannite Precipitated from Acid Mine Drainage: Phase Transformation, Sulphate Release and Surface Properties." *Appl. Geochem.,* 20(1), 179-191.

Jorand, F., Appenzeller, B. M. R., Abdelmoula, M., Refait, P., Block, J. C., Genin, J. M. R. (2000). "Assessment of Vivianite Formation in Shewanella Putrefaciens Culture." *Environ. Technol.,* 21(9), 1001-1005.

Khoe, G.H., Huang, J.C.Y., Robins, R.G. (1991). "Precipitation Chemistry of the Aqueous Ferrous Arsenate System." D.R. Gaskell, eds., *Extraction and Processing Div. Congr. '91, TMS,* New Orleans, LA, 103–115.

Kirk, M., Holm, T., Park, J., Jin, Q., Sanford, R., Fouke, B., Bethke, C. (2004). "Bacterial Sulfate Reduction Limits Natural Arsenic Contamination in Groundwater." *Geology,* 32(11), 953-956.

Kjeldsen, P., Barlaz, M., Rooker, A., Baun, A., Ledin, A., Christensen, T. (2002). "Present and Long-Term Composition of MSW Landfill Leachate: A Review." *Crit. Rev. Environ. Sci. Technol.,* 32(4), 297-336.

Knorr, K., and Blodau, C. (2007). "Controls on Schwertmannite Transformation Rates and Products." *Appl. Geochem.,* 22(9), 2006-2015.

Kocar, B. D., Borch, T., Fendorf, S. (2010). "Arsenic Repartitioning during Biogenic Sulfidization and Transformation of Ferrihydrite." *Geochim. Cosmochim. Acta,* 74(3), 980-994.

Kocar, B. D., Herbel, M. J., Tufano, K. J., Fendorf, S. (2006). "Contrasting Effects of Dissimilatory Iron(III) and Arsenic(V) Reduction on Arsenic Retention and Transport." *Environ. Sci. Technol.,* 40(21), 6715-6721.

Lafferty, B., and Loeppert, R. (2005). "Methyl Arsenic Adsorption and Desorption Behavior on Iron Oxides." *Environ. Sci. Technol.,* 39(7), 2120-2127.

Lagno, F., Rocha, S. D. F., Chryssoulis, S., Demopoulos, G. P. (2010). "Scorodite Encapsulation by Controlled Deposition of Aluminum Phosphate Coatings." *J. Hazard. Mater.,* 181(1-3), 526-534.

Lande, J., Webb, S.M., Mehta, A. (2007). *Area Diffraction Machine,* <http://groups.google.com.ezproxy2.library.arizona.edu/group/area-diffraction-machine>.

Lauchnor, E. G., Schultz, L. N., Bugni, S., Mitchell, A. C., Cunningham, A. B., Gerlach, R. (2013). "Bacterially Induced Calcium Carbonate Precipitation and Strontium Coprecipitation in a Porous Media Flow System." *Environ. Sci. Technol.,* 47(3), 1557-1564.

Le Berre, J. F., Gauvin, R., Demopoulos, G. P. (2008). "A Study of the Crystallization Kinetics of Scorodite Via the Transformation of Poorly Crystalline Ferric Arsenate in Weakly Acidic Solution." *Colloid Surf. A-Physicochem. Eng. Asp.,* 315(1-3), 117-129.

Le Berre, J. F., Gauvin, R., Demopoulos, G. P. (2007). "Characterization of Poorly-Crystalline Ferric Arsenate Precipitated from Equimolar Fe(III)-as(V) Solutions in the pH Range 2 to 8." *Metall. Mater. Trans. B-Proc. Metall. Mater. Proc. Sci.,* 38(5), 751-762.

Lee, J., Jang, C., Wang, S., Liang, C., Liu, C. (2008). "Delineation of Spatial Redox Zones using Discriminant Analysis and Geochemical Modelling in Arsenic-Affected Alluvial Aquifers." *Hydrol. Process.,* 22(16), 3029-3041.

Lee, Y. J., Stephens, P. W., Tang, Y., Li, W., Phillips, B. L., Parise, J. B., Reeder, R. J. (2009). "Arsenate Substitution in Hydroxylapatite: Structural Characterization of the Ca-5(PxAs1-xO4)(3)OH Solid Solution." *Am. Mineral.,* 94(5-6), 666-675.

Li, M., Cheng, X., Guo, H. (2013). "Heavy Metal Removal by Biomineralization of Urease Producing Bacteria Isolated from Soil." *Int. Biodeterior. Biodegrad.,* 76, 81-85.

Li, Y., Low, G. K., Scott, J. A., Amal, R. (2011). "Microbial Transformation of Arsenic Species in Municipal Landfill Leachate." *J. Hazard. Mater.,* 188(1-3), 140-147.

Li, Y., Low, G. K. -., Scott, J. A., Amal, R. (2010a). "Arsenic Speciation in Municipal Landfill Leachate." *Chemosphere,* 79(8), 794-801.

Li, Y., Church, J. S., Woodhead, A. L., Moussa, F. (2010b). "Preparation and Characterization of Silica Coated Iron Oxide Magnetic Nano-Particles." *Spectroc. Acta Pt. A-Molec. Biomolec. Spectr.,* 76(5), 484-489.

Liu, H., Wei, Y., Sun, Y. (2005a). "The Formation of Hematite from Ferrihydrite using Fe(II) as a Catalyst." *Journal of Molecular Catalysis A-Chemical,* 226(1), 135-140.

Liu, H., Wei, Y., Sun, Y. (2005b). "Study of the Catalytic Action of Fe(II) on the Phase Transformation of Ferrihydrite at a Low Temperature." *Acta Chimica Sinica,* 63(5), 391-395.

Liu, H., Wei, Y., Sun, Y., Wei, W. (2005c). "Dependence of the Mechanism of Phase Transformation of Fe(III) Hydroxide on pH." *Colloids and Surfaces A-Physicochemical and Engineering Aspects,* 252(2-3), 201-205.

Liu, H., Guo, H., Li, P., Wei, Y. (2008a). "The Transformation of Ferrihydrite in the Presence of Trace Fe(II): The Effect of the Anionic Media." *Journal of Solid State Chemistry,* 181(10), 2666-2671.

Liu, S., Jing, C., Meng, X. (2008b). "Arsenic Re-Mobilization in Water Treatment Adsorbents, Under Reducing Conditions: Part II. XAS and Modeling Study." *Sci. Total Environ.,* 392(1), 137-144.

Lowers, H. A., Breit, G. N., Foster, A. L., Whitney, J., Yount, J., Uddin, N., Muneem, A. (2007). "Arsenic Incorporation into Authigenic Pyrite, Bengal Basin Sediment, Bangladesh." *Geochim. Cosmochim. Acta,* 71(11), 2699-2717.

Ludvigsen, L., Albrechtsen, H., Ringelberg, D., Ekelund, F., Christensen, T. (1999). "Distribution and Composition of Microbial Populations in Landfill Leachate Contaminated Aquifer (Grindsted, Denmark)." *Microb. Ecol.,* 37(3), 197-207.

Mahapatra, P., Sarangi, D., Mishra, B. (1993). "A New Method of Preparation of Solid-Solutions of Calcium-Cadmium-Lead Hydroxylapatite and their Characterization by X-Ray, Electronmicrography and Ir-Spectra." *Indian J. Chem. Sect A-Inorg. Phys. Theor. Anal. Chem.,* 32(6), 525-530.

Mahapatra, P., Mahapatra, L., Mishra, B. (1989). "Physicochemical Studies on Solid-Solutions of Calcium Phosphorus Arsenic Hydroxyapatites." *Bull. Chem. Soc. Jpn.,* 62(10), 3272-3277.

Mamindy-Pajany, Y., Hurel, C., Marmier, N., Romeo, M. (2011). "Arsenic (V) Adsorption from Aqueous Solution Onto Goethite, Hematite, Magnetite and Zero-Valent Iron: Effects of pH, Concentration and Reversibility." *Desalination,* 281, 93-99.

Mambote, R.C.M., Reuters, M.A., van Sandwijk, A., Krijgsman, P. (2001). “Immobilization of arsenic in crystalline form from aqueous solution by hydrothermal processing above 483.15K.” *Miner. Eng.,* 14(4) 391-403.

Manceau, A. (2011). "Critical Evaluation of the Revised Akdalaite Model for Ferrihydrite." *Am. Mineral.,* 96(4), 521-533.

Manceau, A. (2009). "Evaluation of the Structural Model for Ferrihydrite Derived from Real-Space Modelling of High-Energy X-Ray Diffraction Data." *Clay Miner.,* 44(1), 19-34.

Manceau, A. (2012). "Comment on "Direct Observation of Tetrahedrally Coordinated Fe(III) in Ferrihydrite"." *Environ. Sci. Technol.,* 46(12), 6882-6884.

Mandal, B., and Suzuki, K. (2002). "Arsenic Round the World: A Review." *Talanta,* 58(1), 201-235.

Manning, B., Fendorf, S., Goldberg, S. (1998). "Surface Structures and Stability of Arsenic(III) on Goethite: Spectroscopic Evidence for Inner-Sphere Complexes." *Environ. Sci. Technol.,* 32(16), 2383-2388.

Marquez, M., Gaspar, J., Bessler, K. E., Magela, G. (2006). "Process Mineralogy of Bacterial Oxidized Gold Ore in Sao Bento Mine (Brasil)." *Hydrometallurgy,* 83(1-4), 114-123.

Masscheleyn, P., Delaune, R., Patrick, W. (1991). "Effect of Redox Potential and Ph on Arsenic Speciation and Solubility in a Contaminated Soil." *Environ. Sci. Technol.,* 25(8), 1414-1419.

McArthur, J., Banerjee, D., Hudson-Edwards, K., Mishra, R., Purohit, R., Ravenscroft, P., Cronin, A., Howarth, R., Chatterjee, A., Talukder, T., Lowry, D., Houghton, S., Chadha, D. (2004). "Natural Organic Matter in Sedimentary Basins and its Relation to Arsenic in Anoxic Ground Water: The Example of West Bengal and its Worldwide Implications." *Appl. Geochem.,* 19(8), 1255-1293.

McCormick, M., Bouwer, E., Adriaens, P. (2002). "Carbon Tetrachloride Transformation in a Model Iron-Reducing Culture: Relative Kinetics of Biotic and Abiotic Reactions." *Environ. Sci. Technol.,* 36(3), 403-410.

Mitchell, W., Goldberg, S., Al-Abadleh, H. A. (2011). "In Situ ATR-FTIR and Surface Complexation Modeling Studies on the Adsorption of Dimethylarsinic Acid and p-Arsanilic Acid on Iron-(Oxyhydr)Oxides." *J. Colloid Interface Sci.,* 358(2), 534-540.

Mohan, D., and Pittman, C. U., Jr. (2007). "Arsenic Removal from water/wastewater using Adsorbents - A Critical Review." *J. Hazard. Mater.,* 142(1-2), 1-53.

Mohapatra, D., Singh, P., Zhang, W., Pullammanappallil, P. (2005). "The Effect of Citrate, Oxalate, Acetate, Silicate and Phosphate on Stability of Synthetic Arsenic-Loaded Ferrihydrite and Al-Ferrihydrite." *J. Hazard. Mater.,* 124(1-3), 95-100.

Morin, G., Juillot, F., Casiot, C., Bruneel, O., Personne, J., Elbaz-Poulichet, F., Leblanc, M., Ildefonse, P., Calas, G. (2003). "Bacterial Formation of Tooeleite and Mixed Arsenic(III) Or Arsenic(V)-Iron(III) Gels in the Carnoulbs Acid Mine Drainage, France. A XANES, XRD, and SEM Study." *Environ. Sci. Technol.,* 37(9), 1705-1712.

Morin, G., Wang, Y., Ona-Nguema, G., Juillot, F., Calas, G., Menguy, N., Aubry, E., Bargar, J. R., Brown, G. E., Jr. (2009). "EXAFS and HRTEM Evidence for as(III)-Containing Surface Precipitates on Nanocrystalline Magnetite: Implications for as Sequestration." *Langmuir,* 25(16), 9119-9128.

Morin, G., Rousse, G., Elkaim, E. (2007). "Crystal Structure of Tooeleite, Fe-6(AsO3)(4)SO4(OH)(4)Center Dot 4H(2)O, a New Iron Arsenite Oxyhydroxysulfate Mineral Relevant to Acid Mine Drainage." *Am. Mineral.,* 92(1), 193-197.

Mukiibi, M., Ela, W. P., Saez, A. E. (2008). "Effect of Ferrous Iron on Arsenate Sorption to Amorphous Ferric Hydroxide." *Ann. NY Acad. Sci.,* 1140, 335-345.

Nishimura, T., and Robins, R. G. (2008). "Confirmation that Tooeleite is a Ferric Arsenite Sulfate Hydrate, and is Relevant to Arsenic Stabilisation." *Minerals Eng,* 21(4), 246-251.

Nriagu, J., and Dell, C. (1974). "Diagenetic Formation of Iron Phosphates in Recent Lake Sediments." *Am. Mineral.,* 59(9-10), 934-946.

Nriagu, J. (1972). "Stability of Vivianite and Ion-Pair Formation in System $Fe_3(PO_4)_2$-H_3PO_4-H_2O." *Geochim. Cosmochim. Acta,* 36(4), 459-470.

O'Day, P., Vlassopoulos, D., Root, R., Rivera, N. (2004). "The Influence of Sulfur and Iron on Dissolved Arsenic Concentrations in the Shallow Subsurface Under Changing Redox Conditions." *Proc. Natl. Acad. Sci. U. S. A.,* 101(38), 13703-13708.

Oliva, J., De Pablo, J., Cortina, J., Cama, J., Ayora, C. (2011). "Removal of Cadmium, Copper, Nickel, Cobalt and Mercury from Water by Apatite II (TM): Column Experiments." *J. Hazard. Mater.,* 194, 312-323.

Paige, C., Snodgrass, W., Nicholson, R., Scharer, J., He, Q. (1997). "The Effect of Phosphate on the Transformation of Ferrihydrite into Crystalline Products in Alkaline Media." *Water Air Soil Pollut.,* 97(3-4), 397-412.

Paikaray, S., and Peiffer, S. (2010). "Dissolution Kinetics of Sulfate from Schwertmannite Under Variable pH Conditions." *Mine Water and the Environment,* 29(4), 263-269.

Pallud, C., Masue-Slowey, Y., Fendorf, S. (2010). "Aggregate-Scale Spatial Heterogeneity in Reductive Transformation of Ferrihydrite Resulting from Coupled Biogeochemical and Physical Processes." *Geochim. Cosmochim. Acta,* 74(10), 2811-2825.

Parkhurst, D.L., and Appelo, C.A.J. (1999). “User’s Guide to PHREEQC (Version 2), A Computer Program for Speciation, Batch-reaction, One-dimensional Transport, and Inverse Geochemical Calculations.” *US Geol. Surv.,Water-Resour. Invest. Rep.* 99-4259.

Pedersen, H. D., Postma, D., Jakobsen, R. (2006). "Release of Arsenic Associated with the Reduction and Transformation of Iron Oxides." *Geochim. Cosmochim. Acta,* 70(16), 4116-4129.

Pedersen, H., Postma, D., Jakobsen, R., Larsen, O. (2005). "Fast Transformation of Iron Oxyhydroxides by the Catalytic Action of Aqueous Fe(II)." *Geochim. Cosmochim. Acta,* 69(16), 3967-3977.

Postma, D. (1981). "Formation of Siderite and Vivianite and the Pore-Water Composition of a Recent Bog Sediment in Denmark." *Chem. Geol.,* 31(3), 225-244.

Postma, D., Larsen, F., Hue, N. T. M., Duc, M. T., Viet, P. H., Nhan, P. Q., Jessen, S. (2007). "Arsenic in Groundwater of the Red River Floodplain, Vietnam: Controlling Geochemical Processes and Reactive Transport Modeling." *Geochim. Cosmochim. Acta,* 71(21), 5054-5071.

Radoicic, T. K., and Raicevic, S. (2008). "In Situ Lead Stabilization using Natural and Synthetic Apatite." *Chem. Ind. Chem. Eng. Q.,* 14(4), 269-271.

Rancourt, D. G., and Meunier, J. -. (2008). "Constraints on Structural Models of Ferrihydrite as a Nanocrystalline Material." *Am. Mineral.,* 93(8-9), 1412-1417.

Regenspurg, S., and Peiffer, S. (2005). "Arsenate and Chromate Incorporation in Schwertmannite." *Appl. Geochem.,* 20(6), 1226-1239.

Regenspurg, S., Brand, A., Peiffer, S. (2004). "Formation and Stability of Schwertmannite in Acidic Mining Lakes." *Geochim. Cosmochim. Acta,* 68(6), 1185-1197.

Rennert, T., Totsche, K. U., Heister, K., Kersten, M., Thieme, J. (2012). "Advanced Spectroscopic, Microscopic, and Tomographic Characterization Techniques to Study Biogeochemical Interfaces in Soil." *Journal of Soils and Sediments,* 12(1), 3-23.

Riveros, P., Dutrizac, J., Spencer, P. (2001). "Arsenic Disposal Practices in the Metallurgical Industry." *Can. Metall. Q.,* 40(4), 395-420.

Robins, R. (1987). "Solubility and Stability of Scorodite, $FeAsO_4.2H_2O$ - Discussion." *Am. Mineral.,* 72(7-8), 842-844.

Roden, E., Leonardo, M., Ferris, F. (2002). "Immobilization of Strontium during Iron Biomineralization Coupled to Dissimilatory Hydrous Ferric Oxide Reduction." *Geochim. Cosmochim. Acta,* 66(16), 2823-2839.

Roden, E., and Zachara, J. (1996). "Microbial Reduction of Crystalline Iron(III) Oxides: Influence of Oxide Surface Area and Potential for Cell Growth." *Environ. Sci. Technol.,* 30(5), 1618-1628.

Root, R., Alday, F., Fathordoobadi, S., Ela, W.P., Chorover, J. "Sulfate controls the transformation of As species in ferric-based sorbents subjected to simulated landfill conditions." *Environ. Sci. Technol.,* under review, es-2013-02083h.

Sadiq, M., Locke, A., Spiers, G., Pearson, D. (2002). "Geochemical Behavior of Arsenic in Kelly Lake, Ontario." *Water Air Soil Pollut.,* 141(1-4), 299-312.

Sadiq, M. (1997). "Arsenic Chemistry in Soils: An Overview of Thermodynamic Predictions and Field Observations." *Water Air and Soil Pollution,* 93(1-4), 117-136.

Salome, K. R., Green, S. J., Beazley, M. J., Webb, S. M., Kostka, J. E., Taillefert, M. (2013). "The Role of Anaerobic Respiration in the Immobilization of Uranium through Biomineralization of Phosphate Minerals." *Geochim. Cosmochim. Acta,* 106, 344-363.

Schwertmann, U., and Carlson, L. (2005). "The pH-Dependent Transformation of Schwertmannite to Goethite at 25 Degrees C." *Clay Miner.,* 40(1), 63-66.

Schwertmann, U., Cornell, R.M. (1991). *Iron Oxides in the Laboratory: Preparation and Characterization.* VCH, New York.

Seidel, H., Gorsch, K., Amstatter, K., Mattusch, J. (2005). "Immobilization of Arsenic in a Tailings Material by Ferrous Iron Treatment." *Water Res.,* 39(17), 4073-4082.

Selvin, N., Upton, J., Simms, J., Barnes, J. (2002). "Arsenic treatment technology for groundwaters", *Wa. Sci. Technol.* 2(1), 11-16.

Sharp, J. O., Lezama-Pacheco, J. S., Schofield, E. J., Junier, P., Ulrich, K., Chinni, S., Veeramani, H., Margot-Roquier, C., Webb, S. M., Tebo, B. M., Giammar, D. E., Bargar, J. R., Bernier-Latmani, R. (2011). "Uranium Speciation and Stability After Reductive Immobilization in Aquifer Sediments." *Geochim. Cosmochim. Acta,* 75(21), 6497-6510.

Shaw, J. K., Fathordoobadi, S., Zelinski, B. J., Ela, W. P., Saez, A. E. (2008). "Stabilization of Arsenic-Bearing Solid Residuals in Polymeric Matrices." *J. Hazard. Mater.,* 152(3), 1115-1121.

Silva, J., Vargas de Mello, J. W., Gasparon, M., Pereira Abrahao, W. A. (2012). "Effects of Competing Anions and Iron Bioreduction on Arsenic Desorption." *Water Air Soil Pollut.,* 223(9), 5707-5717.

Singh, T., and Pant, K. (2006). "Solidification/stabilization of Arsenic Containing Solid Wastes using Portland Cement, Fly Ash and Polymeric Materials." *J. Hazard. Mater.,* 131(1-3), 29-36.

Smedley, P., and Kinniburgh, D. (2002). "A Review of the Source, Behaviour and Distribution of Arsenic in Natural Waters." *Appl. Geochem.,* 17(5), 517-568.

Stuckman, M. Y., Lenhart, J. J., Walker, H. W. (2011). "Abiotic Properties of Landfill Leachate Controlling Arsenic Release from Drinking Water Adsorbents." *Water Res.,* 45(16), 4782-4792.

Sturman, B.D. (1976). “New data for kottigite and parasymplesite.” *Can. Mineral.* 14, 437-441.

Taylor, K. G., and Boult, S. (2007). "The Role of Grain Dissolution and Diagenetic Mineral Precipitation in the Cycling of Metals and Phosphorus: A Study of a Contaminated Urban Freshwater Sediment." *Appl. Geochem.,* 22(7), 1344-1358.

Thinnappan, V., Merrifield, C. M., Islam, F. S., Polya, D. A., Wincott, P., Wogelius, R. A. (2008). "A Combined Experimental Study of Vivianite and as (V) Reactivity in the pH Range 2-11." *Appl. Geochem.,* 23(11), 3187-3204.

Tokunaga, T. K., Olson, K. R., Wan, J. (2003). "Moisture Characteristics of Hanford Gravels: Bulk, Grain-Surface, and Intragranular Components." *Vadose Zone J.,* 2(3), 322-329.

Tronc, E., Belleville, P., Jolivet, J., Livage, J. (1992). "Transformation of Ferric Hydroxide into Spinel by Fe(II) Adsorption." *Langmuir,* 8(1), 313-319.

Tufano, K. J., Benner, S. G., Mayer, K. U., Marcus, M. A., Nico, P. S., Fendorf, S. (2009). "Aggregate-Scale Heterogeneity in Iron (Hydr)Oxide Reductive Transformations." *Vadose Zone Journal,* 8(4), 1004-1012.

Tufano, K. J., and Fendorf, S. (2008). "Confounding Impacts of Iron Reduction on Arsenic Retention." *Environ. Sci. Technol.,* 42(13), 4777-4783.

U.S. Environmental Protection Agency (2003). “Arsenic Treatment Technology Evaluation Handbook for Small Systems.” USEPA, Washington, DC.

U.S. Environmental Protection Agency (2002). “Arsenic Treatment Technologies for Soil, Waste, and Water”, USEPA, Washington, DC EPA-542-R-02-004.

U.S. Environmental Protection Agency (2001). “National Primary Drinking Water Regulations: Arsenic and Clarifications to Compliance and New Source Contaminants Monitoring Final Rule” USEPA, Washington, DC.

U.S. Environmental Protection Agency (2000). “Technologies and Costs for Removal of Arsenic from Drinking Water.” USEPA, Washington, DC.

U.S. Environmental Protection Agency (1992). “Method 1311: Toxicity Characteristic Leaching Procedure.” USEPA, Washington, DC http://www.epa.gov/sw-846/pdfs/1311.pdf.

van Geen, A., Zheng, Y., Cheng, Z., Aziz, Z., Horneman, A., Dhar, R., Mailloux, B., Stute, M., Weinman, B., Goodbred, S., Seddique, A., Hope, M., Ahmed, K. (2006). "A Transect of Groundwater and Sediment Properties in Araihazar, Bangladesh: Further Evidence of Decoupling between as and Fe Mobilization." *Chem. Geol.,* 228(1-3), 85-96.

Violante, A., and Pigna, M. (2002). "Competitive Sorption of Arsenate and Phosphate on Different Clay Minerals and Soils." *Soil Sci. Soc. Am. J.,* 66(6), 1788-1796.

Vircikova, E., Molnar, L., Lech, P., Reitznerova, E. (1995). "Solubilities of Amorphous Fe-As Precipitates." *Hydrometallurgy,* 38(2), 111-123.

Voigt, D., Brantley, S., Hennet, R. (1996). "Chemical Fixation of Arsenic in Contaminated Soils." *Appl. Geochem.,* 11(5), 633-643.

Wang, S., and Mulligan, C. N. (2006). "Effect of Natural Organic Matter on Arsenic Release from Soils and Sediments into Groundwater." *Environ. Geochem. Health,* 28(3), 197-214.

Wang, Y., Morin, G., Ona-Nguema, G., Juillot, F., Calas, G., Brown, G. E., Jr. (2011). "Distinctive Arsenic(V) Trapping Modes by Magnetite Nanoparticles Induced by Different Sorption Processes." *Environ. Sci. Technol.,* 45(17), 7258-7266.

Wang, Y., Morin, G., Ona-Nguema, G., Menguy, N., Juillot, F., Aubry, E., Guyot, F., Calas, G., Brown, G. E., Jr. (2008). "Arsenite Sorption at the Magnetite-Water Interface during Aqueous Precipitation of Magnetite: EXAFS Evidence for a New Arsenite Surface Complex." *Geochim. Cosmochim. Acta,* 72(11), 2573-2586.

Warren, L., Maurice, P., Parmar, N., Ferris, F. (2001). "Microbially Mediated Calcium Carbonate Precipitation: Implications for Interpreting Calcite Precipitation and for Solid-Phase Capture of Inorganic Contaminants." *Geomicrobiol. J.,* 18(1), 93-115.

Welch, A., Westjohn, D., Helsel, D., Wanty, R. (2000). "Arsenic in Ground Water of the United States: Occurrence and Geochemistry." *Ground Water,* 38(4), 589-604.

World Health Organization (2001). “Arsenic in drinking water.” WHO, Geneva, Switzerland, Fact Sheet No. 210.

Wilkin, R., and Ford, R. (2006). "Arsenic Solid-Phase Partitioning in Reducing Sediments of a Contaminated Wetland." *Chem. Geol.,* 228(1-3), 156-174.

Wilkin, R. (2003). "Arsenic Uptake Processes in Reducing Environments: Implications for Active Remediation and Natural Attenuation." *Abstracts of Papers of the American Chemical Society,* 226, U587-U587.

Willett, I. R. (1985). "The Reductive Dissolution of Phosphated Ferrihydrite and Strengite." *Aust. J. Soil Res.,* 23(2), 237-244.

Wilson, F., and Hawkins, D. (1978). "Arsenic in Streams, Stream Sediments, and Ground-Water, Fairbanks Area, Alaska." *Environ. Geol.,* 2(4), 195-202.

Wolthers, M., Charlet, L., Van der Weijden, C., Van der Linde, P., Rickard, D. (2005). "Arsenic Mobility in the Ambient Sulfidic Environment: Sorption of Arsenic(V) and Arsenic(III) Onto Disordered Mackinawite." *Geochim. Cosmochim. Acta,* 69(14), 3483-3492.

Yang, D., Hu, J., Fu, S. (2009). "Controlled Synthesis of Magnetite-Silica Nanocomposites Via a Seeded Sol-Gel Approach." *J. Phys. Chem. C,* 113(18), 7646-7651.

Yang, L., Steefel, C. I., Marcus, M. A., Bargar, J. R. (2010). "Kinetics of Fe(II)-Catalyzed Transformation of 6-Line Ferrihydrite Under Anaerobic Flow Conditions." *Environ. Sci. Technol.,* 44(14), 5469-5475.

Yee, N., Shaw, S., Benning, L. G., Nguyen, T. H. (2006). "The Rate of Ferrihydrite Transformation to Goethite Via the Fe(II) Pathway." *Am. Mineral.,* 91(1), 92-96.

Zachara, J., Fredrickson, J., Li, S., Kennedy, D., Smith, S., Gassman, P. (1998). "Bacterial Reduction of Crystalline Fe3+ Oxides in Single Phase Suspensions and Subsurface Materials." *Am. Mineral.,* 83(11-12), 1426-1443.

Zhang, G., Dong, H., Jiang, H., Kukkadapu, R. K., Kim, J., Eberl, D., Xu, Z. (2009). "Biomineralization Associated with Microbial Reduction of Fe3+ and Oxidation of Fe2+ in Solid Minerals." *Am. Mineral.,* 94(7), 1049-1058.

Zhao, H., and Stanforth, R. (2001). "Competitive Adsorption of Phosphate and Arsenate on Goethite." *Environ. Sci. Technol.,* 35(24), 4753-4757.

Zheng, Y., Stute, M., van Geen, A., Gavrieli, I., Dhar, R., Simpson, H., Schlosser, P., Ahmed, K. (2004). "Redox Control of Arsenic Mobilization in Bangladesh Groundwater." *Appl. Geochem.,* 19(2), 201-214.

“Ferrisymplesite” <http://www.mindat.org/min-1502.html>, (June 1, 2013).